

12-2001

Petrological and Geochemical Analyses and economic potential of some Milestones and Siliceous rocks in northern United Arab Emirates.

Mohammed Ahmed A. Ibrahim

Follow this and additional works at: https://scholarworks.uaeu.ac.ae/all_theses

Part of the [Environmental Sciences Commons](#)

Recommended Citation

Ahmed A. Ibrahim, Mohammed, "Petrological and Geochemical Analyses and economic potential of some Milestones and Siliceous rocks in northern United Arab Emirates." (2001). *Theses*. 564.
https://scholarworks.uaeu.ac.ae/all_theses/564

This Thesis is brought to you for free and open access by the Electronic Theses and Dissertations at Scholarworks@UAEU. It has been accepted for inclusion in Theses by an authorized administrator of Scholarworks@UAEU. For more information, please contact fadl.musa@uaeu.ac.ae.

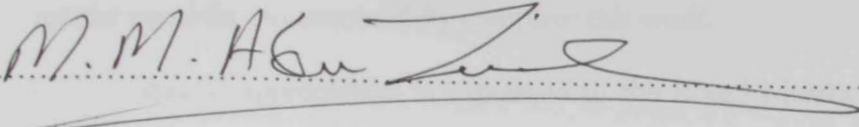
**PETROLOGICAL AND GEOCHEMICAL
ANALYSES AND ECONOMIC POTENTIAL OF
SOME LIMESTONES AND SILICEOUS ROCKS IN
NORTHERN UNITED ARAB EMIRATES**

**By
Mohammed Ahmed A. Ibrahim**

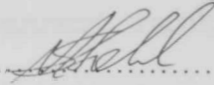
**A Thesis submitted to the Faculty of Science,
United Arab Emirates University in partial
fulfillment of the requirements for the Degree
of Master of Science in Environmental Sciences**

**Faculty of Science
UAE University
December 2001**

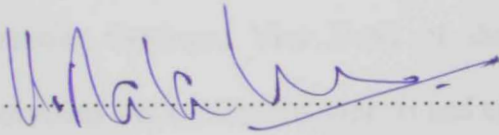
The Thesis of Mohammed Ahmed Ail Ebrahim for the Degree of Master of Science in Environmental is approved.



Examining Committee Member, Prof. Mohamed M. Abu-Zeid



Examining Committee Member, Dr. Mamdouh Shebl



Examining Committee Member, : Dr. V. Balasubramaniam

Dean of the Graduate Studies, Dr. Hadeef Rashed Al-Owa

United Arab Emirates University
2001/2002

ACKNOWLEDGMENTS

First of all, I thank Almighty Allah for His Blessings and for providing me the capability to successfully complete this work.

Special appreciation is expressed to the Board Member of the Ras Al Khaimah Cement Company for giving me the opportunity to complete my study in this field.

I am deeply indebted to Prof. Mohamed M. Abu-Zeid (Professor of Mineralogy and Sedimentary Petrology; Chairman of the Geology Department, Faculty of Science, United Arab Emirate University) and Dr. Fathy H. Mohamed (Associate Professor of Geochemistry, Geology Department, Faculty of Science, UAEU) who suggested, planned and supervised this research project. Their sincere guidance, fruitful discussions, critical reviewing of the manuscript and unlimited assistance during the various phases of this work greatly aided its completion.

Thanks are extended to Dr. Abdullah Al Musallam (Assistant Professor of Economic Geology, Vice Dean of the Faculty of Science, UAEU) for his kind supervision and continuous support and encouragement.

I am grateful to Dr. Mohamed Mersal (Geology Department, UAEU) for providing valuable help during microscopic examinations. Appreciation is extended to Mr. Hamdi Kandil, Mr. Magdi Mohib and Mr. Iyman Elsaay for their sincere efforts during various phases of this research project. I am also grateful to all of those who in some way or the other have helped me for the completion of this work.

Finally, I would like to express my deep gratitude and special thanks to my great family for their patience and support during all phases of this work.

ABSTRACT

Combined microscopic, heavy-mineral, X-ray diffraction and chemical analyses have been carried out on the Jurassic limestones, the Upper Cretaceous Hawasina cherts and the coastal and inland sand dunes in several localities in the Ras Al Khaimah Emirate. The obtained results revealed that cherts are represented by a number of subfacies; namely: ferruginous radiolarian ribbon chert, carbonaceous radiolarian ribbon chert, colloform ribbon chert, calcareous chert and siliceous mudstone. These rocks consist of (in order of decreasing abundance): quartz, calcite, dolomite and hematite. The carbonate rocks are made up of lime mudstone, wackestone, packstone and, rarely, crystalline limestone. Various types of wackestone and packstone were recorded. Mineralogically, these limestones consist of calcite and much lesser proportions of quartz and dolomite. Diagenesis greatly modified the original textural and compositional characteristics of the rocks especially the limestones. On the other hand, the light fractions of the coastal sand dunes contain higher concentrations of carbonate lithoclasts and skeletal grains and lower proportions of quartz and chert than those of the inland dunes. Also, the heavy fractions of the former sediments are slightly more enriched in opaques, pyroxenes, epidotes and hornblende while depleted in rutile, tourmaline, garnet and monazite.

The obtained geochemical data confirm the presence of the main chert types; namely: (i) radiolarites (R), (ii) calcareous cherts (CC), and (iii) siliceous mudstones (SM). Each type has a homogeneous and characteristics major and trace element compositions. Silica values are highest (90%-98%) in radiolarites and lowest (49%-72%) in calcareous cherts. The relatively high Al/(Al+Fe+Mn) ratios in most cherts, reflects the importance of the terrigenous sources in their genesis. This is further

confirmed by the increase of TiO_2 , Al_2O_3 , MgO , Fe_2O_3 and HFSE (High Field Strength Elements). The cherts exhibit LREE (Light Rare Earth Elements) fractionated patterns with moderate negative Eu anomalies. R-mode cluster analysis shows three clusters. The first is for the carbonate minerals, the second includes the terrigenous components and the third is the silica cluster. Factor analysis produced a two-factor model which accounts for 85.85% of the data variability. The first is the terrigenous factor (TiO_2 , Al_2O_3 , FeO , K_2O , P_2O_5 , Rb, Ga, Zr and REE), and the second is the carbonate factor.

The majority of the studied limestones and a few of the chert rocks are compositionally similar to those presently used by the Ras Al Khaimah Rock Company for cement production and, consequently, can be considered for possible future needs. On the other hand, the compositional characteristics of the dune sands, especially the coastal dunes, do not permit their use as a possible source of silica.

TABLE OF CONTENTS

	Page
CHAPTER I - INTRODUCTION	1
1.1 Geomorphology.....	1
1.1.1 The Structural Ridge of the Mountain Region.....	1
1.1.2 The Western Bajada of the Gravel Plain.....	3
1.1.3 The Sandy Desert or Structural Plain.....	3
1.1.4 The Coastal Plain.....	3
1.1.5 Mountains.....	6
1.1.6 Alluvial Fans.....	8
1.2 Geology and Structural Setting.....	8
1.2.1 Hajar Supergruop: Mosozoic - Early Tertiary carbonate platform.....	11
1.2.2 Sumeini Group: carbonate slope deposition.....	14
1.2.3 Hawasina Compex: deep-water passive margin sediments.....	17
1.2.4 Triassic Zulla Formation: starved base of slope.....	18
1.2.5 Late Triassic - Jurassic Guweyza Formation: redeposited deep-sea carbonate.....	18
1.2.6 Late Jurassic - Early Cretaceous Sid'r Formation: siliceous deposition.....	19
1.2.7 Structurally higher Hawasina units.....	21
1.2.8 Haybi Complex: more outboard units.....	23
1.2.9 Ayam Formation: condensed shelf deposition.....	23
1.3 Aim of the Study.....	24
CHAPTER II - MATERIALS AND METHODS OF STUDY	25
2.1 Materials.....	25
2.2 Methods of study.....	25
CHAPTER III – PETROGRAPHY	28
3.1 The Chert Facies.....	28
3.1.1 Ferruginous Radiolarian Ribbon Chert.....	28
3.1.2 Carbonaceous Radiolarian Ribbon Chert.....	28
3.1.3 Colloform Ribbon Chert.....	30

	Page
3.1.4	Calcareous Chert..... 30
3.1.5	Siliceous Claystone..... 30
3.2	The carbonate Facies..... 35
3.2.1	Lime Mudstone..... 35
3.2.2	Wackstone..... 35
3.2.3	Packstone..... 37
3.2.4	Crystalline Limestone..... 43
3.3	Sand Dunes..... 43
3.3.1	Carbonate Dune Sands..... 43
3.3.2	Non carbonate Dune sands..... 43
3.4	The Diabasic Sheet..... 46
CHAPTER IV - MINERALOGY	47
4.1	Mineralogy of Cherts..... 47
4.2	Mineralogy of Carbonate Rocks..... 47
4.3	Mineralogy of the Sand Dunes..... 49
4.4	Mineralogy of Diabase Sheet..... 50
CHAPTER V – GEOCHEMISTRY	61
5.1	Distribution of Elements..... 61
5.1.1	Major Elements..... 61
5.1.2	Trace Elements..... 67
5.1.3	Rare Earth Elements (REE)..... 70
5.2	Multivariate Statistics..... 78
5.2.1	Correlation Coefficients..... 78
5.2.2	Cluster Analyses..... 78
CHAPTER VI - ECONOMIC POTENTIAL	91
6.1	Introduction..... 91
6.2	Ras Al-Khaimah Cement History..... 92
6.3	The Cement Production Process..... 93
6.4	Raw Materials Available in the Ras Al-Khaimah Emirate.. 97
CHAPTER VII - SUMMARY AND CONCLUSIONS	106
REFERENCES	112

LIST OF FIGURES

		Page
Fig.1.1	Simplified geomorphologic map of the Northern United Arab Emirates showing the location of the study area	2
Fig.1.2	Geologic map of the Northern United Arab Emirates.....	5
Fig.1.3	Generalized tectonic map of the Northern United Arab Emirates...	9
Fig.1.4	Geologic map of the Dibba Zone	10
Fig.1.5	Sections across the Dibba Zone	12
Fig.1.6	Stratigraphy of the Dibba Zone.....	15
Fig.2.1	Geologic map showing the sample locations.....	26
Fig.3.1	A photomicrograph of ferruginous radiolarian ribbon chert.....	29
Fig.3.2	A closeup view of the ferruginous radiolarian ribbon chert.....	29
Fig.3.3	A photomicrograph of the ferruginous radiolarian ribbon chert.....	31
Fig.3.4	A photomicrograph of the carbonaceous radiolarian chert.....	31
Fig.3.5	A photomicrograph of the carbonaceous radiolarian chert.....	32
Fig.3.6	A photomicrograph of the colloform ribbon chert.....	32
Fig.3.7	A photomicrograph of the colloform ribbon chert.....	33
Fig.3.8	A photomicrograph of the calcareous chert.....	33
Fig.3.9	A photomicrograph of the calcareous chert.....	34
Fig.3.10	A photomicrograph of the siliceous claystone.....	34
Fig.3.11	A photomicrograph of the siliceous claystone.....	36
Fig.3.12	A photomicrograph of the conglomerate subfacies.....	36
Fig.3.13	A photomicrograph of the lime mudstone facies.....	38
Fig.3.14	A photomicrograph of the peloidal bioclastic wackestone.....	38
Fig.3.15	A photomicrograph of the peloidal bioclastic wackestone	39
Fig.3.16	A photomicrograph of the Orbitolina bioclastic wackestone.....	39
Fig.3.17	A photomicrograph of the algal bioclastic packstone.....	41
Fig.3.18	A photomicrograph of the algal bioclastic packstone.....	41
Fig.3.19	A photomicrograph of pelecypodal bioclastic packstone.....	42
Fig.3.20	A photomicrograph of pelecypodal bioclastic packstone.....	42
Fig.3.21	A photomicrograph of Orbitalina bioclastic packstone.....	44
Fig.3.22	A photomicrograph of the crystalline limestone.....	44

	Page
Fig.3.23 A photomicrograph of the carbonate dune sand.....	45
Fig.3.24 A photomicrograph of the lithic dune sand.....	45
Fig.3.25 A photomicrograph of the diabasic.....	46
Fig.4.1 X-ray diffraction patterns of Idan chert samples.....	51
Fig.4.2 X-ray diffraction patterns of Al Gail chert samples.....	52
Fig.4.3 X-ray diffraction patterns of Saram chert samples.....	53
Fig.4.4 X-ray diffraction patterns of Saram chert samples.....	54
Fig.4.5 X-ray diffraction patterns of Al Rams chert samples.....	55
Fig.4.6 X-ray diffraction patterns of Idan carbonate samples.....	56
Fig.4.7 X-ray diffraction patterns of Al Gail carbonate samples.....	57
Fig.4.8 X-ray diffraction patterns of Saram carbonate samples.....	58
Fig.4.9 X-ray diffraction patterns of Khor Khowair samples.....	59
Fig.4.10 X-ray diffraction patterns of Idan diabase sheet sample.....	60
Fig.5.1 A binary relationship of Al versus Ti for the studied cherts.....	65
Fig.5.2 Al to metal ration versus Ti in the studied cherts.....	66
Fig.5.3 Fe/Ti versus Al/(Al+Fe+Mn) for the studied cherts.....	66
Fig.5.4 Plot of Ti/100, Zr & Yx3 for the studied chets.....	69
Fig.5.5 Chondrite-normalized REE patterns for the siliceous mudstones....	71
Fig.5.6 Chondrite-normalized REE patterns for the calcareous cherts.....	72
Fig.5.7 Chondrite-normalized REE patterns for the radiolarites.....	73
Fig.5.8 A binary relationship of Total REE versus FeO in the studied cherts	74
Fig.5.9 A binary relationship of Total REE versus Al ₂ O ₃ in the studied cherts.....	74
Fig.5.10 A binary relationship of Total REE versus TiO ₂ in the studied cherts	75
Fig.5.11 A binary relationship of Total REE versus K ₂ O in the studied cherts	75
Fig.5.12 A binary relationship of Total REE versus Zr in the studied cherts	76
Fig.5.13 A binary relationship of Total REE versus SiO ₂ in the studied cherts	76
Fig.5.14 A binary relationship of Total REE versus CaO in the studied cherts	77
Fig.5.15 Dendrogram (R-mode) of major and trace elements.....	82
Fig.5.16 Dendrogram for the studied chert samples using the 14 elements and REE.....	82

	Page
Fig.5.17 Dendrogram (Q-mode) for the studied cherts by using selected major and trace elements.....	85
Fig.5.18 Dendrogram (Q-mode) for the studied cherts by using major oxides.	86
Fig.5.19 Dendrogram (Q-mode) for the studied cherts by using trace elements together with the Tree.....	86
Fig.5.20 The loading of the representative major and trace elements in the chert samples on both factor 1 and factor 2.....	90
Fig.6.1 A panorama looking North of the limestone quarry in Khor Khowair	95
Fig.6.2 A flow chart showing the various stages of cement preparation in the cement plant.....	96
Fig.6.3 A map of the Ras Al Khaimah limestone quarry in Khor Khowair	98
Fig.6.4 A photograph (looking east) of the RRC limestone quarry in Khor Khowair.....	99
Fig.6.5 Close up view (looking east) of the limestone quarry in Khor Khowair showing the extensive thickness (average about 1500 m) of the limestone succession.....	99
Fig.6.6 A photograph (looking North) of the limestone quarry of the Steven Rock Company (SRC).....	101
Fig.6.6 A photograph showing the red banded ribbon cherts in the Idna silica rock quarry of the Ras Al Khaimah Rock Company.....	103

LIST OF TABLES

		Page
Table 4.1	Mineral composition of the chert facies as revealed by X-ray diffractometry.....	48
Table 4.2	Mineral composition of the carbonate facies as revealed by X-ray diffractometry.....	48
Table 4.3A	Mineral composition of the coastal and inland sand dunes (Light Fractions).....	49
Table 4.3B	Mineral composition of the coastal and inland sand dunes (Heavy Fractions).....	49
Table 4.4	Mineral composition of the diabase sheet as revealed by X-ray diffractometry.....	50
Table 5.1	Major and Minor elements composition of the various rock types and sand dunes	62
Table 5.2	Trace and REE Compositions of the various rock types and sand dunes.....	68
Table 5.3	The correlation matrix of major oxides data in the studied cherts.....	79
Table 5.4	The correlation matrix of minor elements data in the studied cherts....	79
Table 5.5	The correlation matrix of major oxides and trace elements in the chert samples from the studied area.....	80
Table 5.6	R-Mode Varimax rotated Factor matrix for the studied chert samples..	89
Table 6.1	Comparison between the chemical compositions of the studied limestones and those used by RAKCC.....	102
Table 6.2	Comparison between the chemical composition of the studied cherts and dune sands and those used by RAKCC.....	105

CHAPTER I

INTRODUCTION

CHAPTER I

INTRODUCTION

CHAPTER I

INTRODUCTION

The northern most part of the United Arab Emirates (U.A.E.) is occupied by the Ras Al-Khaimah (R.A.K) Emirate which has got a reputation for being the greenest of all the emirates. It has the highest amount of rainfall and the highest supplies of groundwater due to its proximity to the Hajar Mountains. Ras Al-Khaimah has enjoyed only a limited success in the oil industry, but it has sufficiently encouraged other industrial activities and investments. One of the Ras Al-Khaimah's major resources is represented by the industrial materials such as limestones from the Hajar Mountains (Northern part of Oman Mountains) at Musandam Peninsula and the siliceous rocks which are exposed in the Hawasina sequence (Northern part of Oman Mountains) at Dibba Zone and Al Rams area. These two types of material are essential for the cement industry. Presently, a limestone and siliceous rock quarries have been opened in the area by the Ras Al-Khaimah Rock Company, and a siliceous rock quarry at Al Rams area has been utilized by the Union Cement Company.

1.1 Geomorphology

The northern part of UAE, which comprises the study area including Khor Khowair, Al Rams, Al Gail and Idan, represents the northern extension of the Oman Mountains chain. The region displays the following geomorphic units (Fig. 1.1):

1.1.1 The Structural Ridge of the Mountain Region

The structural ridge of the mountain region occupies the eastern portion of the area and rises to more than 2000 m (a.s.l) in the northern tip close to Shaam. The major portion

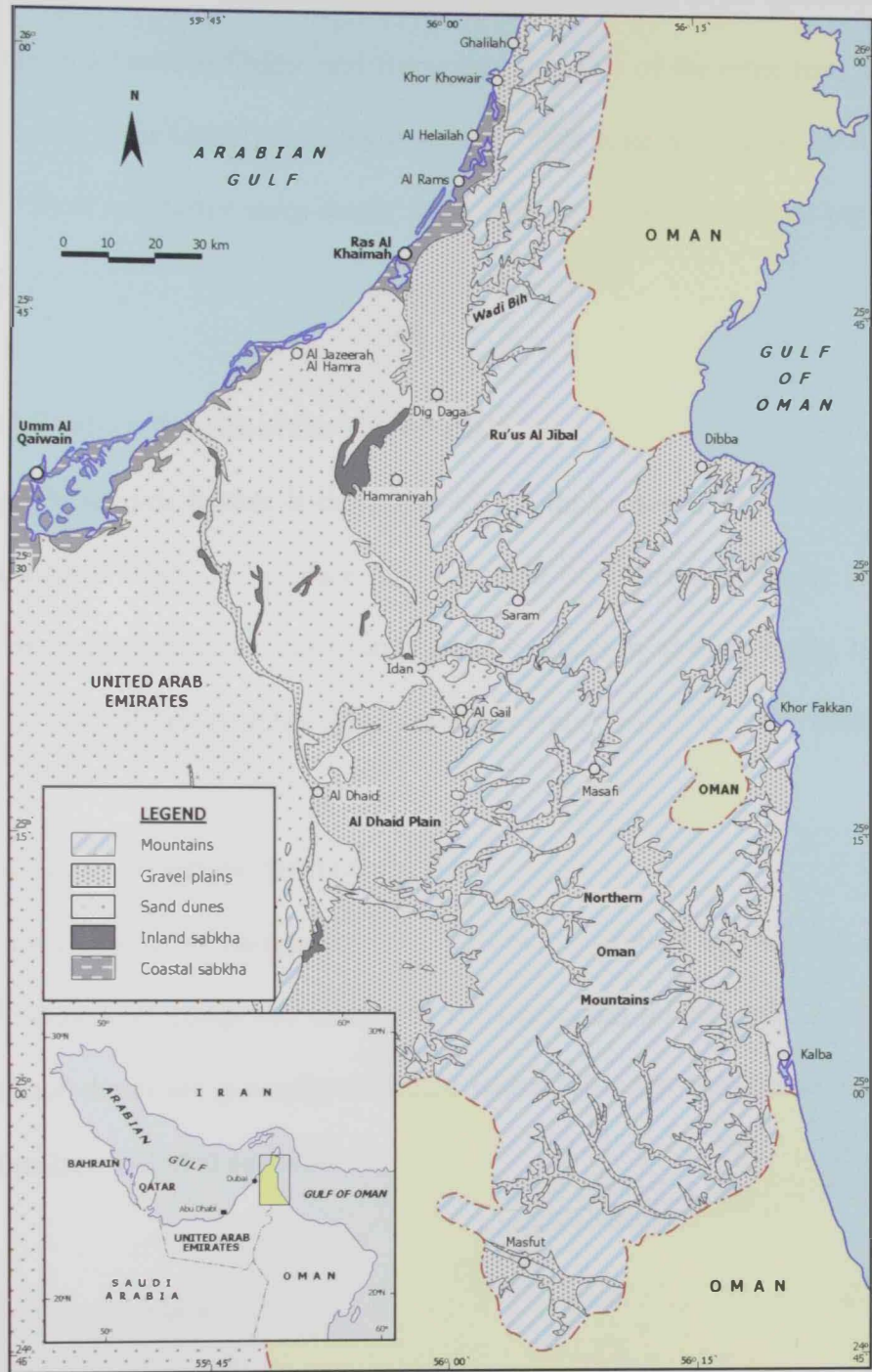


Fig.1.1 Simplified geomorphologic map of the Northern United Arab Emirates showing the location of the study areas (simplified from the UAE National Atlas, 1993).

of the ridge is underlain by carbonate rocks which are dominantly barren with regard to soils and vegetation. Wadi and morphotectonic depressions are filled with ample amounts of downwash deposits which constitute characteristic features of the landscape.

In the area between Shaam and Burayrats, the edge of the ridge rises abruptly from a narrow coastal plain which is missing at Shaam. This edge is prominently dissected by the outlets of short and rather steep wadis which add more to the complex topography of the area.

1.1.2 The Western Bajada of the Gravel Plain

This geomorphic feature is composed of a complex set of alluvial fans along the base of the structural ridge. The surface of the Bajada is underlain either by flattened gravely deposits or mudflat deposits and is, in places, occupied by shifting sands. In the north, the plain is known as Jiri plain which separates the mountain range from the desert foreland.

1.1.3 The Sandy Desert or Structural Plain

This area forms a triangle bounded by coastal sabkhas and the sea in the northern area. The dunes are composed mainly of carbonate and quartz sand. In Ras Al Khaimah area, the sand dunes are generally elongated with a NE - SW orientation and the interdunal depressions have deflated bottoms.

1.1.4 The Coastal Plain

This is the area of tidal flats and sabkhas bordering the Arabian Gulf. In the area near Ras Al Khaimah, littoral erosion may be observed, the coastal flats and cliffs of dune sands form the shoreline.

The land exhibits typical features of arid zone geomorphology with degradation of the major portion of the surface. The area is also arid with regard to vegetation, soil, presence of sand dunes and development of salt encrustations (salinization) in the interdunal depressions locally known as "sabkha". The Wadi Al Bih area lies in the extension of the Oman Mountains chain, consisting of Ru'us Al Jibal mountain range or the structural ridge as defined by IWACO (1986) (Fig.1.2). The remaining areas can be classified as lowlands. The area shows indications of land features designating post wet climatic conditions which were prevailing during the Late Tertiary and, occasionally, the Quaternary.

The structural setting of the carbonate rocks affects the shape of the landscape. Except in the west (thrust fault) and south (Hawasina contact), the dipping of beds generally does not exceed 20 degrees. This contributes to the formation of sub-vertical cuts of the deeply-incised wadis in canyon-like valleys, and to the development of elevated flat areas on gently-sloping beds. Different levels can be distinguished in the flat area on gently-dipping slopes in the proximity of the two major wadis (AL Bih and Naqab) with the elevations: 170-230 m, 500-550 m and 790 - 840 m. Sporadic small-scale agricultural activities exist on these high mountain flats.

The lowlands, especially the alluvial fans, experience an intensive agricultural development. Three distinct fans are present on the western edge of the mountain range, originating from Wadi Al Naqab, Wadi Al Bih and Wadi Galillah. The slope distribution is uniform and the surface gradient is about 0.011. Most of the cultivation is concentrated at the foot of the alluvial cone where the finer outwash materials predominate. Where the alluvial fan changes into gravel plain, the Wadi channel course disappears and the surface becomes irregular. These areas are used for larger-scale agricultural farms and only the lowest parts are left as barren boulder fields (original surface of the gravel plain).

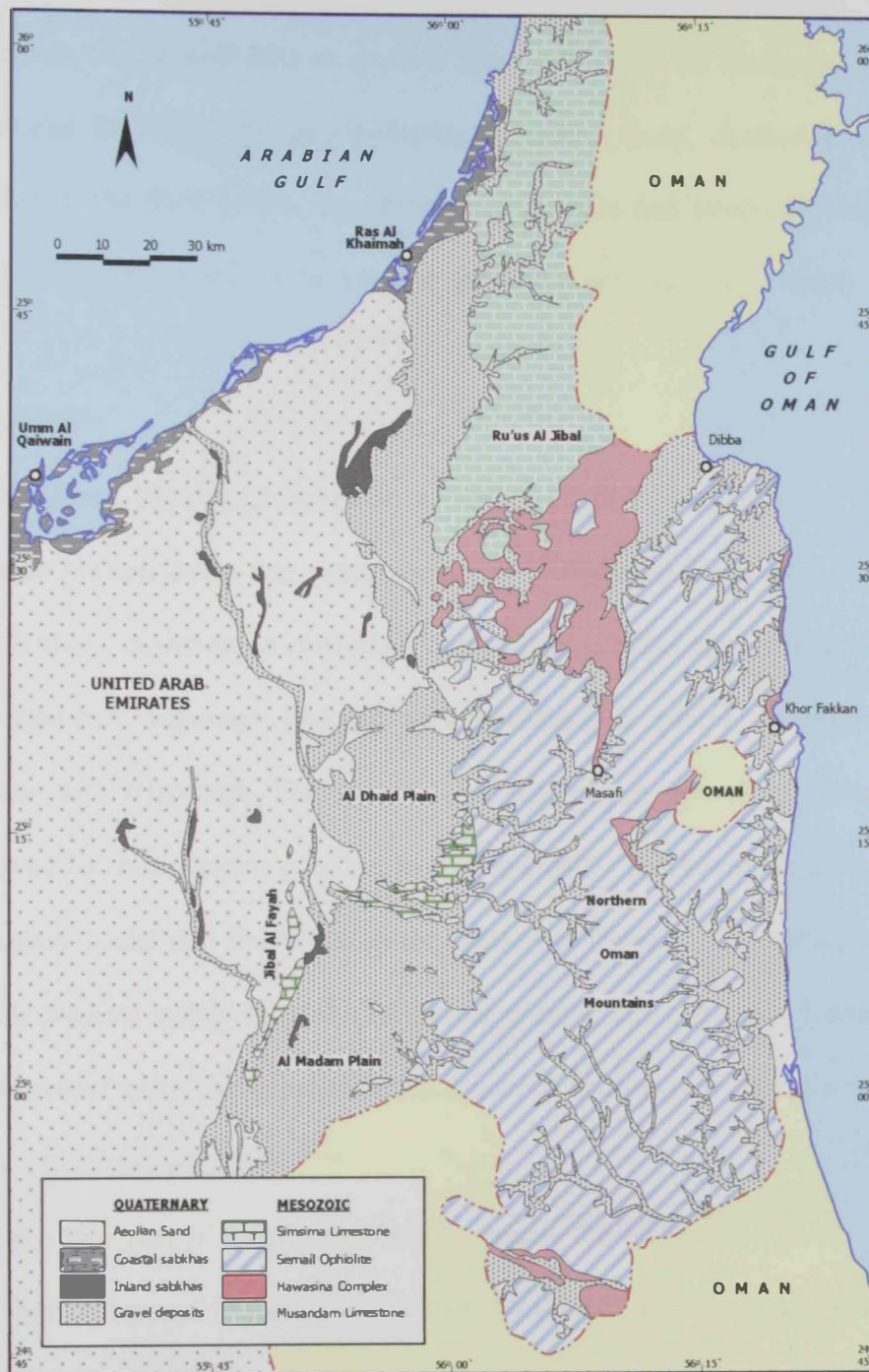


Fig. 1.2 Geologic map of the Northern United Arab Emirates (simplified from the UAE National Atlas, 1993).

Two levels having different stages of incision can be distinguished in the area; both supporting scattered cultivation. The first level is bound to the main wadi channels with direct outlets to the sea (Wadi Shaam, Wadi Al Bih and Wadi Al Naqab). The elevations range between 50 m and 200 m (a.s.l.). The other type of landscape with scattered cultivation can be found on gently-sloping mountain faces, drained by minor wadis. Contributing to the main wadis, they form deep cloughs and steep cliffs separating these two levels. Tiny cultivations can be found as far as 850 m (a.s.l.) (e.g. Hagil).

1.1.5 Mountains

The Oman Mountains comprise a number of different groups of rocks most of which can be broken down into many smaller units (Glennie *et al*, 1974; Glennie, 1995). The present study, however, is concerned only with two major classes of rocks. The first is an autochthonous sequence (formed and remained in place) ranging in age from Precambrian to Cretaceous. The second class comprises two allochthonous sequences (rocks moved to their present position from elsewhere). The lower sequence is composed of sedimentary rocks and is known as the Hawasina Group. It is overlain by the Semail suite which consists mainly of a slab of former oceanic crust. A brief description of these three fundamental units, the autochthonous sequence and the two allochthonous sequences, is given in the following.

The upper part of the Autochthonous unit is the Hajar Supergroup, a sedimentary sequence that is exposed in parts of the Oman Mountains and continues beneath the desert to the south and west. The major part of this sedimentary sequence was deposited on the bottom of shallow seas on the continental shelf or platform that covered much of Arabia between the Mid-or Late Permian period and the Late Cretaceous time.

The allochthonous Hawasina sediments were deposited on the floor of the Neo-Tethys ocean (the Neo-Tethys) which, between about 270 and 70 million years ago, covered the NE of the Arabia. During most of that time span, Arabia (then formed the NE corner of Africa) was moving slowly westwards as the ocean on its eastern margin grew wider. As will be explained shortly, this increase in ocean width resulted from the creation of a new oceanic crust in the middle of the Neo-Tethys (which actually consisted of two parts: Neo-Tethys 1 and Neo-Tethys 2).

Overlying the Hawasina is the other allochthonous unit, the Semail Ophiolite suite. This consists of a thick slab of a former oceanic crust that was created on the floor of Neo-Tethys 2 between about 70 and 105 million years ago. These three groups of rocks are used to lie side-by-side; the Arabian shelf to the west, the newly-created oceanic crust (Semail Ophiolite) to the east, with the Hawasina sediments overlying older oceanic crust in between. Presently, they exist as a thick pile of one stacked sequence on the top of the other. This stacking process began possibly 105 million years before the present, and took about 35 Ma to be completed. The stacking did not create a mountain range, possibly because the autochthonous rocks were held down by the great weight of the overlying Semail ophiolitic sequence, but rather formed a chain of essentially low-relief islands roughly along the site of the present mountains. It was not until 40 Ma later that the Oman Mountains began to be pushed up into a high mountain range. This was about the time when India started to collide with the southern edge of Eurasian (Europe plus Asia) plate to be followed by the creation of a new oceanic area beneath the Red Sea with the separation of Arabia from Africa.

1.1.6 Alluvial Fans

Alluvial fans are significant landforms in the Wadi Al Bih area. They are widespread, having uniform slope distribution and the surface gradient is about 0.011. Where the alluvial fan changes into gravel plain, the course of wadi channel disappears and the surface becomes irregular. Near the wadi mouth, the high resistivities may indicate the presence of basement bedrock at shallow depths.

1.2 Geology and Structural Setting

The Dibba Zone in the Northern Oman Mountains (Fig.1.3) represents a transition between a Late Paleozoic-Mesozoic continental margin and an oceanic basin. This critical area links a continent-ocean boundary to the southeast in the Gulf of Oman to a continent-continent collision zone to the northwest in the Zagros area (Falcon, 1967; Stocklin, 1968 and 1974; White and Ross, 1979).

The Dibba Zone is an elongate, 10 km wide, NE-SW-trending topographic depression between the carbonate successions of the Musandam shelf to the northwest and the Semail Ophiolite to the southeast. The geology of the area of the Dibba Zone has been studied in detail by Robertson *et al.* (1990). Based on this study, the following is a brief description of the main geological characteristics:

The study area of the Dibba Zone forms an oblique-rifted (transitional) segment of the Arabian passive margin (Fig.1.4). Five major thrust units are recognized:

- 1- The Musandam shelf carbonates: a Late Paleozoic-Mesozoic allochthonous carbonate platform unit.
- 2- The Sumeini Group: relatively large, intact thrust sheets of Mesozoic carbonate slope facies.
- 3- The Hawasina Complex: a complicated stack of thrust sheets of Mesozoic deep-water carbonate platform slope, continental rise and abyssal plain sediments.

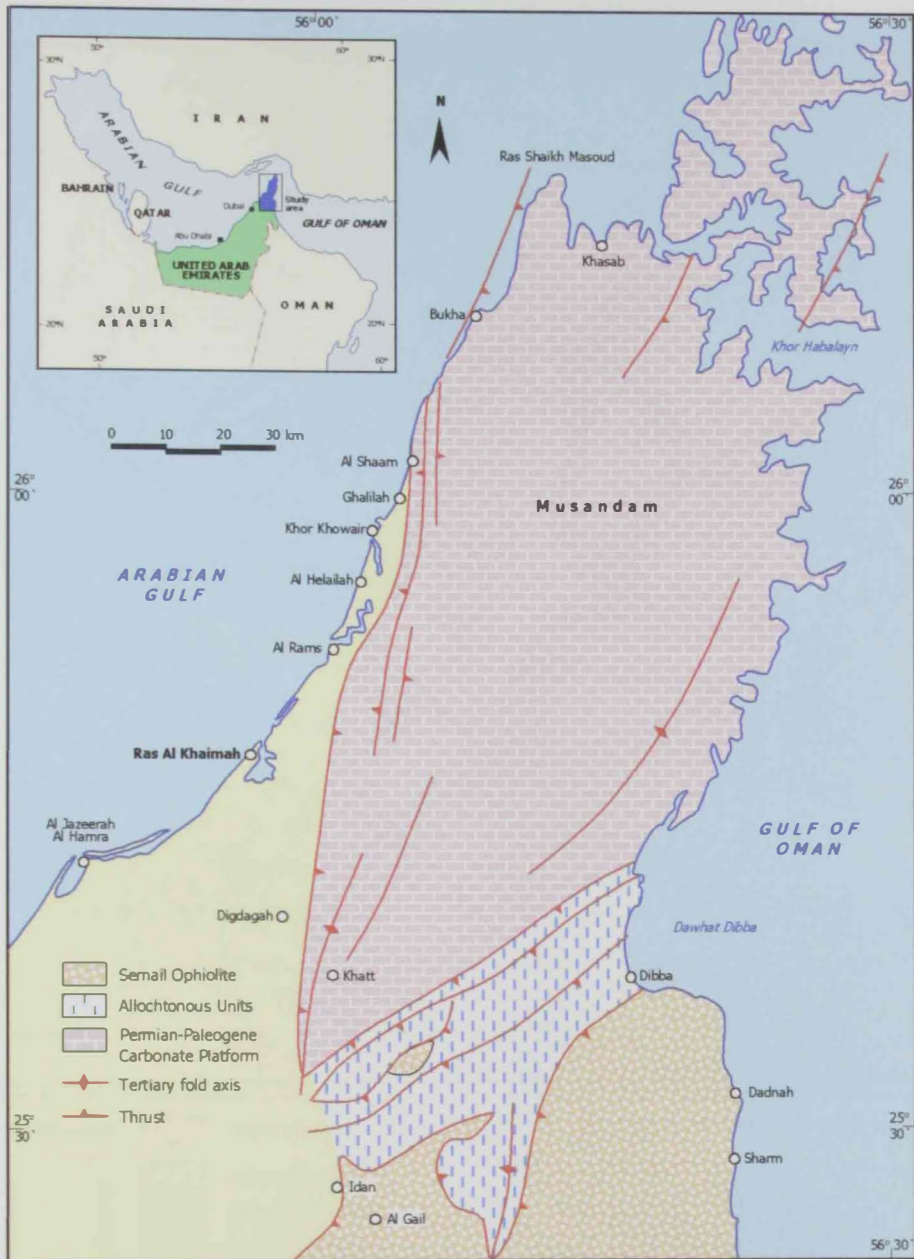


Fig.1.3 Generalized tectonic map of the Northern United Arab Emirates (modified after Harland *et al.*, 1982).

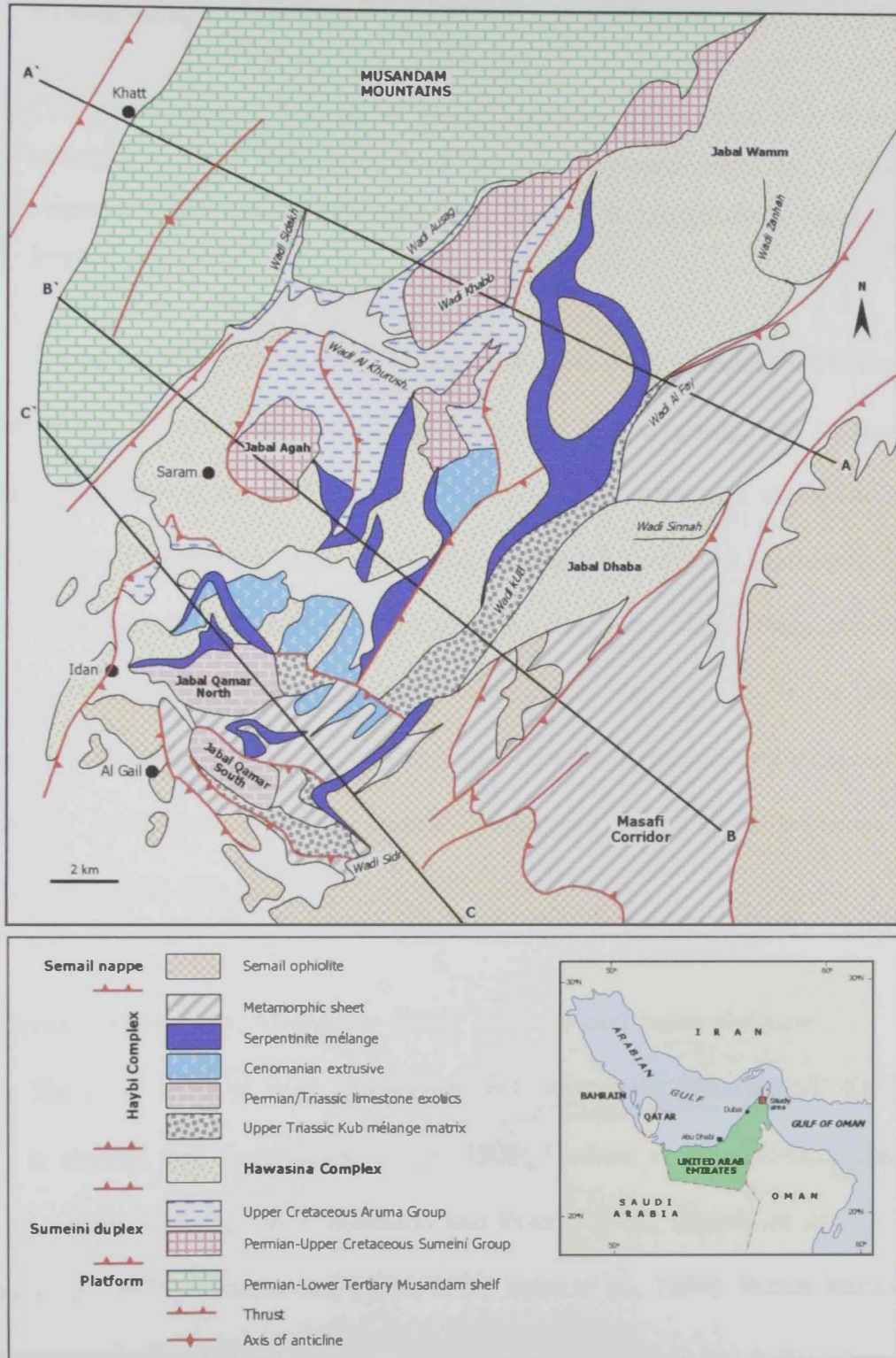


Fig.1.4 Geologic map of the Dibba Zone (modified after Harland *et al.*, 1982).

- 4- The Haybi Complex: comprising sedimentary and tectonic mélange, up to mountain-sized limestone units ('olistoliths' or Oman Exotics), alkaline and tholeiitic volcanics, and greenschist - and amphibolite - facies metamorphic rocks forming the sole of the Semail Ophiolite (Searle and Malpas, 1980 and 1982).
- 5- The overriding Late Cretaceous Semail Ophiolite thrust sheet. The thrust stack is assumed to have been assembled by continentward-migrating thrusting, with originally more distal (outboard) units located at progressively higher structural levels.

During the mid-Tertiary time, 3.5 km thick sheet of Musandam shelf carbonate was thrust about 15 km westwards along the Hagab thrust giving rise to huge domal culminations (Searle *et al.*, 1983; Searle, 1988 b) (Fig.1.3). Along the southeastern edge of the Musandam Peninsula, a major culmination apparently collapsed southeastwards along an important normal fault, explaining the presence of a large Semail Ophiolite slice down in the structural stacking order in the north of the study area (Fig.1.4). In the Dibba Zone, deformation of assumed mid Tertiary age gave rise to large, asymmetrical, west-facing 'whaleback' folds, accompanied by reverse faulting and limited out-of-sequence thrusting (Searle *et al.*, 1983) (Fig.1.5).

1.2.1 Hajar Supergroup: Mesozoic – Early Tertiary carbonate platform

The a. c. 3500 m thick Musandam shelf succession from Ras Al Khaimah and Oman is already well documented (Lees, 1928; Hudson *et al.*, 1954a,b; Hudson and Chatton, 1959; Hudson, 1960; Allemann and Peters, 1972; Glennie *et al.*, 1973, 1974; Biehler *et al.*, 1975; Ricateau and Riche, 1980; Rabu *et al.*, 1990). Salient features can be briefly summarized as follows:

The mainly dolomitic Permian and Triassic platform sediments (Bih, Hagil and Milaha Fms.) consist of shallowing upwards intertidal to supratidal cycles that pass

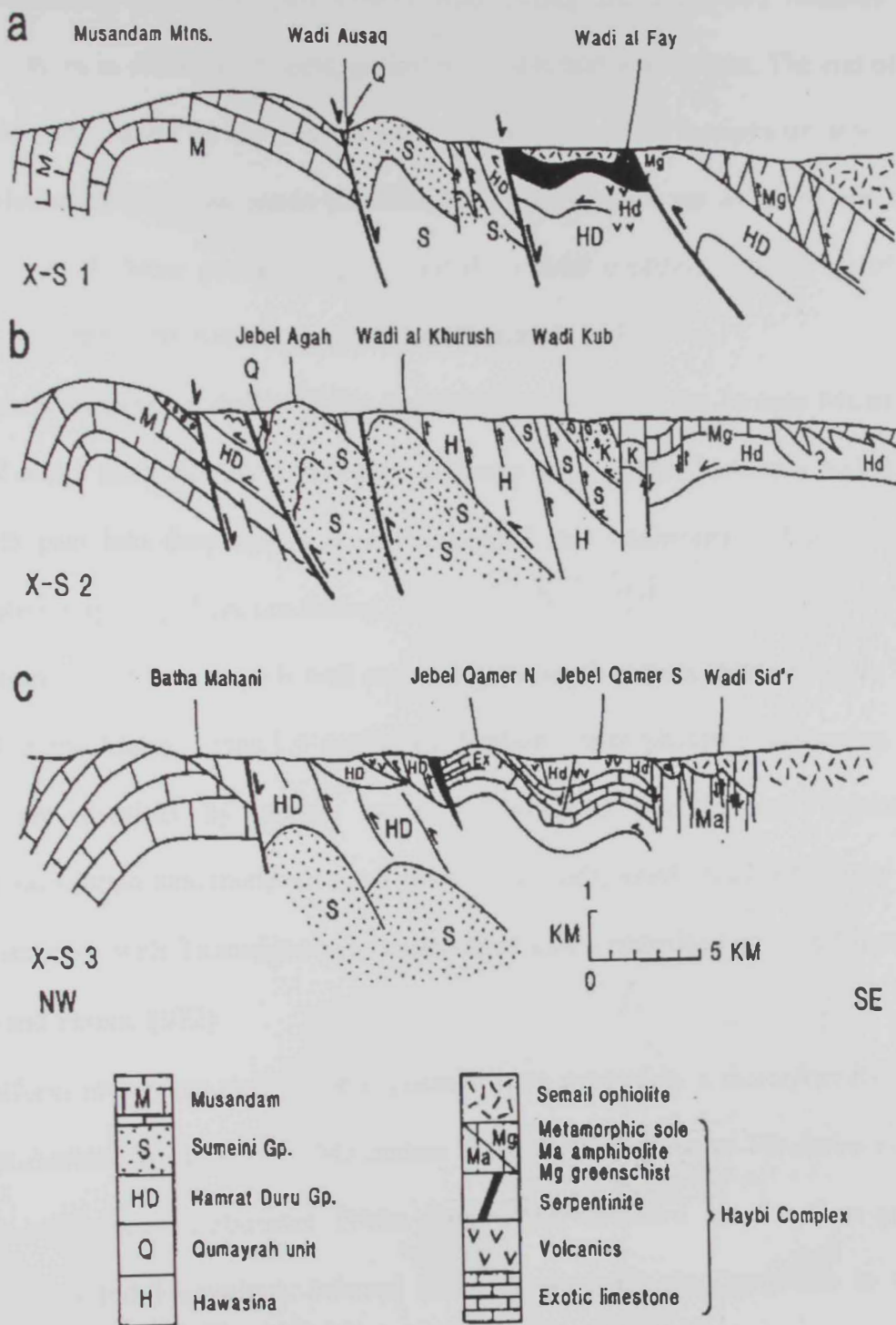


Fig.1.5 Sections across the Dibba Zone (simplified from the sections of Searle, 1988).

laterally towards the shelf edge into higher-energy facies. In the Late Triassic, fore-reef talus conglomerates were developed around Wadi Ausag and comprised boulders and blocks up to 40 m in diameter of coral, grainstone, oolite and wackestone. The end of the Triassic time was marked by the emergence of the platform, with ferruginous deposition and progradation of quartzose sands (Ghalilah Fm.) towards, but not as far as, the shelf edge. The controls were probably uplift related to final continental break-up of the Gondwana, combined with eustatic sea-level fall (Vail *et al.*, 1977).

Re-establishment of shallow-water conditions gave rise to the Jurassic Musandam Group 1, 2 and 3 carbonate platform cycles (Glennie *et al.*, 1974; Richateau and Riche, 1980) which pass into deep open-marine thin-bedded lime mudstones of Late Jurassic-Early Cretaceous age (e.g. Miaolica facies).

The upper platform slope is well exposed in the northwestern Dibba Zone, in Wadi Ausag and Batha Mahani (Figs.1.4 and 1.5a). Shallow water platform carbonates, with Kornubia, are overlain by deeper water, well-bedded porcellaneous calpionellid limestones, radiolarian lime mudstones and red to pink marls, interbedded with slump beds and conglomerates with Tithonian-to Berriasian-aged clasts embedded in a muddy matrix (Allemann and Peters, 1972).

Platform emergence and/or non-deposition were marked by a disconformity at the base of the Arabian Wasia Group (Musandam Cycle 4). Transgressive lithofacies initially comprised argillaceous carbonates (Nahr Umr Fm.), followed by the finer-grained sediments (Mauddud Formation). Inferred shallowing-upwards then gave rise to mixed terrigenous and carbonate sequences of mid-Albian to Cenomanian age (Natih Formation) (Hughes Clarke, 1988).

Flexural upwarping associated with the beginning of the Ophiolite obduction episode (Robertson, 1987) resulted in the erosion of up to 600 m of the shelf edge and the

upper slope succession, down to the Albian horizons in the Batha Mahani and Wadi Ausag areas. As the Semail ophiolite overthrust the platform margin, inner-shelf areas further northwest were loaded and subsided giving rise to a foreland basin in which ophiolite-derived sediments (Guweyza Fm.) accumulated rapidly (Glennie *et al.*, 1974; Patton and O'Connor, 1988). Final overthrusting of the Semail ophiolite took place in Late Campanian – Early Maastrichtian time. However, there is little evidence that the Ophiolite moved far over the Musandam shelf. The most far traveled Hawasina sediments, still preserved, are exposed in the Hagil window and as two very small klippen in the central Musandam Mountains (Biehler *et al.*, 1975).

Following emplacement of the Semail ophiolite, a carbonate shelf was re-established, as the Paleocene-Eocene Pabdeh Group and the Oligocene Asmari Formation (Fig.1.6). Regional compression during the Late Oligocene – Miocene time was related to collision in the Zagros area (Searle 1988b) and the Musandam platform underwent large-scale folding, while the higher levels of the succession were thrust at least 15 km to the west along the Hagab thrust, associated with the development of a foreland basin succession (Pabdeh basin) to the west.

1.2.2 Sumeini Group: carbonate slope deposition

Jurassic and Cretaceous carbonate slope facies (Sumeini Group) are well exposed in the Dibba Zone (Figs.1.3 to 1.6). The Jurassic succession in the north (Wadi Khabb) is dominated by about 700 m of dark gray to black, decimeter-bedded, unburrowed lime mudstone and minor grainstone that contain calcified radiolarians, rare crinoids and small shell fragments, but are otherwise mainly unfossiliferous (a Member of Mayhah Fm.; Glennie *et al.*, 1974). Slump scars are common. They are up to 30 m long to 5 m deep. Submarine slopes were for a long period steep and unstable. The Jurassic-mid Cretaceous

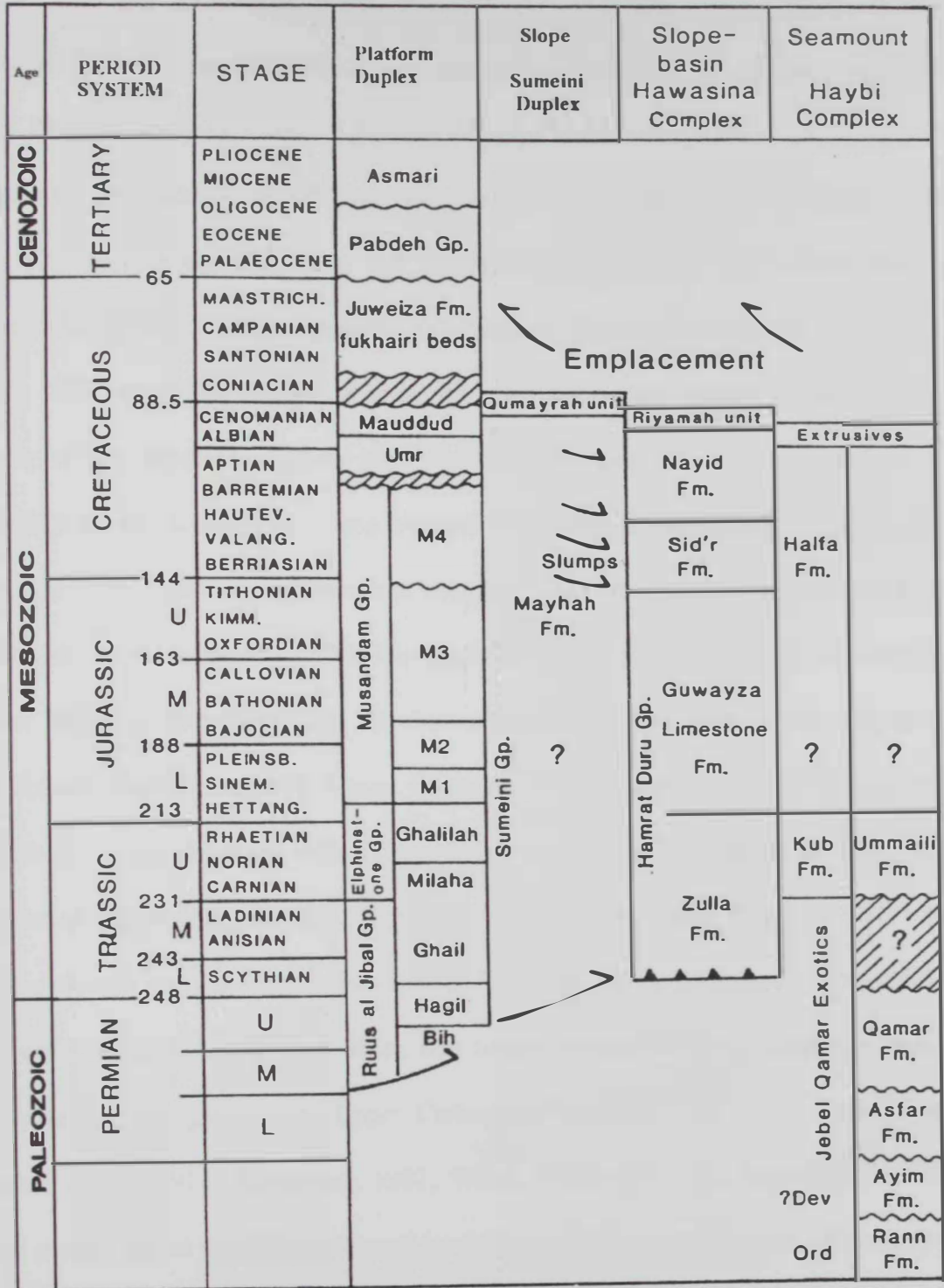


Fig.1.6 Stratigraphy of the Dibba Zone.(Time scale after Harland et al., 1982).

limestones represent Bahama-type periplatform ooze. The succession in the Dibba Zone then passes upwards into 100-300 m of limestone-conglomerates and slumps, followed in turn by shale and thin-bedded limestone of the Qumayrah unit (Muti Formation). Further south, similar limestone debris flows are exposed in the Jabal Agah window (Figs. 1.34 and 1.5b). Platform lime mudstones of Jurassic – Early Cretaceous age there are transgressively overlain by thin-bedded micritic limestone, with planktonic foraminifers of Early Albian to Early Cenomanian age (Allemann and Peters, 1972). Overlying thin-bedded deep-water limestones, marls and conglomerates are dated as Santonian-Coniacian (Allemann and Peters, 1972) to probably Early Campanian. The succession records collapse and mass-wasting of the upper parts of the carbonate slope in early Late Cretaceous time, and is equivalent to the C Member of the Mayhah Formation in the Sumeini area (Watts and Garrison, 1986). Similar fault-bounded conglomerates of Aptian-Albian age exist below the Hagab thrust in the Hagil Window (Lakshaifa Fm. of Hudson *et al.*, 1945b). Other smaller bodies of Sumeini Group, like the carbonates south of Wadi Al Khurush (Figs. 1.4 & 1.5b) are interbedded with Upper Cretaceous syntectonic radiolarian facies, and are equivalent to the Riyamah unit of the Muti Formation. The stratigraphically highest redeposited carbonates (slumps and debris flows) of the Upper Cretaceous part of the Sumeini Group are disconformably overlain by up to 300 m of sheared imbricated, non-calcareous brown mudstone and shale, thin-bedded calciturbidites and minor rudites, that are collectively assigned to the Upper Cretaceous Qumayrah unit of the Muti Formation (Glennie *et al.*, 1974; Robertson, 1987; Watts, 1990) (Fig. 1.5). The Qumayrah unit is folded around thrust culminations cored by the Sumeini Group (e.g. north of Tawiyayn and southwest of Jabal Agah) and is also sandwiched between these thrust sheets and the overlying carbonates of the Musandam shelf (e.g. Wadi Ausag – Wadi Khabb) (Figs. 1.4 & 1.5a). The Qumayrah units are attributed to flexural downward and collapse of the edge of

the carbonate platform to form a foredeep that was developed prior to overthrusting (Robertson, 1987).

1.2.3 Hawasina Complex: deep-water passive margin sediments

Mesozoic deep-water successions of the Hawasina Complex are exposed in generally structurally higher thrust sheets. The sedimentary structures in all the successions are consistent with deposition from high – to low - density turbidity currents (cf. Bouma, 1962; Hiscott and Middleton, 1979; Lowe, 1982), superimposed on a ‘background’ input of hemipelagic mud, fine-grained carbonate and true pelagic sediments that are mainly radiolarian. In the tectonostratigraphic scheme of Glennie *et al.* (1973, 1974), only a small outcrop of the Hamrat Dura Group was identified in Batha Mahani (Fig.1.5). Other successions were assigned by Glennie *et al.* (1974) to the structurally lower and coarser-grained Dibba Formation, and to the higher and more distal calcareous Dhera Formation and the siliceous Shamal Formation. Cooper (1986, 1987) made the minimum necessary changes to bring the stratigraphy into line with international usage (Hedberg, 1976; Holland *et al.*, 1978) (Fig.1.6) and the terms Dhera, Dibba and Shamal Formations are now abandoned. In the Dibba Zone, deep-water platform-derived sediments are placed in the Hamrat Dura Group and comprise the Late Permian to Late Triassic Zulla Formation (mainly shale and limestone), the Late Triassic to mid Jurassic Guweyza Limestone (revised name) (mainly redeposited limestone), the Late Jurassic – Early Cretaceous (Tithonian – Barremian) Sid’r Formation (mainly chert) and the Albian – Cenomanian Nayid Formation (mainly redeposited limestone). The Guweyza Sandstone (Late Triassic) is not recognized in this area.

1.2.4 Triassic Zulla Formation: starved base of slope

In the central and northern Oman Mountains, the Zulla Formation is widely exposed and comprises mostly shale and muddy limestone (e.g. in the Hawasina window; Glennie *et al.*, 1974; Graham, 1980; Cooper, 1990). In the Dibba Zone, local recognition of the Zulla Formation (Figs.1.5 and 1.6) is based on limited age data and lithological correlation.

In the southwest at Batha Mahani, a succession of shale passes upward into thin – to medium-bedded calcilutite, silicified limestone and oolitic calcarenite containing curved, thin-shelled pelagic bivalve fragments. Nodular silicification is ubiquitous. Radiolarians from red cherts immediately indicate Late Norian to Hettangian age. Three kilometers north of the village of Idan, a poorly-exposed succession comprises ‘exotic’ limestone conglomerates, weathered volcanics, shale and thin calcarenite (Hawasina unit 2 of Searle *et al.*, 1980).

The Zulla Formation comprises shallow water carbonate sediments derived from the Musandam shelf, particularly oolitic that were redeposited down a steep escarpment margin and accumulated as small clastic wedges. Slope areas (e.g. Yamahah) were largely by-passed. The newly-rifted slope was unstable and repeatedly slumped, giving rise to intraformational platy-limestone breccias. Widespread tectonic instability during the Late Triassic triggered the development of lenticular conglomerates composed of reef edge-derived materials. Fine-grained terrigenous background sediments accumulated under oxidizing conditions. Base of slope areas remained volcanically active. Slope like unit was covered by a wedge of finer-grained sediments, similar to those of the Hamrat Dura Group in the Hatta Zone; c. 60 km to the south (Robertson *et al.*, 1990).

1.2.5 Late Triassic – Jurassic Guweyza Formation: redeposited deep-sea carbonate

Time – equivalent sediments of the Early Jurassic Guweyza Formation that are

exposed elsewhere in the Oman Mountains are represented in the Dibba Zone by redeposited oolitic limestones.

In Batha Mahani, a small outcrop, previously mapped as the Hamrat Dura Group (Glennie *et al.*, 1974), comprises decimeter-to metre-bedded oolitic calcarenite that is inter-bedded with red shale, mainly low in the succession. There, the Zulla Formation is locally conformably overlain by intact sequences comprising 25 m of silicified limestone, chert and shale, that pass upwards into 10 m of decimeter-bedded oolitic limestone, with inter-bedded green shale.

At Idan, the Guweyza Formation comprises 33 m of centimeter-bedded, fine-grained, rippled calcarenite. Each bed passes into structureless, chalky weather wackestones in which chert nodules are preferentially concentrated in the finer-grained fractions.

Throughout the Dibba Zone, the Guweyza Formation is capped by a conglomeratic horizon, except locally in the north in the Yamahah section where there is a rapid transition to silicified limestone and cherts of the Sid'r Formation. The dominance of green shale and cherts in deeper water, basinal areas (e.g. Batha Mahani) suggests that diagenetic conditions were mainly reducing; more oxidizing settings were more apparent in rise continental areas.

The conglomerates record extensional faulting, collapse of the platform edge and erosion of the submerged basement outcrops. The abundance of conglomerates contrasts with equivalent stratigraphic levels further south in the central mountains, as in the Hawasina window and the Hamrat Dura (Cooper, 1990). This indicates that the Dibba Zone was particularly tectonically active throughout most of the Mesozoic time.

1.2.6 Late Jurassic – Early Cretaceous Sid'r Formation: siliceous deposition

The Sid'r Formation is dominated by distinctive red radiolarites of Late Jurassic (Tithonian) to Early Cretaceous (Late Valanginian) age. In the northern Oman Mountains,

the formation is subdivided into a lower calcareous unit and an upper shale unit (Cooper, 1986, 1990).

Successions at Jabal Wamm and Jabal Dhera start with silicified radiolarian wackestone and interbedded shale. Tithonian radiolarian cherts and lenticular pebbly conglomerates are augmented at Jabal Wamm by pink slump-folded radiolarian wackestone. Five measurements of fold facing direction indicate south-directed transport. A massive, up to 8 m thick limestone conglomerate is also regionally developed towards the middle of the formation, and defines a gradational boundary with more shale-rich successions in the upper part of the Sid'r Formation. In this part, the abundance of coarse- and fine-grained carbonate and radiolarian chert is reduced.

In Batha Mahani, the base of the Sid'r Formation (Unit 2 of Searle *et al.*, 1983) comprises a 1-2 m thick interval of recessive-weathering shales, silicified marls and red and green radiolarian cherts, passing upwards into 35 m of variably silicified radiolarian wackestones and marls, with thin laminae of red chert. Pebbly conglomerates, 5-10 cm thick, are distinctly lenticular over 10-30 m laterally. Upwards, white-weathering, cliff-forming, medium-bedded silicified limestones contain abundant replacement dolomite. They are then overlain by 3 m of relatively unsilicified, coarse-grained, 30 cm thick beds of graded calcarenites, with granule-grade bases. The succession finally passes into a 5-15 m thick interval of recessive-weathering, brick red radiolarian cherts and shale. Near Idan, the Sid'r Formation is composed almost entirely of 2-10 cm-bedded, variably silicified, graded radiolarian wackestones (Fig.1.6). Parallel-laminated and/or rippled-bed bases are common. Replacement chert accounts for 50-90 % of the bed thickness. Shale is almost completely absent or restricted to thin laminae

The Sid'r Formation records a combination of enhanced radiolarian productivity, raised sea-level (Vail *et al.*, 1977; Ager, 1981) and/or a raised CCD. Associated tectonic

subsidence and faulting gave rise to the numerous platform-derived rudaceous intercalations. Drawing of the platform in the Late Jurassic – Early Cretaceous time then greatly reduced carbonate input to the basin.

Conglomerates at the top of the lower unit record increased subsidence of the margin; carbonate largely ceased to be transported into the basin and fine-grained turbidities were restricted to the base of the slope. ‘Background’ shale deposition then dominated and red cherts accumulated from radiolarian fall-out (upper unit) in areas shielded from shale accumulation. Much of the chert was formed diagenetically through the dissolution of radiolarian tests and the replacement of the fine-grained and thin – bedded calcareous sediments by silica.

1.2.7 Structurally higher Hawasina units

Several large slices of Hawasina sedimentary rocks are located high in the structural stack between outcrops of the Haybi Complex to the west and the Semail Ophiolite and its metamorphic sole to the east (Figs.1.4 and 1.5b). Proximal base of slope facies includes shelf-derived conglomerate and reef limestone blocks up to 10 m in size. These are unlikely to be distal units formed far from the Arabian continent, but probably came to be in their present high structural position as a result of complex ‘out-of-sequence’ thrusting (i.e. with proximal over distal units) (Searle, 1985; Bernoulli and Weissert, 1987; Cooper, 1988; Barrette and Calon, 1987). Alternatively, these units were initially emplaced ‘in sequence’, but were later downthrown by normal faults located along the northwestern side of the Musandam shelf succession (Searle, 1988a) (Fig.1.5a).

In the Jabal Dhaba area, the inferred out-of-sequence unit is sandwiched between outcrops of *mélange* (Kub *Mélange*, see below) and the Semail nappe and its metamorphic sole (Fig.1.3). Lithofacies are shared and disrupted (i.e. as broken formation) (Fig.1.6), and

comprised of shale, radiolarites, thin-bedded lime mudstone, turbiditic calcarenite, channelized calcirudite and scattered, meter-sized detached blocks of reefal limestone. The lithologies can be correlated with all four formations of the Hamrat Dura Group (Zulla, Guweyza Limestone, Sid'r and Nayid). Diabase sills are quite numerous. At the extreme southern end of this thrust-bounded unit (Fig.1.6), extensively-deformed successions of calciturbidites in beds up to 0.25 m thick are interbedded with ribbon chert that contains radiolarians of mid-Triassic (Late Ladinian) to Late Triassic (Carnian) age.

Northeast of Wadi Kub (Figs.1.4 to 1.6), another major duplex is mainly composed of radiolarian chert of the Sid'r Formation (Shamal Chert of Glennie *et al.*, 1974). This is sandwiched between volcanics of the Haybi Complex, sheared serpentinite below, and broken formation of the Hawasina Complex above. In detail, this unit comprises tightly-imbricate ribbon radiolarian chert, subordinate shale and relatively rare, thin-to medium-bedded silicified calciturbidites, with Calpionellids (Glennie *et al.*, 1974). In the north near Wadi al Khurush (Fig.1.4 and 1.5b), the Shamal Chert locally passes into redeposited limestone typical of the Nayid Formation elsewhere.

The Sid'r Formation as exposed north of Wadi Kub (Shamal Chert) is structurally overlain by an elongate, about 500-1000 m, thrust-bounded outcrop comprising a broken formation. This includes a part of the 'sedimentary mélange' outcrop mapped by Lippard *et al.* (1982). It is made up of lenticular slices of Hawasina rocks up to 3 km long by 0.5 km wide. These are often bounded by thin stands of steeply-inclined, sheared serpentinite that increase in number and thickness northwards. Local sedimentary successions up to 60 m thick comprise bioclast-rich calciturbidites, with rare calcirudite beds up to 0.3 m thick, containing clasts up to 0.3 m in size, and short intervals of ribbon radiolarites.

1.2.8 Haybi Complex: more outboard units

Throughout the Oman Mountains, the Haybi Complex as a whole is very heterogeneous in age, structure and lithology (cf. Searle and Malpas, 1980, 1982; Searle *et al.*, 1980; Searle and Graham, 1982; Lippard and Rex, 1982; Bechennec *et al.*, 1990).

In the Dibba Zone (Fig.1.6), however, notable differences exist. First, in some places, extrusives of the Haybi Complex are thrust between deep - sea sediments of the Hawasina Complex and the metamorphic sole of the Semail Ophiolite. Elsewhere, the Haybi Complex is generally located at the highest structural level below the metamorphic sole. Second, available dates on the extrusives are all Late Cretaceous, rather than Permian or Late Triassic, as in most other areas. Third, the Permian and Late Triassic limestones of the Oman Exotics in the Dibba Zone (at Jabal Qamar) are underlain by Ordovician to Permian successions; elsewhere Late Triassic extrusives are exposed. Fourthly, the Oman Exotics are associated with a distinctively sheared sedimentary *mélange* that has not so far been reported from other areas and is here termed the Khabb *Mélange*.

1.2.9 Ayam Formation: condensed shelf deposition

The base of the conformably overlying Ayam Formation is a 0.15 m thick, Fe, Mn-rich phosphatic pavement comprised of bone material, fish teeth, broken fish scales, preferentially-orientated *Orthocones* and well-rounded, honey-colored quartz grains in a siltstone matrix. Scattered, well-rounded phosphatic lumps contain terrigenous silt. The pavement is overlain by up to 5 m of finely-laminated, thinly-bedded brown shale, argillaceous calcilutite and calcareous siltstone.

The succession passes upwards into rubbly, stylolitic concretionary limestone, with biocalstic limestone lenses up to 0.25 m thick. There is then a 3 m thick distinctive horizon of fine-grained nodular limestone with manganese crusts and nodules up to 0.2 m

in diameter. The manganese occurs in an argillaceous lime-mud matrix, with numerous large burrows, that are mainly orientated parallel to bedding. The formation terminates with up to 3.5 m of brick-red argillaceous micritic limestone and hematitic shale with numerous randomly-orientated *Orthocones*. The Ayam Formation presently can be constrained only between the Ordovician and Early Permian. A Devonian age is possible as the formation, particularly the pelagic limestone and manganese nodules, resembles the Devonian Griotte and Cephalopodenkalk of the Western European Vatican (Tucker, 1974).

1.3 Aim of the Study

The present study deals with the Jurassic to Upper Cretaceous limestones and siliceous rocks exposed in the northern part of the United Arab Emirates at Ras Al Khaimah Emirate. It aims at: (i) determining the petrographic and mineral characteristics of these rocks; (ii) investigating their geochemical attributes; and (iii) assessing their suitability as raw materials for the cement industry in the Emirate.

CHAPTER II

MATERIALS AND METHODS
OF STUDY

CHAPTER II

MATERIALS AND METHODS OF STUDY

2.1 Materials

The materials used in the present study include 21 chert samples collected from the Hawasina succession in the silica quarries at Idan of the Ras Al-Khaimah Rock Company (RRC) and at Al Rams of the Union Cement Company (UCC), together with the exposures at Al Gail and Saram (Fig.2.1). In addition, 15 limestone samples were collected from the different stratigraphic levels in the Khor Khowair limestone quarry of the Ras Al-Khaimah Rock Company.

In order to evaluate the economic potential of dune sands as a source of silica in the cement industry, samples have been collected from the inland and coastal dunes at Al Gail and Al Helailah; respectively. Also, a diabase sheet structurally interbedded with the chert in the Hawasina succession has been sampled.

2.2 Methods of study

A total of 37 thin sections were prepared from the various lithologies were microscopically examined. Out of these, 36 thin sections represent the chert and carbonate rocks and one was prepared from a sample collected from the diabase sheet. In addition, three grain-mounts were prepared from the dune sands, one represents the dunes which lie close to ophiolite exposures and two from those close to carbonate exposures.

Powder samples have been prepared for the X-Ray diffraction analysis. The original sample was first crushed using a jaw crusher. The sample was then ground using

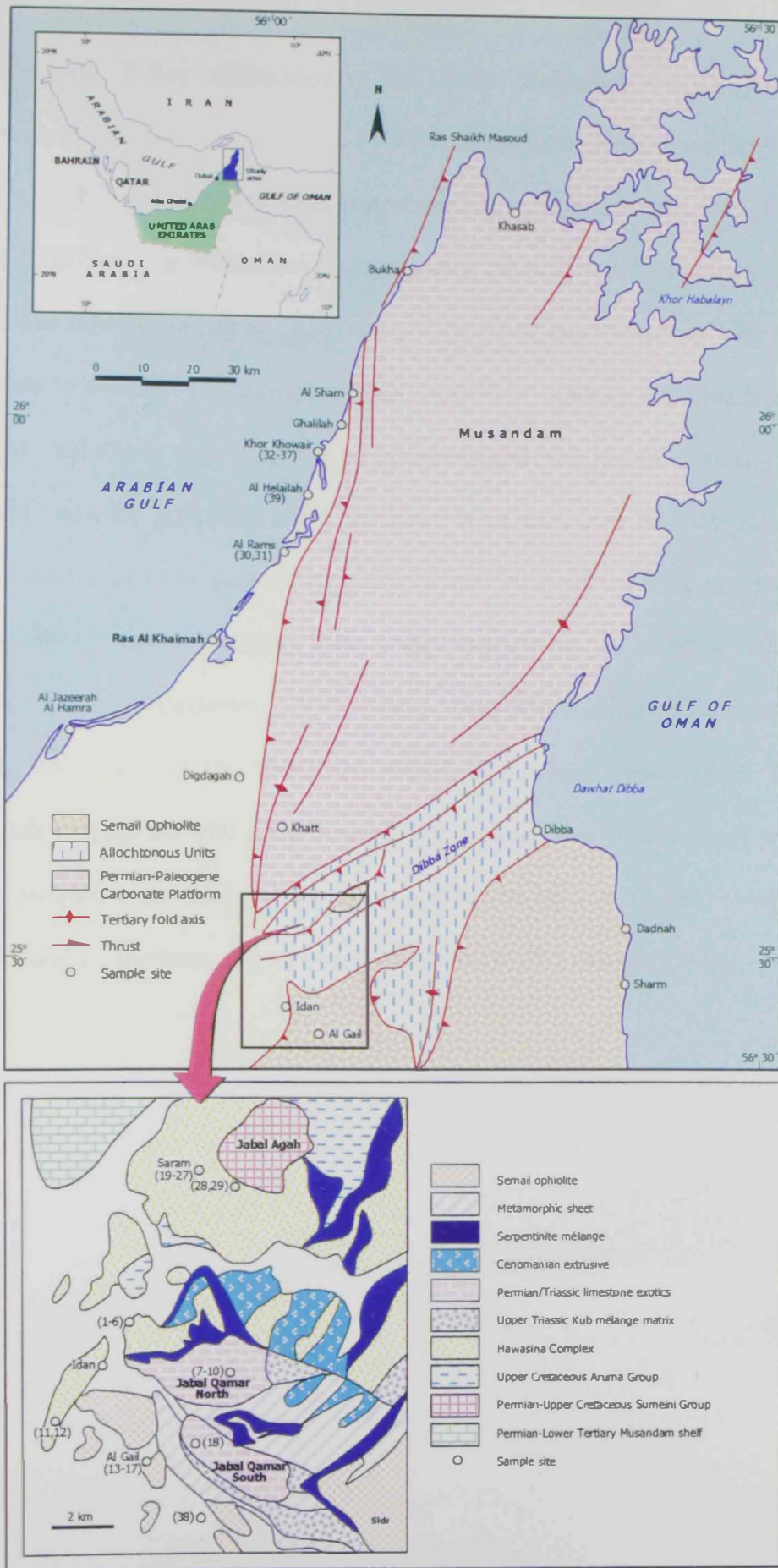


Fig.2.1 Geologic map showing the sample locations.

oscillatory mill. X-Ray diffractometry has been conducted on all the 37 samples representing the various rock types. A Phillips X-Ray diffractometer model PW/1840 with Ni-filter, Cu - K α radiation was used. Instrument settings were 40 kV, 30 mA and scanning speed of 0.05 $^{\circ}$ /sec. The diffraction peaks between $2\theta = 2^{\circ} - 60^{\circ}$ were recorded. Their d-spacings and relative intensities (I/I $_0$) were determined and compared with the published ASTM data to identify the existing minerals. In addition samples collected from the coastal and inland sand dunes were subjected to heavy-mineral analysis using bromoform (sp.g. = 2.87). The obtained light and heavy fractions were examined microscopically and their mineral constituents were quantitatively determined by point-counting of about 300 grains in each slide. Chemical analyses were conducted on the 36 samples representing the various sedimentary lithologies. Chert samples were prepared for the analysis by grinding weighting 250 grams of the clean, non-veined, non-stained, fresh sample in a tungsten carbide mill to pass the 200 mesh screen. The powder was homogenized and split. The obtained samples were analyzed for the major oxides by LiBO fusion using the ICP-ES technique, and for the trace and rare earth elements (REEs) using ICP-MS.

CHAPTER III

PETROGRAPHY

CHAPTER III

PETROGRAPHY

Petrographic examination of thin sections and grain mounts prepared from the sedimentary rocks and dune sands in the study area permitted the recognition of two main facies; namely: the chert facies and the carbonate facies. Based on their composition, each of these facies could be subdivided into a number of subfacies.

3.1 The Chert Facies:

The chert facies exists in almost all the exposures of the study area (Al Rams, Al Gail, Saram, and Idan) except for Khor Khowair. Based on composition and physical appearance of the rocks, the following subfacies could be delineated:

3.1.1 Ferruginous Radiolarian Ribbon Chert:

This subfacies was recognized at Al Rams, Idan and Al Gail, while was not recorded in Saram. The rock is composed of well-sorted, closely-packed radiolarian tests which are filled or replaced with chalcedonic silica that occasionally obliterated their morphological features (Fig.3.1). The radiolarian tests are embedded in a microquartz groundmass that is impregnated with iron oxides (mostly hematite). The latter also fill hair-like fractures (Fig.3.2), whereas larger fractures are partially or completely plugged with meso-to coarse-crystalline interlocked quartz and minor calcite crystals (Fig.3.3).

3.1.2 Carbonaceous Radiolarian Ribbon Chert:

This subfacies was recorded in the localities: Idan, Al Gail and Saram while is absent at Al Rams. The rock is composed of a microquartz groundmass in which are embedded closely-packed, poorly-preserved radiolarian tests and minor diatoms and

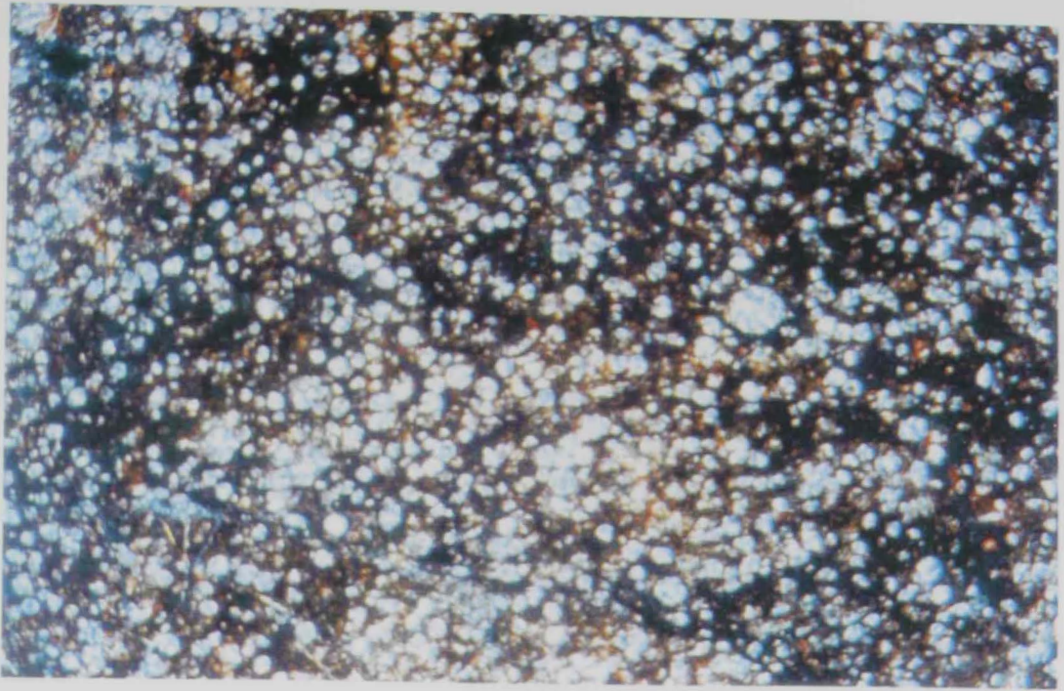


Fig.3.1 A photomicrograph of ferruginous radiolarian ribbon chert. Closely-packed radiolarian tests are embedded in a ferruginous microquartz groundmass. (Sample 1, Cross Polars, X10).

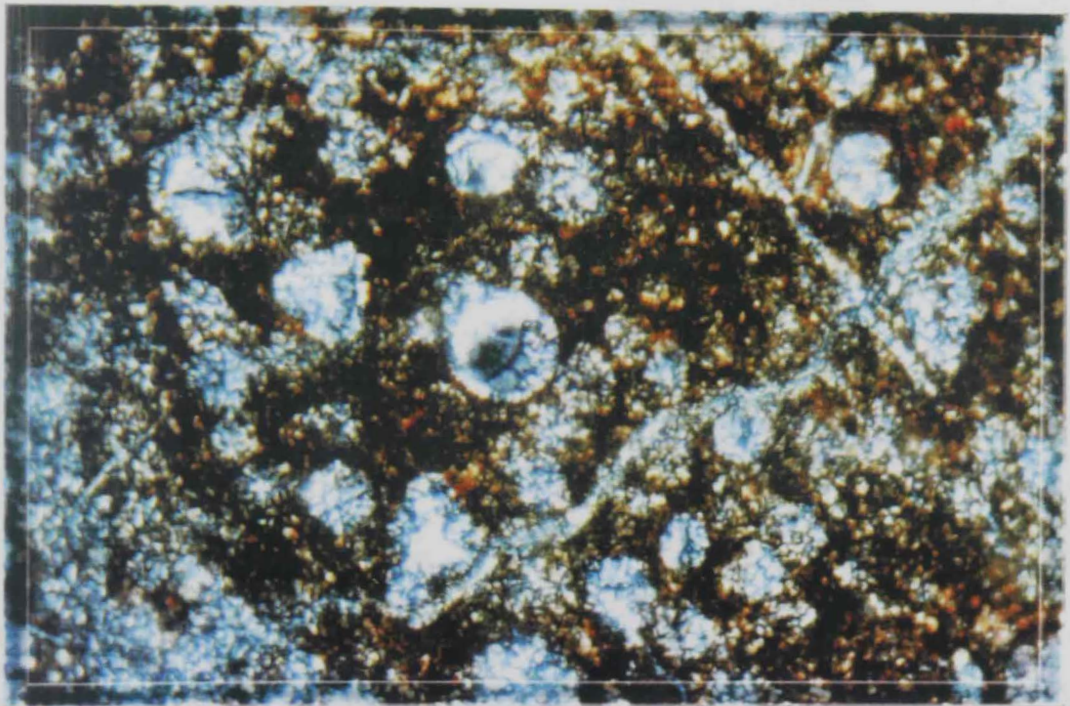


Fig.3.2 A closeup view of the ferruginous radiolarian ribbon chert. Chalcidonic silica replaces the radiolarian skeletons or fills their cavities. (Sample 1, Plain Polars, X25)

siliceous spicules. The groundmass is grayish black in color due to the presence of carbonaceous matter (Fig.3.4). Moreover, scattered, euhedral dolomite rhombs are recorded. Fractures are common and are filled by: dolomite and/or silica. (Fig.3.5).

3.1.3 Colloform Ribbon Chert:

This subfacies was recognized only at Idan and Al Gail. Remarkably, it lacks radiolaria. The rock contains well-developed colloform quartz banding with distinct gradation in crystal size from micro-to coarse-crystalline (Fig.3.6). Occasionally, the rock is highly brecciated (e.g. at Idan) (Fig.3.7). The fractures are filled with two generations of cements: calcite and a subsequent silica cement. Traces of iron oxides are present either as stains or scattered spots.

3.1.4 Calcareous Chert:

It occurs in the Saram, Idan and Al Gail areas while is missing at Al Rams. The rock, which lacks radiolaria, is composed of a mosaic of authigenic microquartz which, most probably, replaced a pre-existing carbonate. The latter seems to have been initially a pelagic limestone (abundant pelagic foraminifers) (Fig.3.8). Scattered euhedral, medium-sized dolomite rhombs suggesting an earlier phase of dolomitization. Fractures are commonly filled with coarse-crystalline silica and subsequent calcite cements. The latter consists of euhedral, bladed interlocking crystals occupying the centers of the fractures. Minor amounts of hematitic materials are recorded (Fig.3.9).

3.1.5 Siliceous Claystone:

This subfacies was recorded at Al Gail, Al Rams and Saram. The rock is characterized by a distinct fissility. It consists of an argillaceous groundmass that was subjected to extensive silicification and contains calcite crystals and silt-sized quartz grains (Fig.3.10, 3.11). Scattered pelagic foraminifers are recorded. Their chambers are

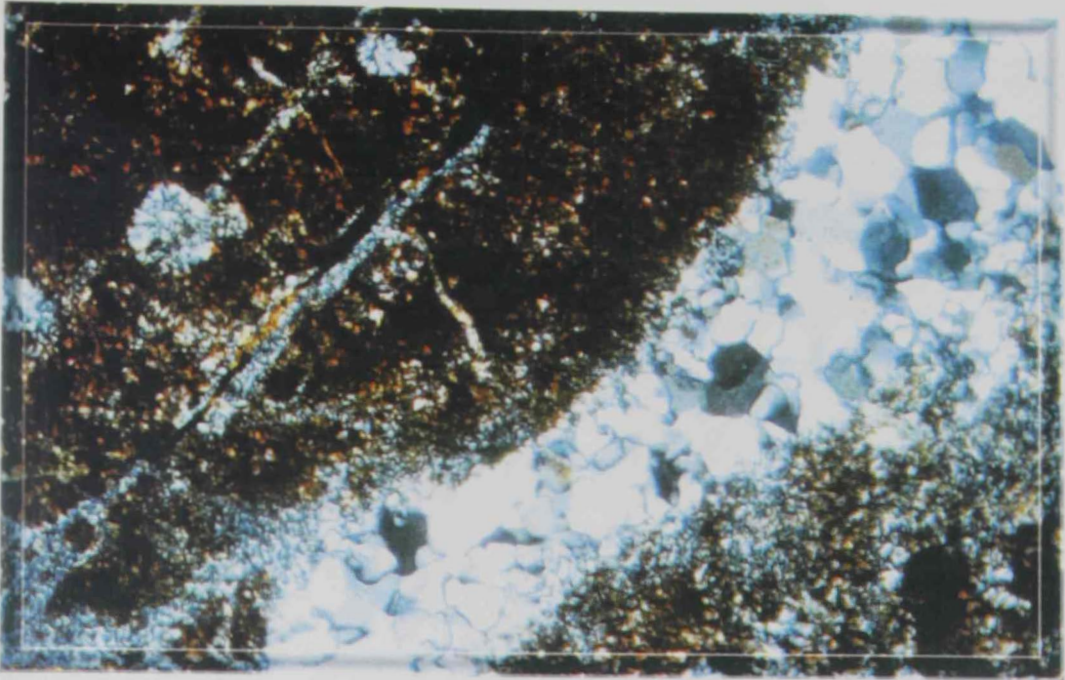


Fig.3.3 A photomicrograph of the ferruginous radiolarian ribbon chert. A large fracture is filled with micro to macrocrystalline quartz. (Sample 1, Crossed Polars, X25).

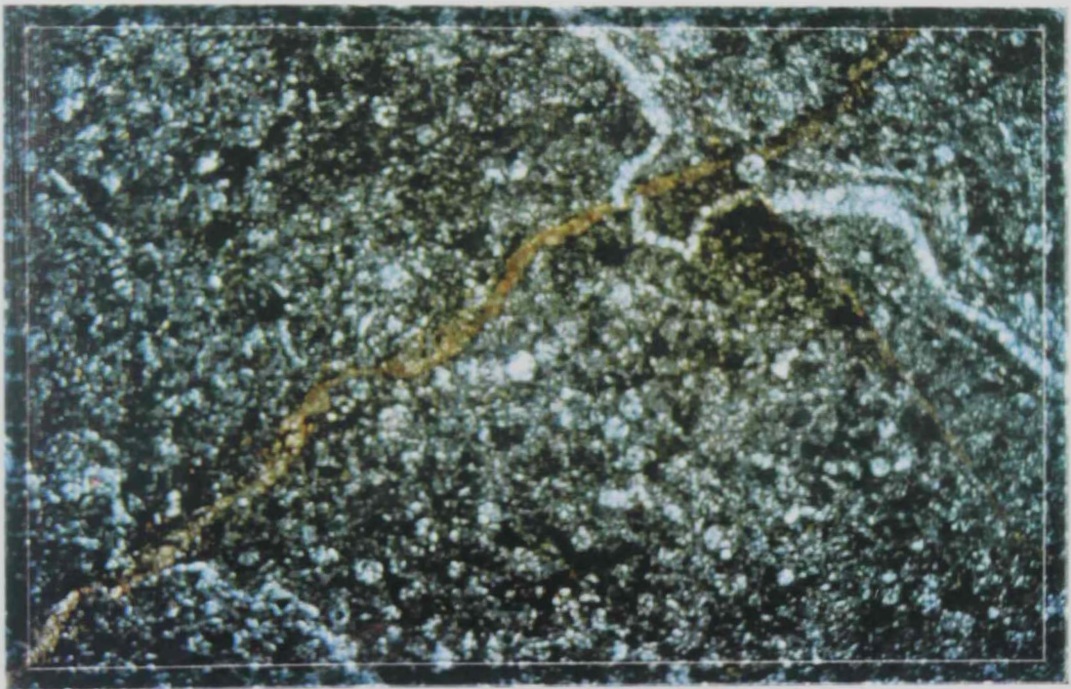


Fig.3.4 A photomicrograph of the carbonaceous radiolarian chert. Abundant poorly-preserved radiolarian test are embedded in a carbonaceous microquartz groundmass. (Sample 4, Crossed Polars, X10).

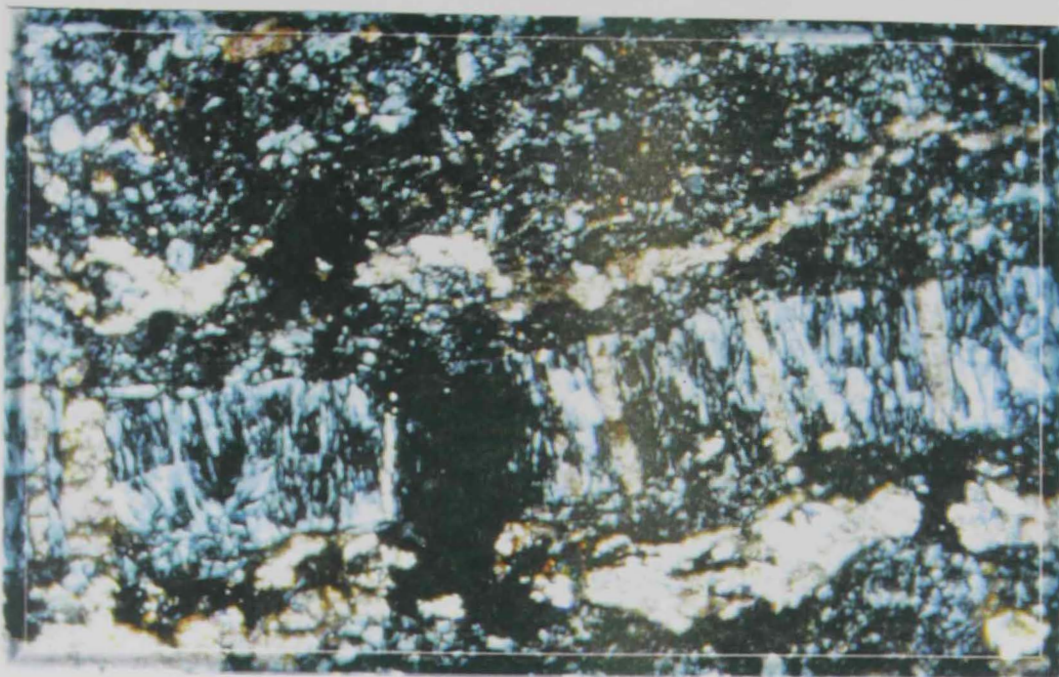


Fig.3.5 A photomicrograph of the carbonaceous radiolarian chert. The fractures are filled with chalcedonic silica. (Sample 4, Crossed Polars, X10).

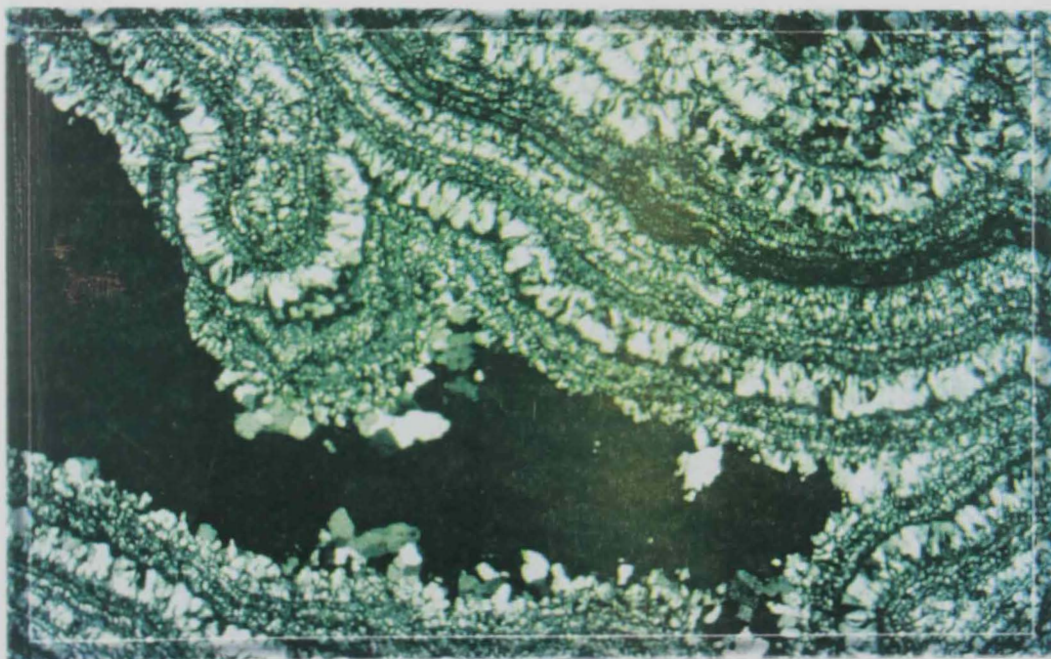


Fig.3.6. A photomicrograph of the colloform ribbon chert. A well-developed colloform texture displays a distinct gradation in crystal size. (Sample 17, Crossed Polars, X25).

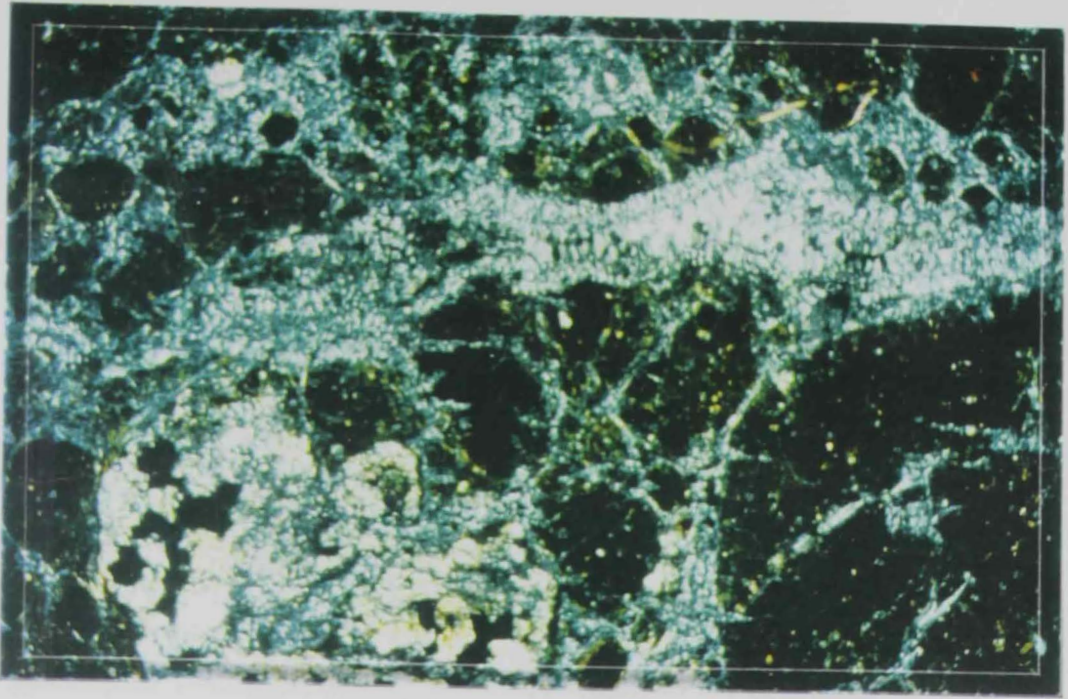


Fig.3.7 A photomicrograph of the colloform ribbon chert. The rock is extensively brecciated and the developed fractures are filled with silica and calcite. (Sample 17, Crossed Polars, X25).

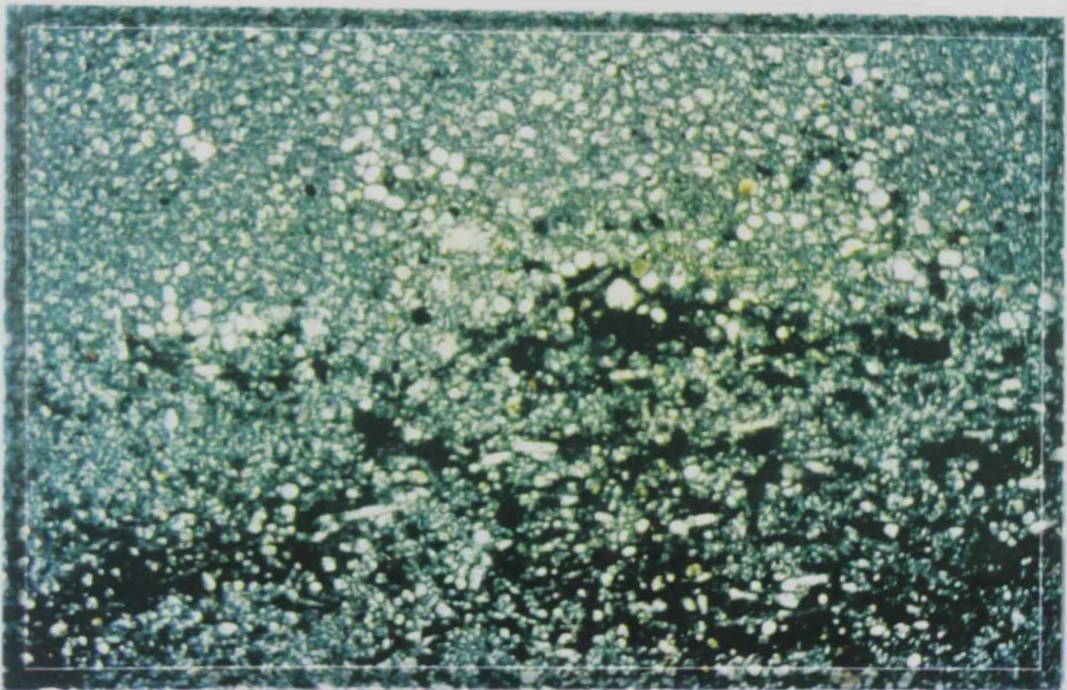


Fig.3.8 A photomicrograph of the calcareous chert. Scattered pelagic foraminifers and poorly-preserved radiolarian tests are embedded in a matrix of calcareous, silt-sized quartz. (Sample 14, Crossed Polars, X10).

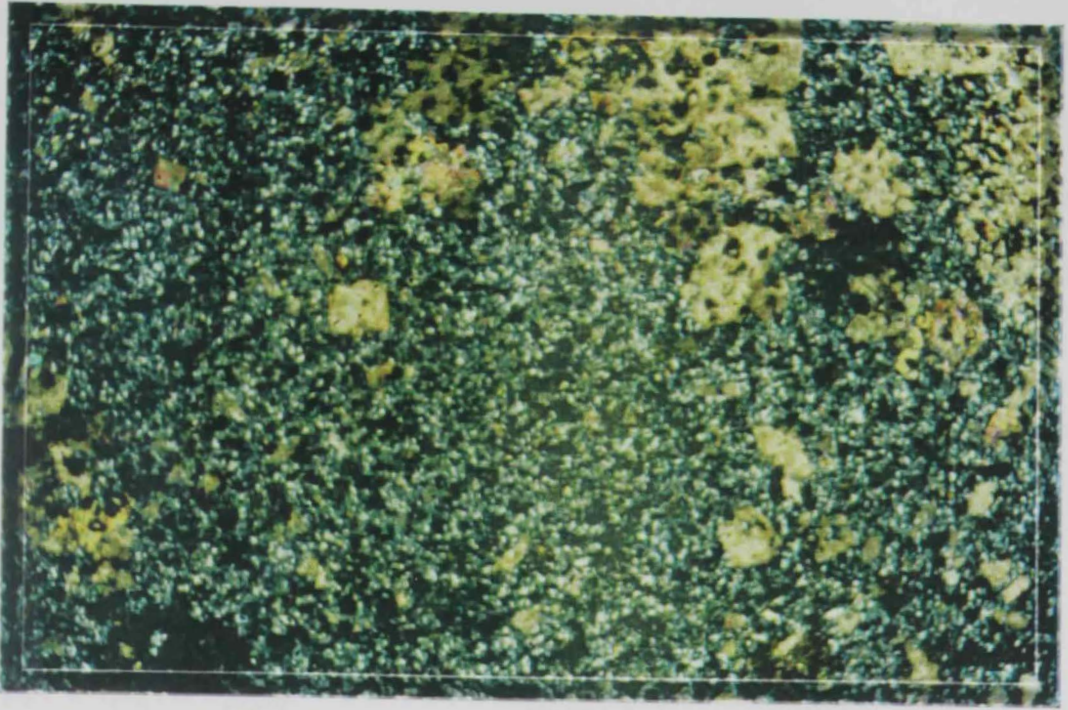


Fig.3.9. A photomicrograph of the calcareous chert. Relics and patches of dolomite rhombs constitute a part of the groundmass. (Sample 20, Crossed Polars, X25).

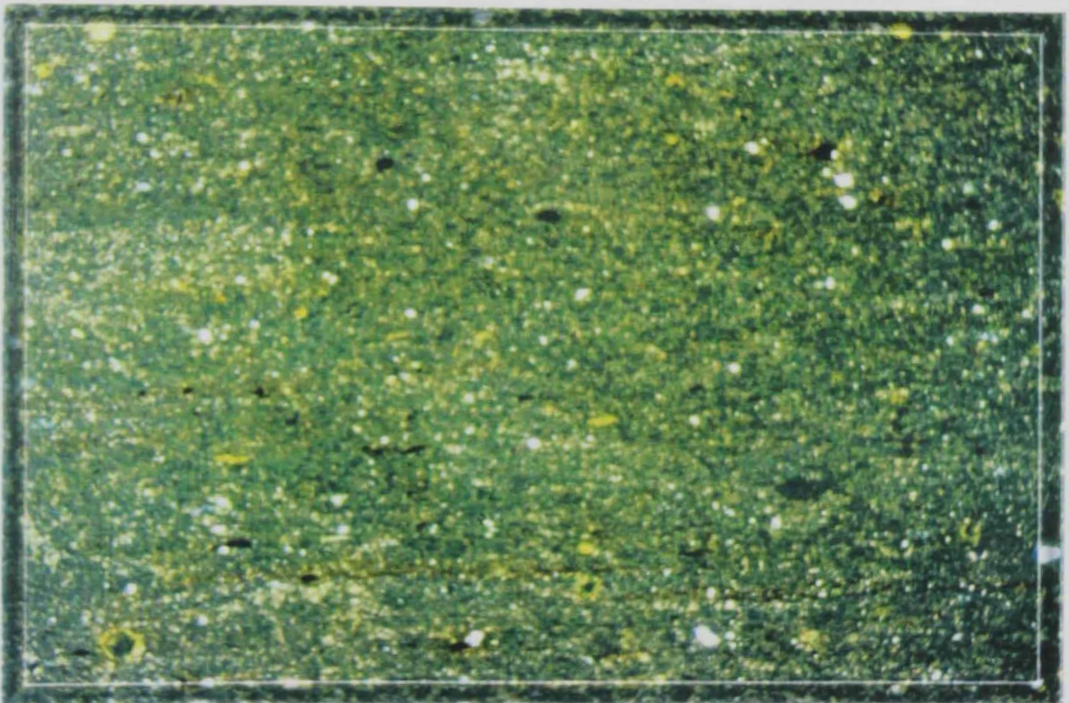


Fig.3.10 A photomicrograph of the siliceous claystone. The rock is composed of a silicified clayey groundmass in which are scattered pelagic forms and silt sized quartz grains. (Sample 19, Crossed Polars, X10).

filled either by calcite crystals or iron oxides. The latter also fill most of the existing hair-like fractures.

In addition to the above-mentioned chert facies types, the sequence at Saram contains a thin lamina of conglomerate. The rock is polymictic and composed mainly of closely-packed, coarse pebbles consisting (Fig.3.12) predominantly of fossiliferous and siliceous limestones. Grains of ophiolitic origin (serpentinite and gabbros) and quartz sand are also present. The lithoclastics are cemented by coarse-crystalline calcite, minor silica and iron oxides.

3.2 The Carbonate Facies:

The carbonate facies types were recorded in all the localities of the study area (Idan, Al Gail, Al Rams, Saram, and Khor Khowair). Based on the textural scheme of limestone classification proposed by Dunham (1962), four subfacies types were recognized.

3.2.1 Lime Mudstone:

It is recognized only at Idan, Al Rams and Saram while is absent at Al Ghail and Khor Khowair. The rock is composed of a groundmass formed of argillaceous lime mud (Fig.3.13). Scattered moldic pores, produced by dissolution of pelagic foraminiferal tests, are present and some are filled with calcite crystals. Fractures are commonly plugged with medium-to coarse-crystalline calcite and, occasionally, silica crystals and minor organic matter.

3.2.2 Wackestone:

This subfacies is recorded only in Khor Khowair area where it constitutes about 43% of the carbonate succession. Based on the dominating carbonate allochems, two wackestone types were recognized:

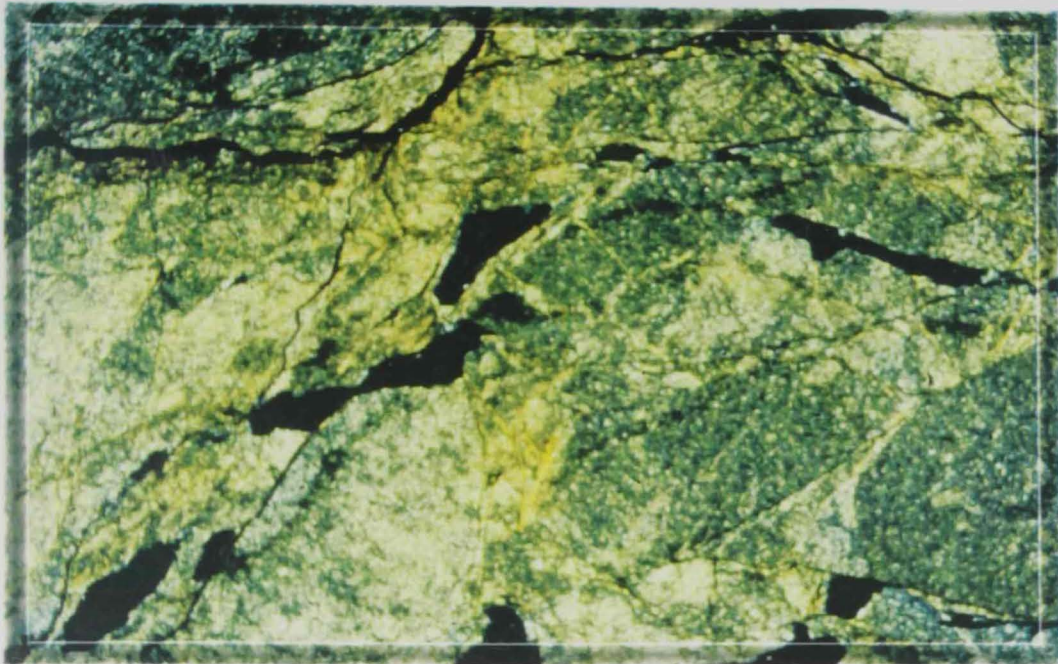


Fig.3.11 A photomicrograph of the siliceous claystone, . The rock is composed of a siliceous clayey groundmass in which are scattered pelagic forms and silt-sized quartz grains. (Sample 31, Crossed Polars, X25).

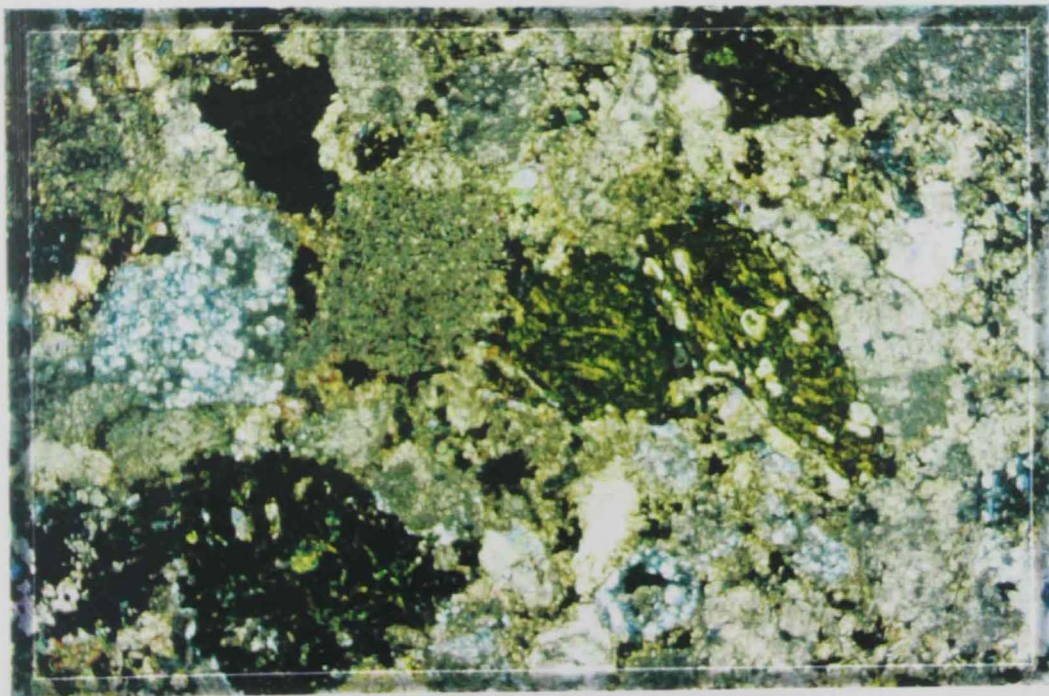


Fig.3.12 A photomicrograph of the conglomerate subfacies. Coarse pebbles of various lithologies are closely-packed and cemented by calcite and silica. (Sample 27, Crossed Polars, X25).

(i) Peloidal bioclastic wackestone:

The rock is composed of an argillaceous lime mud groundmass containing much peloides of varying sizes. (Fig.3.14). Skeletal grains are represented by crinoidal debris, algal and pelecypod shell fragments and scattered foraminiferal tests (Fig.3.15). Calcite cement is present in the form of drusy growths inside some skeletal cavities.

(ii) Orbitolina bioclastic wackestone:

The framework of this rock is composed of skeletal grains including tests of large foraminiferas (*Orbitolina sp.* and *Orbiopsella primaeva*), small foraminiferas (*Globotruncana sp.*) (Fig.3.16), algal grains, crinoidal debris, pelecypod shell fragments, large ostracodal carapaces, calcareous sponges and worm tubes. These grains are embedded in an argillaceous lime mud matrix. Calcite cement occurs in the form of veinlets and drusy growths inside many of the skeletal cavities. Aggrading neomorphism is also recognizable whereby neoformed calcite had destroyed many of the original structural features of the skeletal grains.

3.2.3 Packstone:

This subfacies is recorded in Idan, Al Ghail and Khor Khowair while is missing at Al Rams and Saram. Based on the dominant carbonate grains, three subfacies could be delineated:

(i) Algal bioclastic packstone:

It is recognized in Idan and Al Gail areas. The calcareous algae (Codiaceans and lithothamnium) constitute the majority of the carbonate grains (Fig3.17) and occasionally form a stromatolitic structure. Other skeletal grains consist of (in decreasing order of abundance) bryozoa (*Leiosoecia*), corals (colonial scleractines),

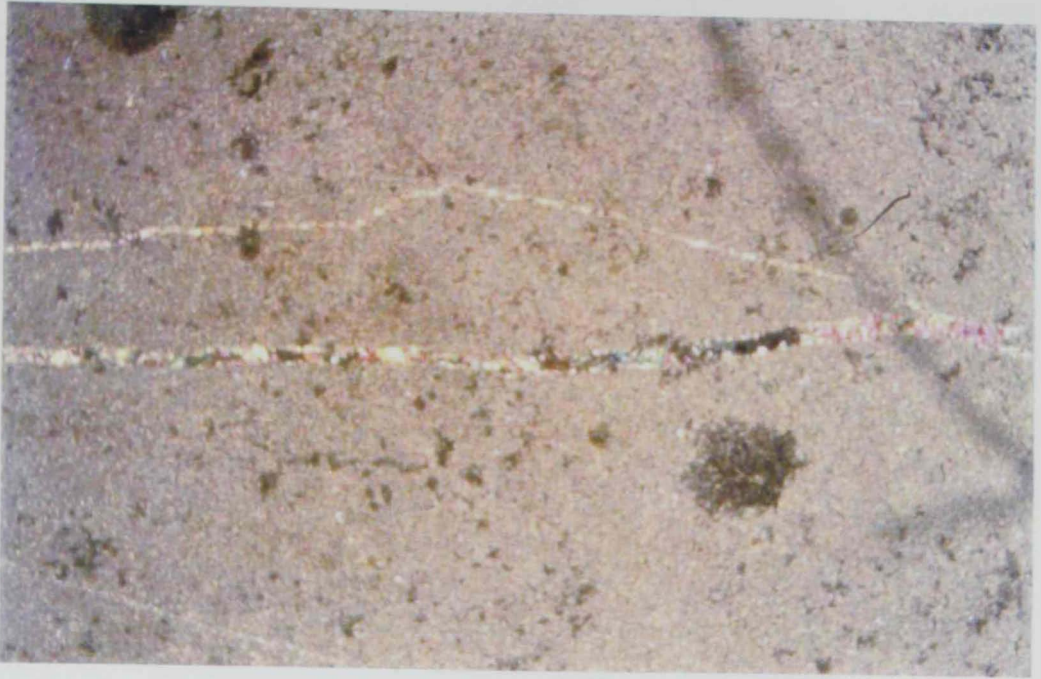


Fig.3.13 A photomicrograph of the lime mudstone facies. A dense, homogeneous lime mud groundmass is dissected by calcite veinlets. (Sample 3, Crossed Polars, X25).

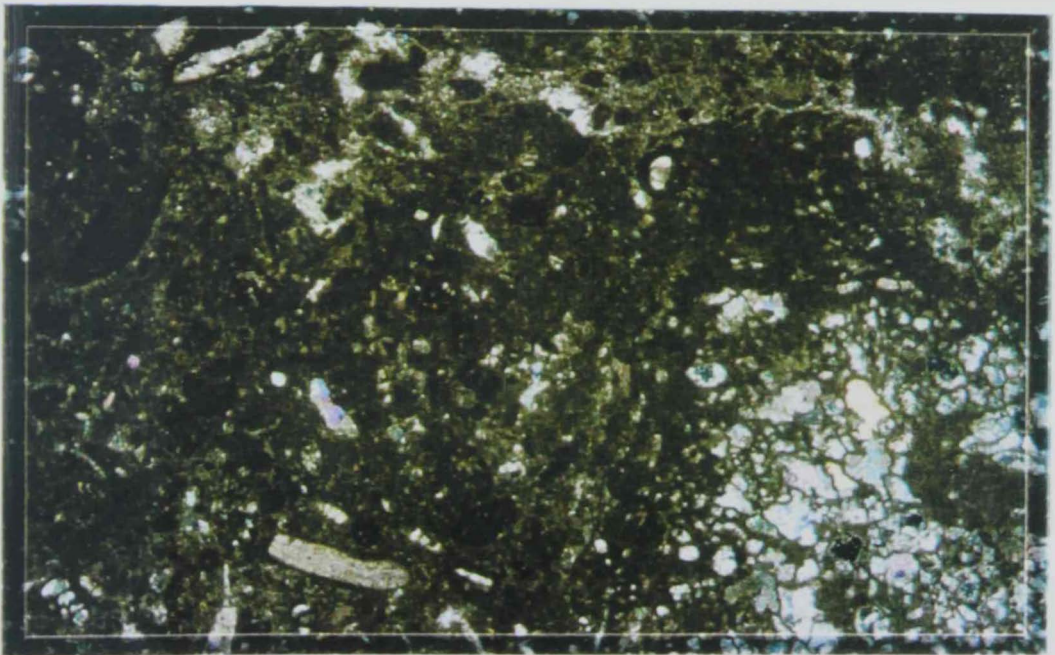


Fig.3.14 A photomicrograph of the peloidal bioclastic wackestone. Peloidal grains, foraminiferal tests and echinoid fragments are embedded in an argillaceous lime mud groundmass. (Sample 32, Crossed Polars, X25).

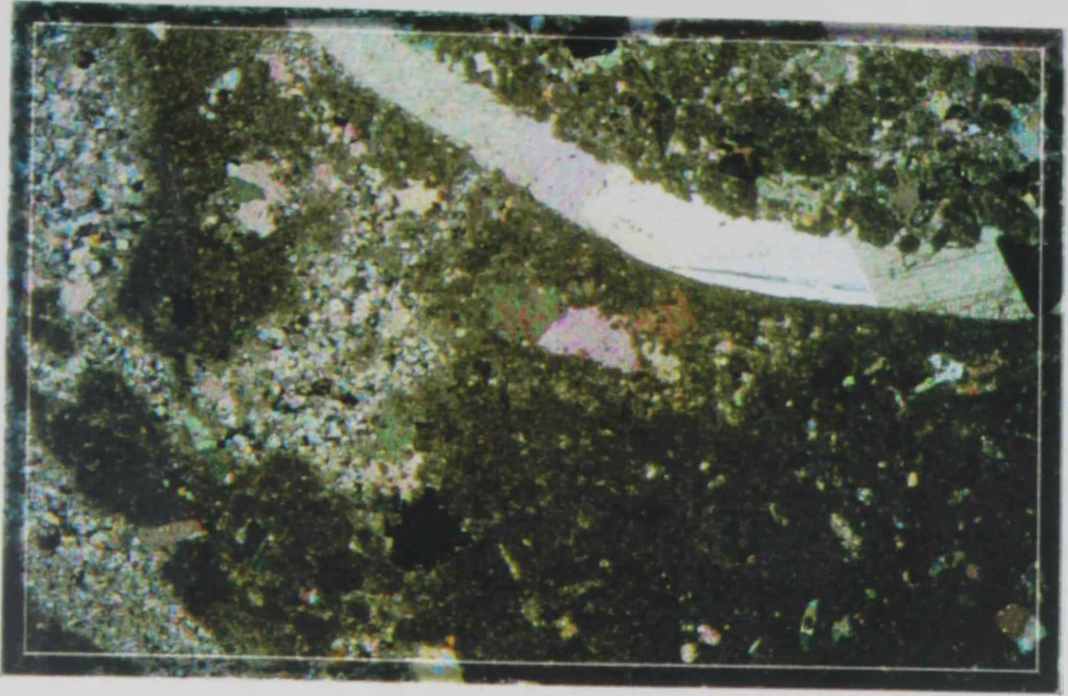


Fig.3.15 A photomicrograph of the peloidal bioclastic wackestone. A large recrystallized crinoidal plate is embedded in a groundmass which is extensively affected by aggrading neomorphism. (Sample 32, Crossed Polars, X25).

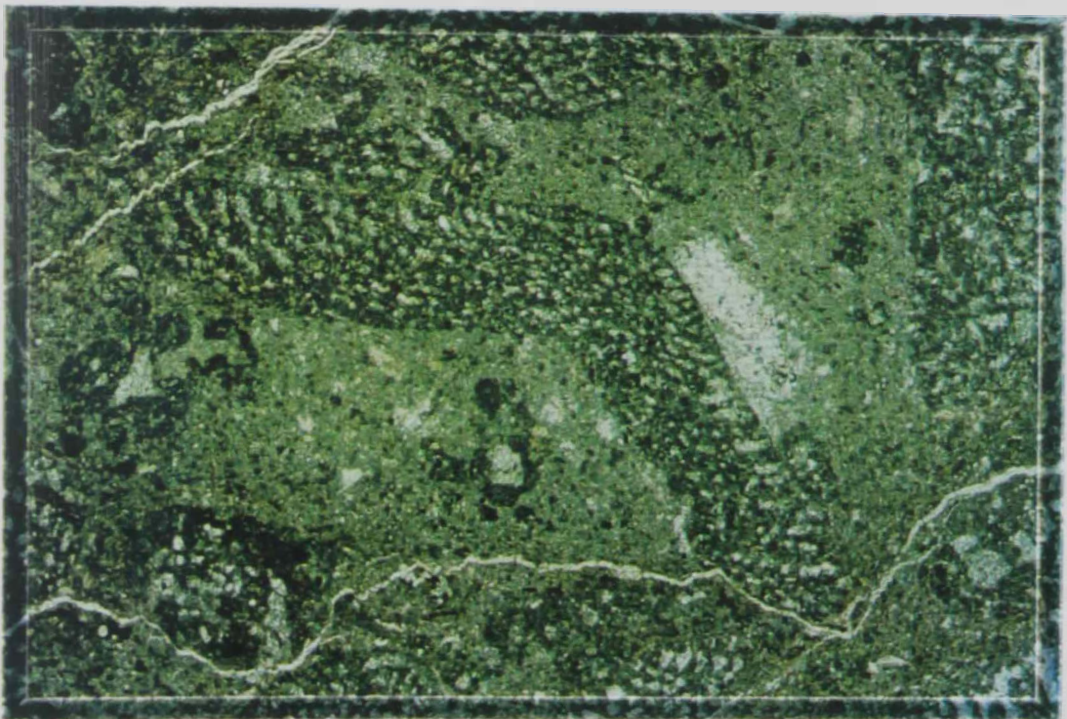


Fig.3.16 A photomicrograph of the Orbitolina bioclastic wackestone. Abundant well-preserved Orbitolinids tests are set in a groundmass of argillaceous lime mud. (Sample 36, Crossed Polars, X25).

crinoidal debris, ostracodal tests and pelecypod shell fragments, together with other unidentified bioclasts. These skeletal grains are cemented by microsparry calcite (Fig.3.18), which later had undergone partial recrystallization. Calcite cements filling many of the fractures and minor silica replacement are also clearly observed. The rock shows extensive aggrading neomorphism. Also, micritic envelopes are frequently recorded encrusting some of the carbonate grains.

(ii) Pelecypodal bioclastic packstone:

This subfacies is recognized only in Khor Khowair. The framework of the rock is formed essentially of pelecypod shells (mainly *Exogyra sp*) and other unidentifiable fossil debris. (Fig.3.19). In addition, crinoidal fragments, foraminiferal tests (*Gaudyrina sp. and Textularia sp.*) and ostracodal carapaces are occasionally recorded. The cement consists mainly of intergranular microsparry calcite, which exists also as drusy growths filling many of the skeletal cavities. Aggrading neomorphism extensively affected this rock type (Fig.3.20) and resulted in partial obliteration of the initial structures of some skeletal grains. Wispy styloilites are also observed.

(iii) Orbitolina peloidal bioclastic packstone:

Well-sorted pellets composed of dense lime mud form the main non-skeletal carbonate grains in this rock. The skeletal grains, on the other hand, are dominantly foraminiferal tests (Fig.3.21) including large forams (*Orbitolina sp.*) and small forams (*Textularia sp., Nodosaria sp., Spiroplectamina sp. and Bolivinooides sp.*). In addition, scattered algal grains, crinoidal debris and pelecypod shell fragments are recorded. The cement consists of intergranular micro-to mesocrystalline calcite which exists also as syntaxial overgrowths around crinoidal debris. Drusy calcite fills many skeletal cavities. Most of the carbonate grains are encrusted by micritic

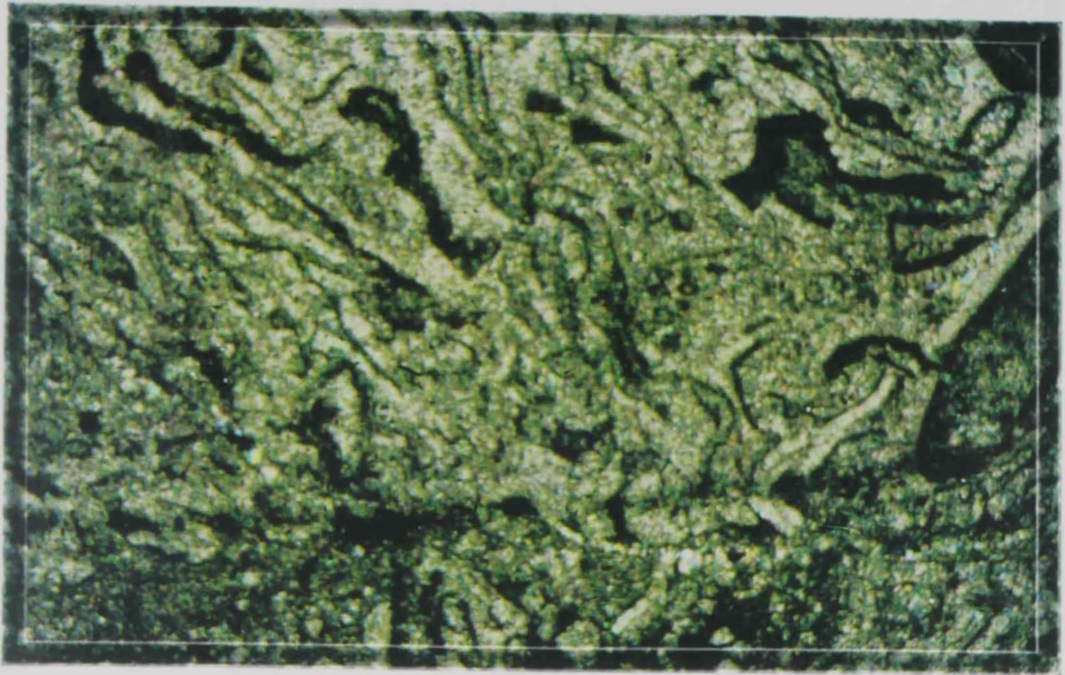


Fig.3.17 A photomicrograph of the algal bioclastic packstone. Different Codiaceans cemented by microsparitic calcite. (Sample 13, Crossed Polars, X25).

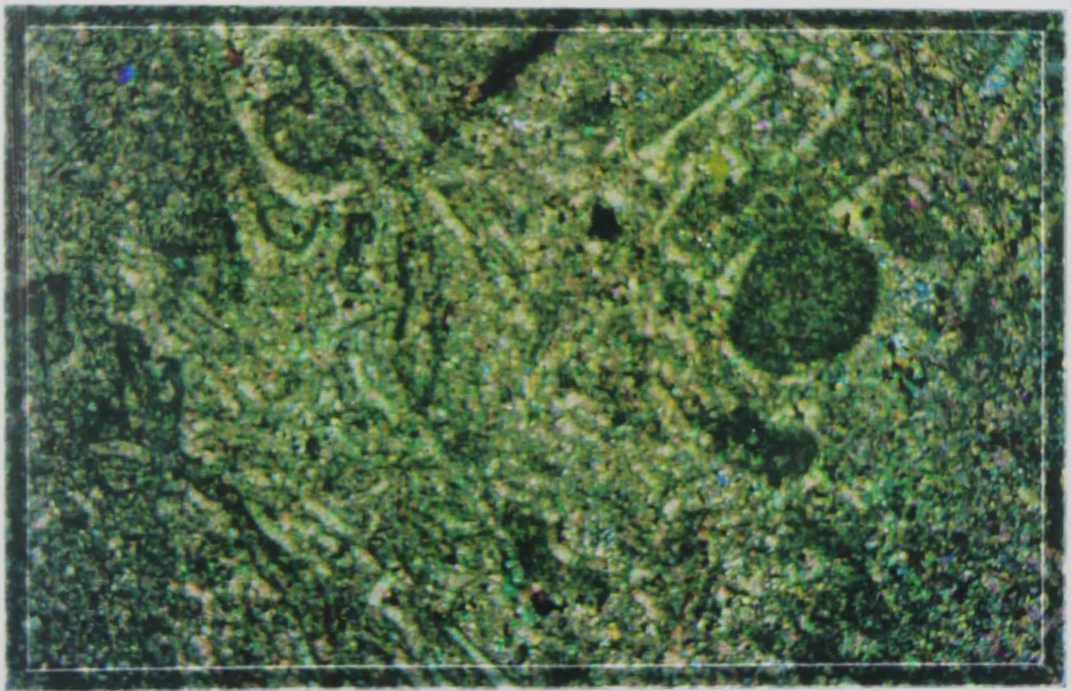


Fig.3.18 A photomicrograph of algal bioclastic packstone. Various Codiaceans are cemented by microsparitic calcite. (Sample 13, Crossed Polars, X25).

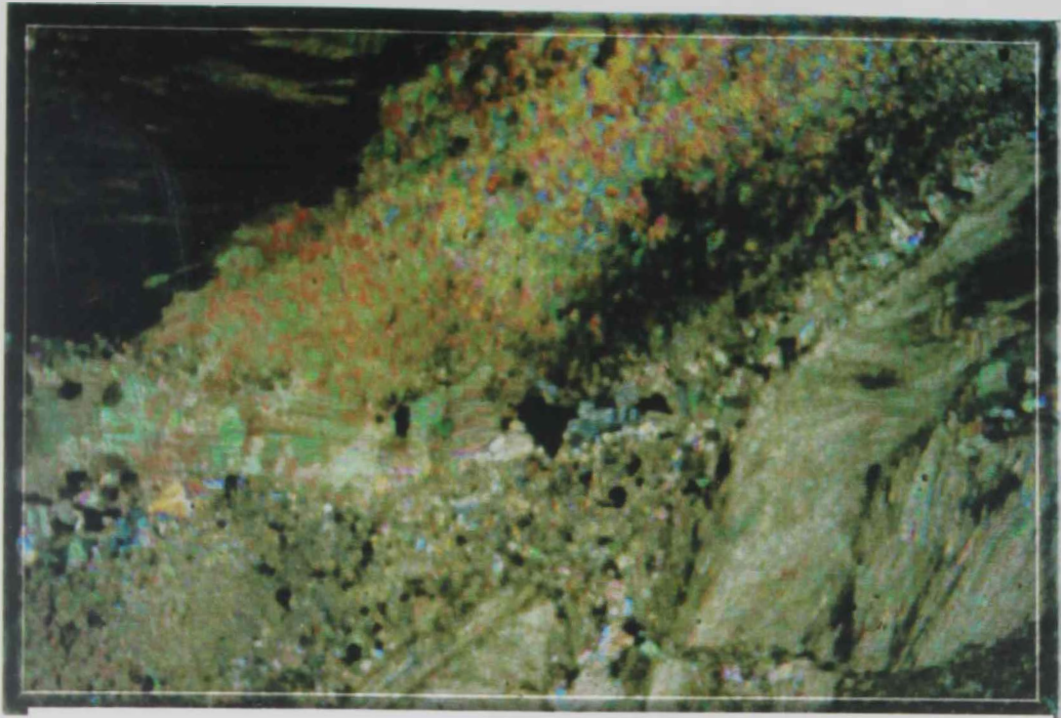


Fig.3.19 A photomicrograph of pelecypodal biocalstic packstone. Pelecypod shells are cemented by microsparry calcite. (Sample 33, Crossed Polars, X25).

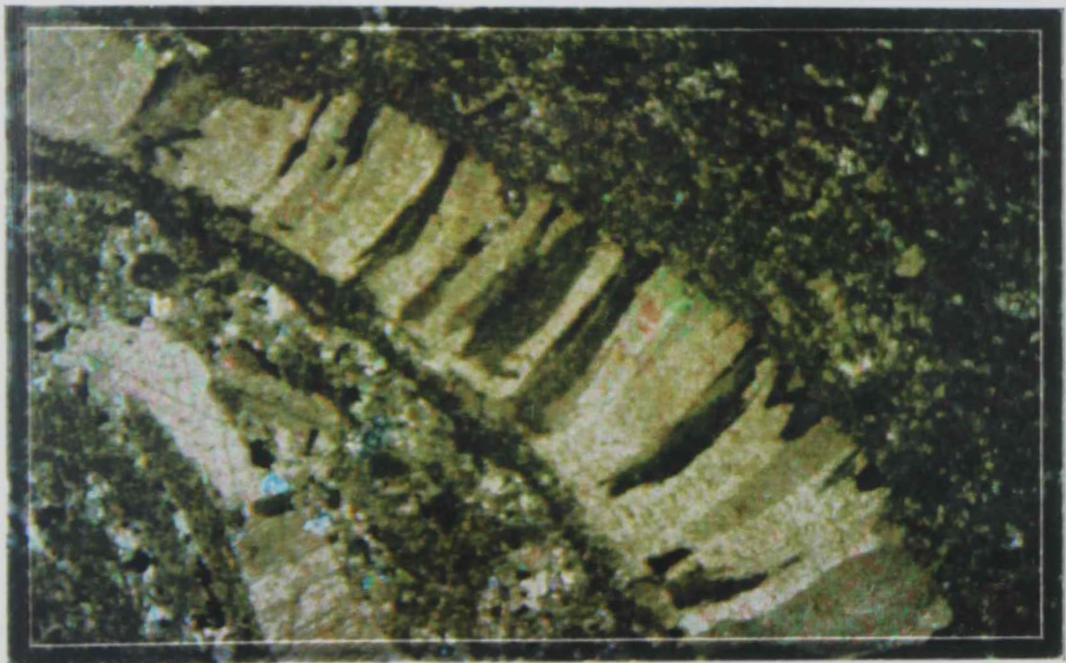


Fig.3.20 A photomicrograph of pelecypodal biocalstic packetone. Recrystallized pelecypod shells and pellets are cemented by microsparry calcite.(Sample 34, Crossed Polars, X25).

envelopes. Aggrading neomorphism is frequently recorded obliterating many of the original skeletal fabrics. The rock contains also wispy stylolites.

3.2.4 Crystalline Limestone:

This facies type is rare whereby its occurrence is restricted to Idan area. The rock is composed of a mosaic of interlocked, coarse crystalline, occasionally zoned calcite crystals (Fig.3.22). This zoning pattern might reflect crystal growth through 3 to 4 stages. Authigenic silica had been deposited in the intercrystal spaces and / or replaced the calcite crystals.

3.3 Sand Dunes

Microscopic examination of samples collected from the inland and coastal dunes in the study area revealed the presence of two main types:

3.3.1 Carbonate Dune Sands:

This type of sands is composed essentially of well-sorted and well-rounded carbonate grains (Fig.3.23). Some of these grains are made up entirely of lime mud while others have nuclei of foraminiferal tests encrusted by microcrystalline calcite. Some grains show typical oolitic structures. The sediment contains also detrital quartz grains, pelecypod shell debris and limestone lithoclasts.

3.3.2 Non Carbonate Dune Sands:

These sands consist mainly of olivine, pyroxene and quartz grains that are generally well-sorted and well-rounded (Fig.3.24). The calcareous sand-sized grains are rather minor.

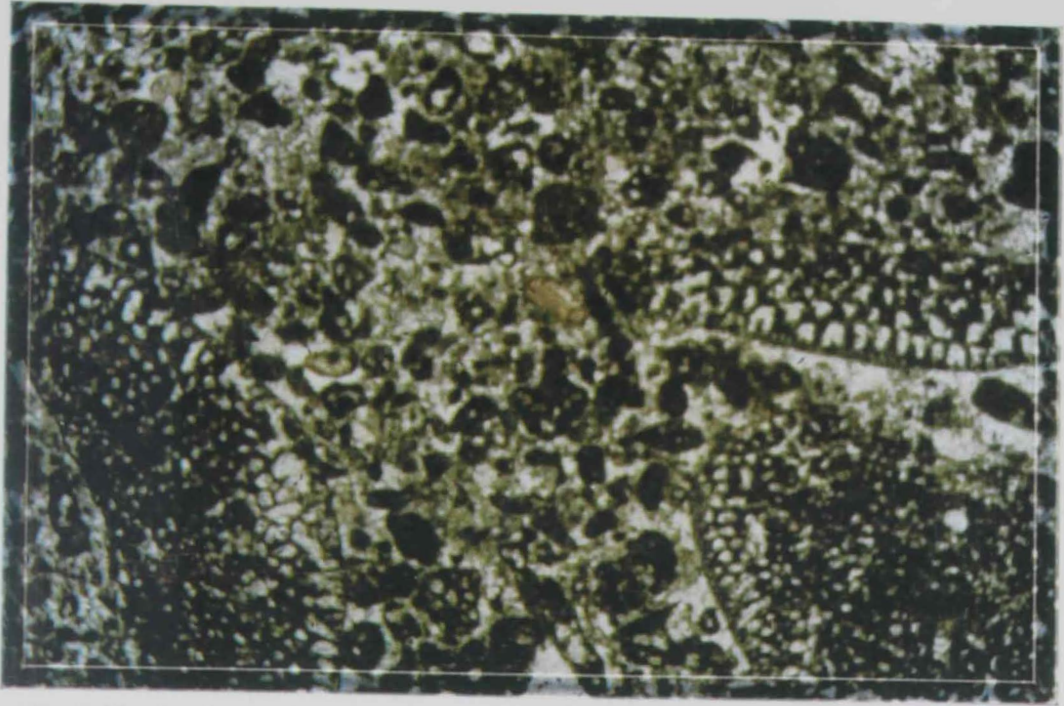


Fig.3.21 A photomicrograph of *Orbitalina* biocalstic packetone. *Orbitalina* and small foraminiferal tests and pellets are cemented by microsparry calcite. (Sample 35, Plain Polars, X25).

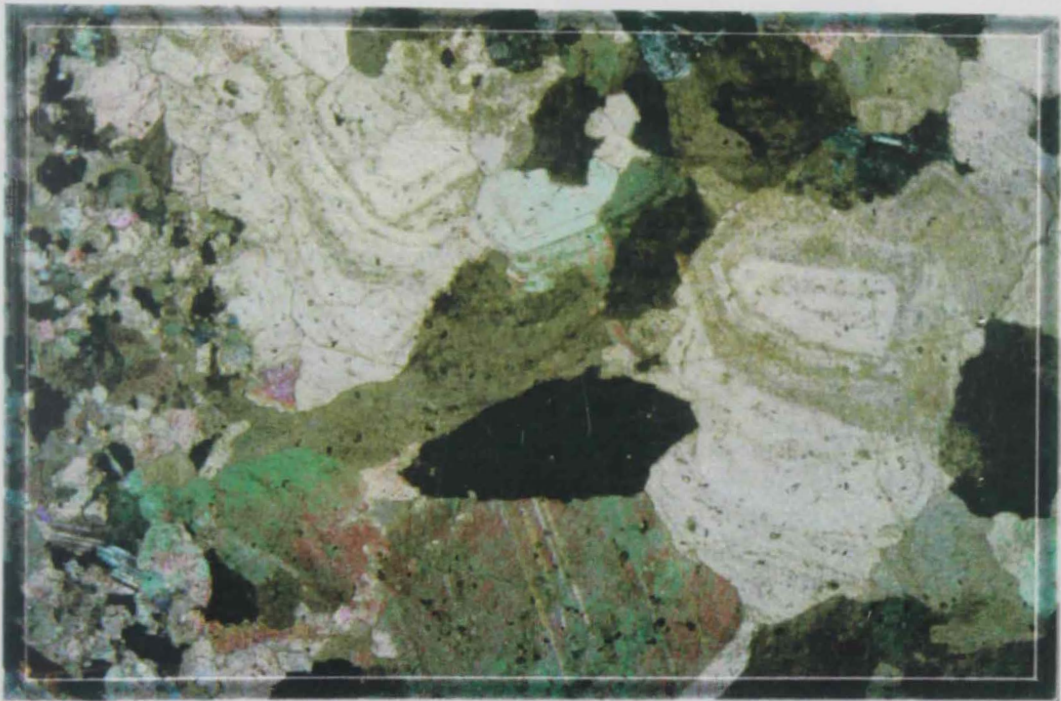


Fig.3.22 A photomicrograph of the crystalline limestone. The rock consists predominately of coarse, zoned and interlocked calcite crystals. (Sample 9, Crossed Polars, X25).

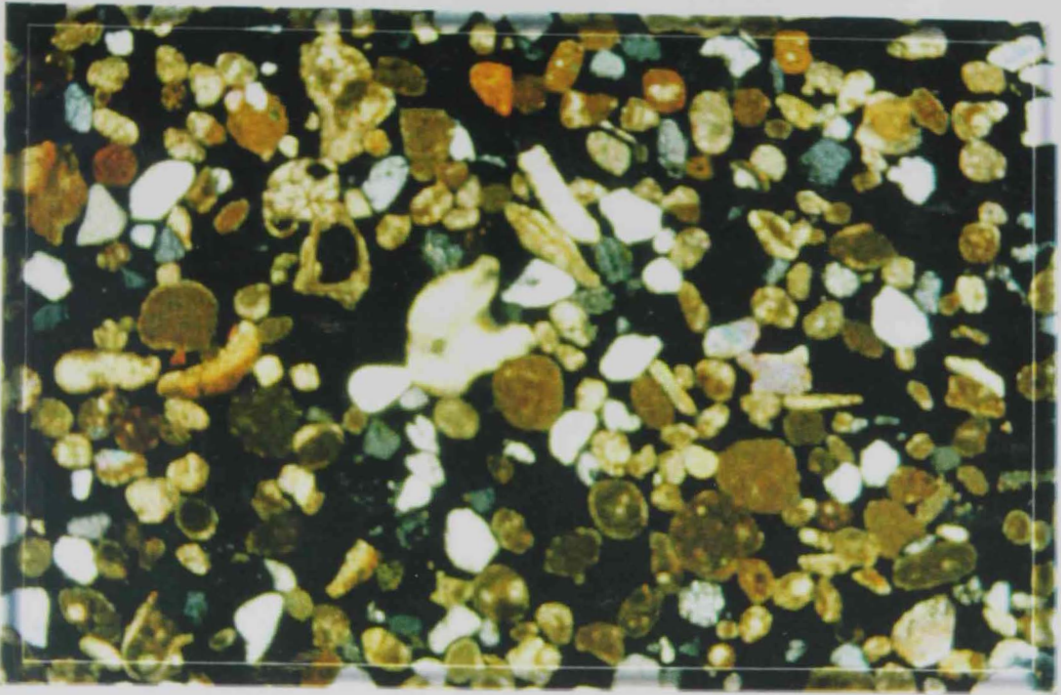


Fig.3.23 A photomicrograph of the carbonate dune sand. The predominantly carbonate grains are mainly well-sorted and well-rounded. (Sample 39, Crossed Polars, X25).

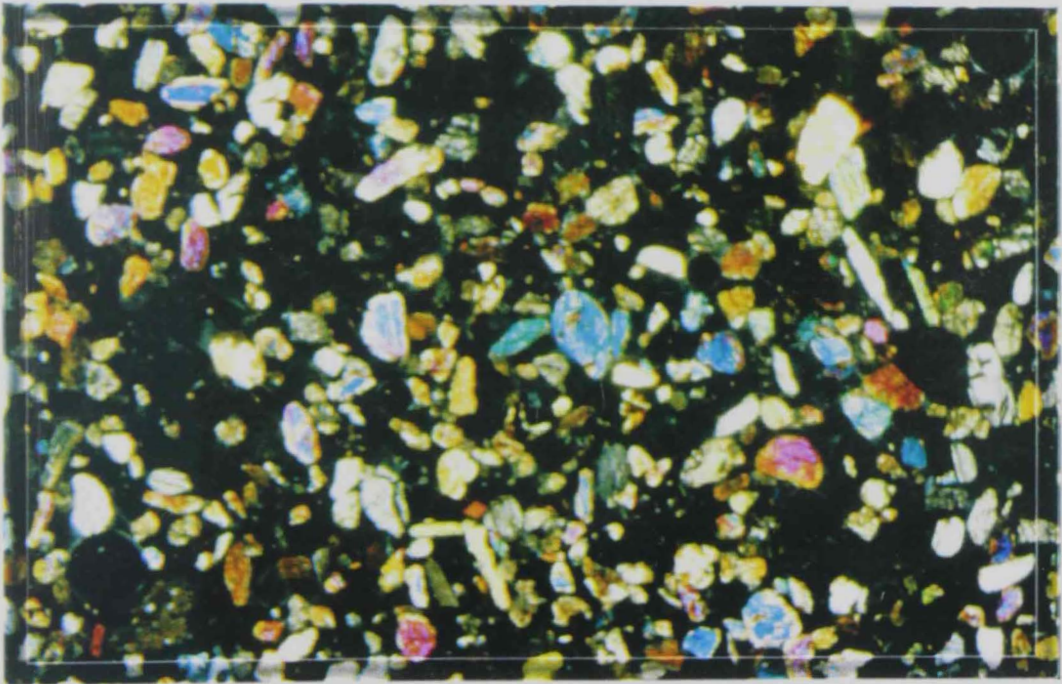


Fig.3.24 A photomicrograph of the lithic dune sand. The grains are mainly monomineralic (predominantly olivine, pyroxene and quartz) well-sorted and well-rounded. (Sample 38, Crossed Polars, X25).

3.4 The Diabasic Sheet:

The rock is fine-grained and dark green in color. The dominant mineral components include calcic plagioclase feldspar and pyroxene. Amphiboles are less abundant, and iron oxides are the main accessory minerals. Feldspars exist as lath-like interlocking crystals. Pyroxene is present in the form of subhedral to euhedral prismatic crystals forming with the feldspar laths a typical diabasic texture (Fig.3.25).

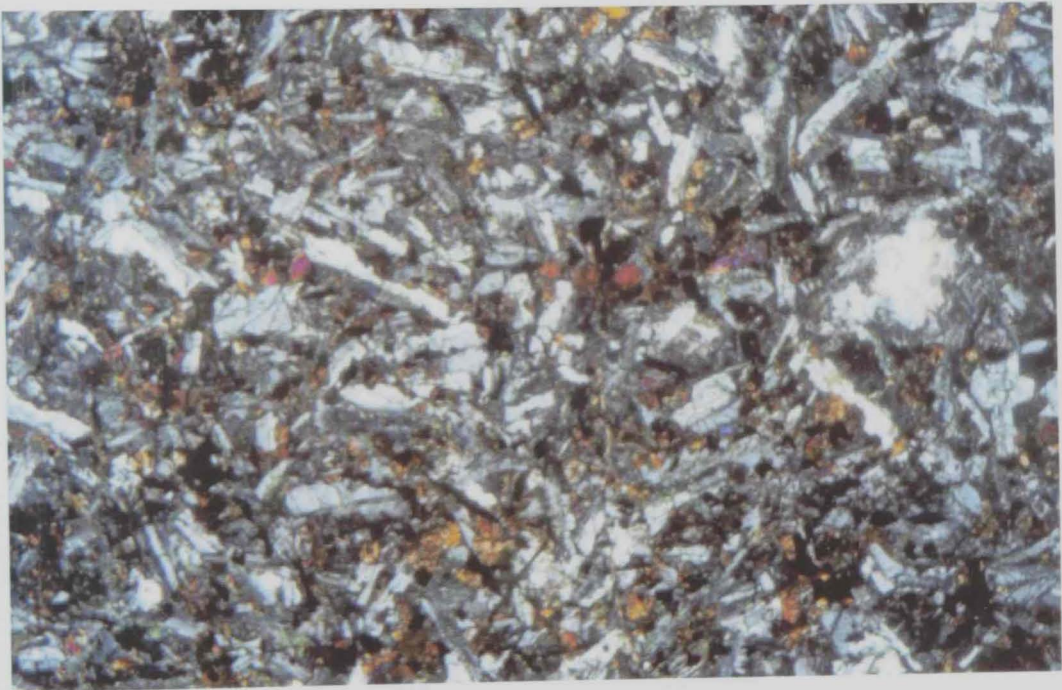


Fig.3.25 A photomicrograph of the diabase. The rock is fine-grained dark green in color. The dominant mineral components are calcic plagioclase feldspar and pyroxene. (Sample 7, Crossed Polars, X25).

CHAPTER IV

MINERALOGY

CHAPTER IV

MINERALOGY

CHAPTER IV

MINERALOGY

X-ray diffraction analysis was utilized to throw more light on the mineral composition of the various rock types and sand dunes in the study area. The obtained X-ray data were used for the semiquantitative determination of the existing minerals based on the intensities of their strongest diffraction peaks. The results obtained are given in Tables (4.1) to (4.4) and illustrated in Figs. (4.1) to (4.9). These results are in accordance with those obtained from the microscopic examination of thin sections (Chapter III).

4.1 Mineralogy of Cherts

Table (4.1) presents the mineral composition of the various chert types in the study localities. It shows that these rocks consist of (in order of decreasing abundance): quartz, calcite, dolomite and hematite. Quartz is the only major component in all localities except for some exposures in Saram where calcite also represents a major constituent. The latter mineral is a subordinate or minor component in some other calcareous cherts in Al Gail and Saram. The presence of dolomite is restricted to the calcareous cherts of Idan in which it represents a subordinate or minor component. Hematite, on the other hand, was detected in only one sample representing the ferruginous radiolarian chert of Idan.

4.2 Mineralogy of Carbonate Rocks

Table (4.2) presents the mineral composition of the various carbonate rocks in the study area. It shows that these rocks are made up of (in order of decreasing abundance): calcite, quartz and dolomite. Calcite is the sole major component in all the carbonates. Quartz exists as a subordinate constituent in some of the lime mudstones and wackestones of Saram. The presence of dolomite is limited to the packstones of Idan in which the mineral represents a minor constituent.

Table (4.1) Mineral composition of the chert facies as revealed by X-ray diffractometry

Locality	Sample No.	Facies Type	Mineral Composition		
			Major	Subordinate	Minor
Idan	1	Ferruginous radiolarian chert	Quartz		Hematite
	2	Radiolarian chert	Quartz		
	3	Radiolarian chert	Quartz		
	4	Calcareous chert	Quartz		Dolomite
	5	Calcareous chert	Quartz	Dolomite	
	6	Siliceous mudstone	Quartz		
Al Gail	13	Siliceous mudstone	Quartz		
	14	Calcareous chert	Quartz	Calcite	
	15	Calcareous chert	Quartz		Calcite
	16	Radiolarian chert	Quartz		
	17	Radiolarian chert	Quartz		
Saram	19	Calcareous chert	Quartz	Calcite	
	20	Calcareous chert	Quartz, Calcite		
	21	Radiolarian chert	Quartz		
	22	Radiolarian chert	Quartz		
	23	Calcareous chert	Quartz	Calcite	
	24	Calcareous chert	Quartz		Calcite
	25	Radiolarian chert	Quartz		
	26	Calcareous chert	Quartz, Calcite		
Al Rams	30	Ferruginous radiolarian chert	Quartz		
	31	Radiolarian chert	Quartz		

Table (4.2) Mineral composition of the carbonate facies as revealed by X-ray diffractometry

Locality	Sample No.	Facies Type	Mineral Composition		
			Major	Subordinate	Minor
Idan	8	Packstone	Calcite		Dolomite
	9	Crystalline limestone	Calcite		
	10	Packstone	Magnesium/Calcite		Dolomite
	11	Crystalline limestone	Calcite		Quartz
	12	Lime mudstone	Calcite		
Al Gail	18	Packstone	Calcite		
Saram	27	Wackestone	Calcite		Quartz
	28	Lime mudstone	Calcite		Quartz
	29	Lime mudstone	Calcite	Quartz	
Khor Khowair	32	Wackestone	Calcite		
	33	Wackestone	Calcite		
	34	Wackestone	Calcite		
	35	Lime mudstone	Calcite		
	36	Wackestone/Packstone	Calcite		
	37	Wackestone/Packstone	Calcite		

4.3 Mineralogy of the Sand Dunes

Tables (4.3) presents the mineral composition of the light and heavy mineral fractions of two samples collected from the coastal and inland sand dunes in the study area. This table shows that the light fraction of the Al Helailah coastal dune sands consists of carbonate clasts and quartz grains together with minor proportions of skeletal grains and traces of feldspars and chert. Their heavy fractions are made up of pyroxenes and opaques in addition to traces of hornblende, garnets, rutile, tourmaline and epidotes. The light fractions of Al Gail inland dunes compositionally resemble those of Al Helailah except for the absence of the skeletal grains. Their heavy fractions are also similar with the exception of the presence of traces of monazite.

Quantitative comparison of the mineralogy of the two types of sand dunes reveals that the light fractions of Al Helailah coastal dunes contain higher concentrations of carbonate lithoclasts and skeletal grains and lower proportions of quartz and chert. Also, the heavy fractions of Al Helailah coastal dunes are slightly more enriched in opaques, pyroxenes, epidote and hornblende whereas depleted in rutile, tourmaline, garnet and monazite.

Table (4.3) Mineral composition of the coastal and inland Sand dunes

(A) Light Fractions

Locality	Mineral Composition %				
	Quartz	Carbonate lithoclasts	Feldspars	Chert	Skeletal grains
Al Helailah (Coastal Dune)	32.7	55.7	1.6	1.6	8.4
Al Gail (Inland Dune)	48.3	46.5	1.6	3.6	-

(B) Heavy Fractions

Locality	Opaques	Pyroxene	Epidote	Rutile	Tourmaline	Hornblende	Garnets	Staurolite	Monazite
Al Helailah (Coastal Dune)	36.1	57.5	0.8	1.0	1.0	1.8	1.8	-	-
Al Gail (Inland Dune)	34.3	56.0	0.4	1.3	2.3	1.5	4.0	-	0.2

4.4 Mineralogy of Diabase Sheet

Table (4.4) presents the mineral composition of a sample representing the diabase rock at Idan. It shows that this sample is composed of quartz and plagioclase together with lesser concentrations of magnetite and clay minerals.

Table (4.4) Mineral composition of the diabase sheet as revealed by X-ray diffractometry

Locality	Sample No.	Facies Type	Mineral Composition		
			Major	Subordinate	Minor
Idan	7	Diabase	Quartz, Plagioclase	Magnetite, clay Mineral	-

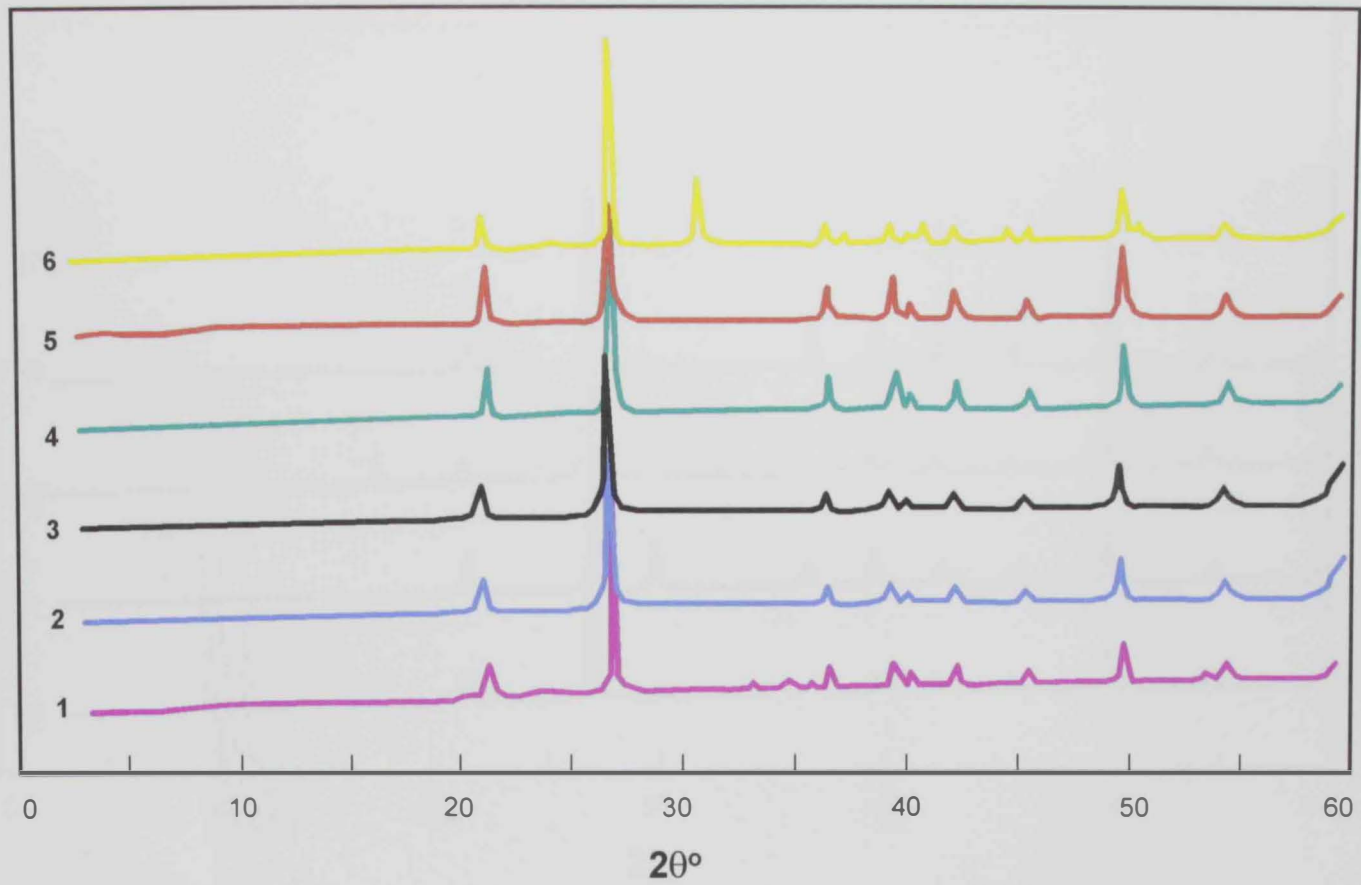


Fig. 4.1: X-ray diffraction patterns of Idan chert samples

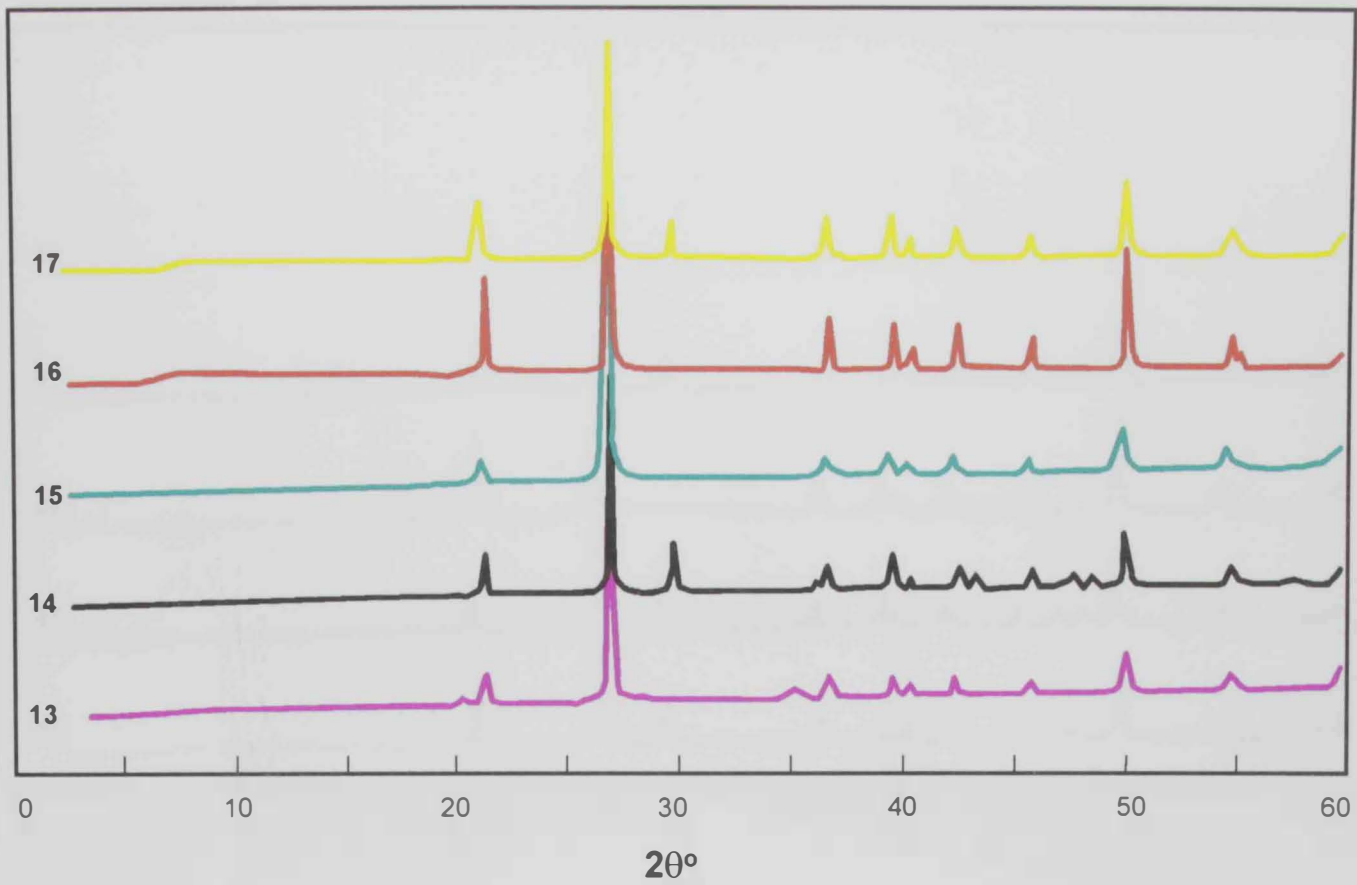


Fig. 4.2: X-ray diffraction patterns of Al Gail chert samples

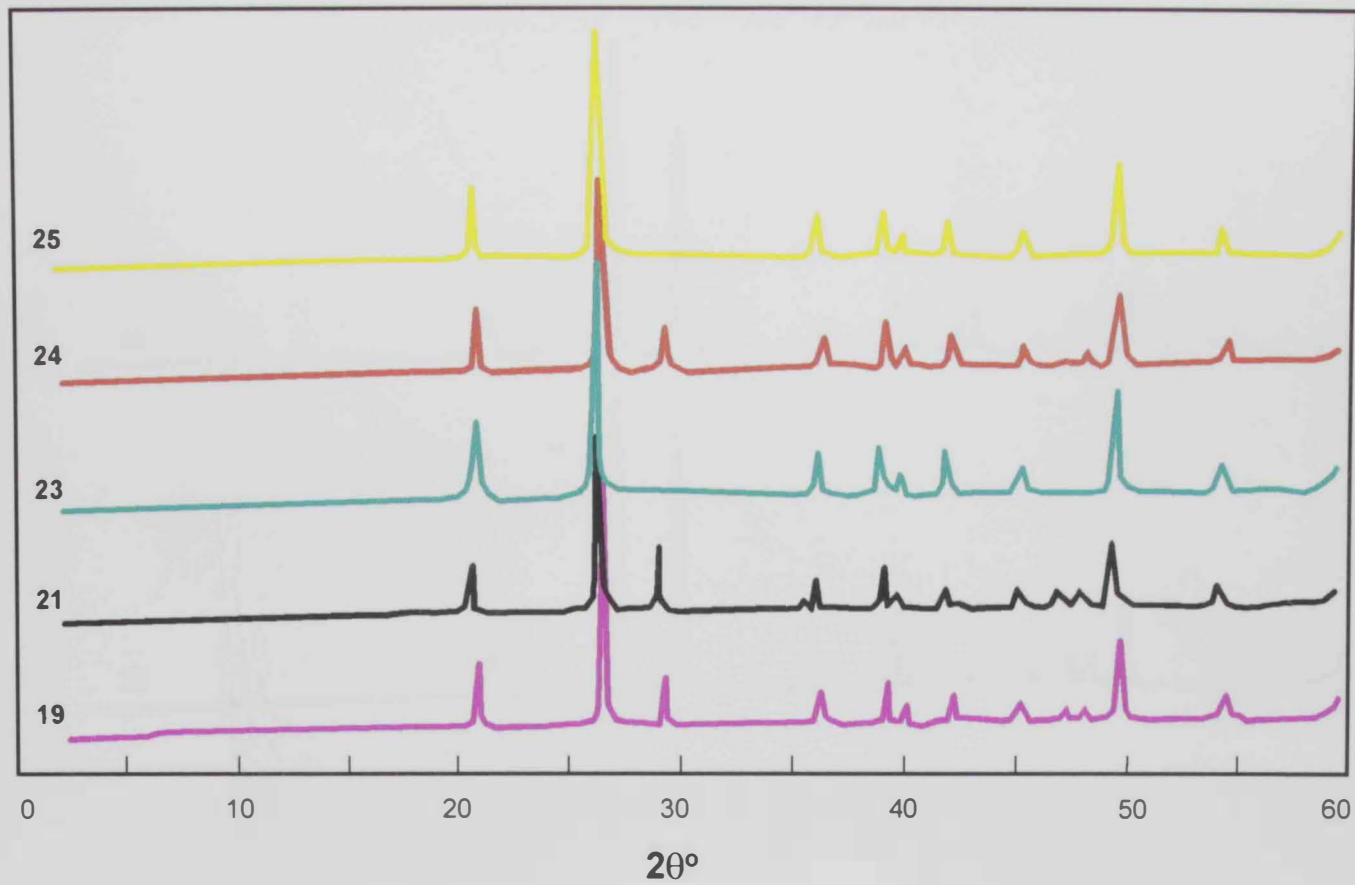


Fig. 4.3: X-ray diffraction patterns of Saram chert samples

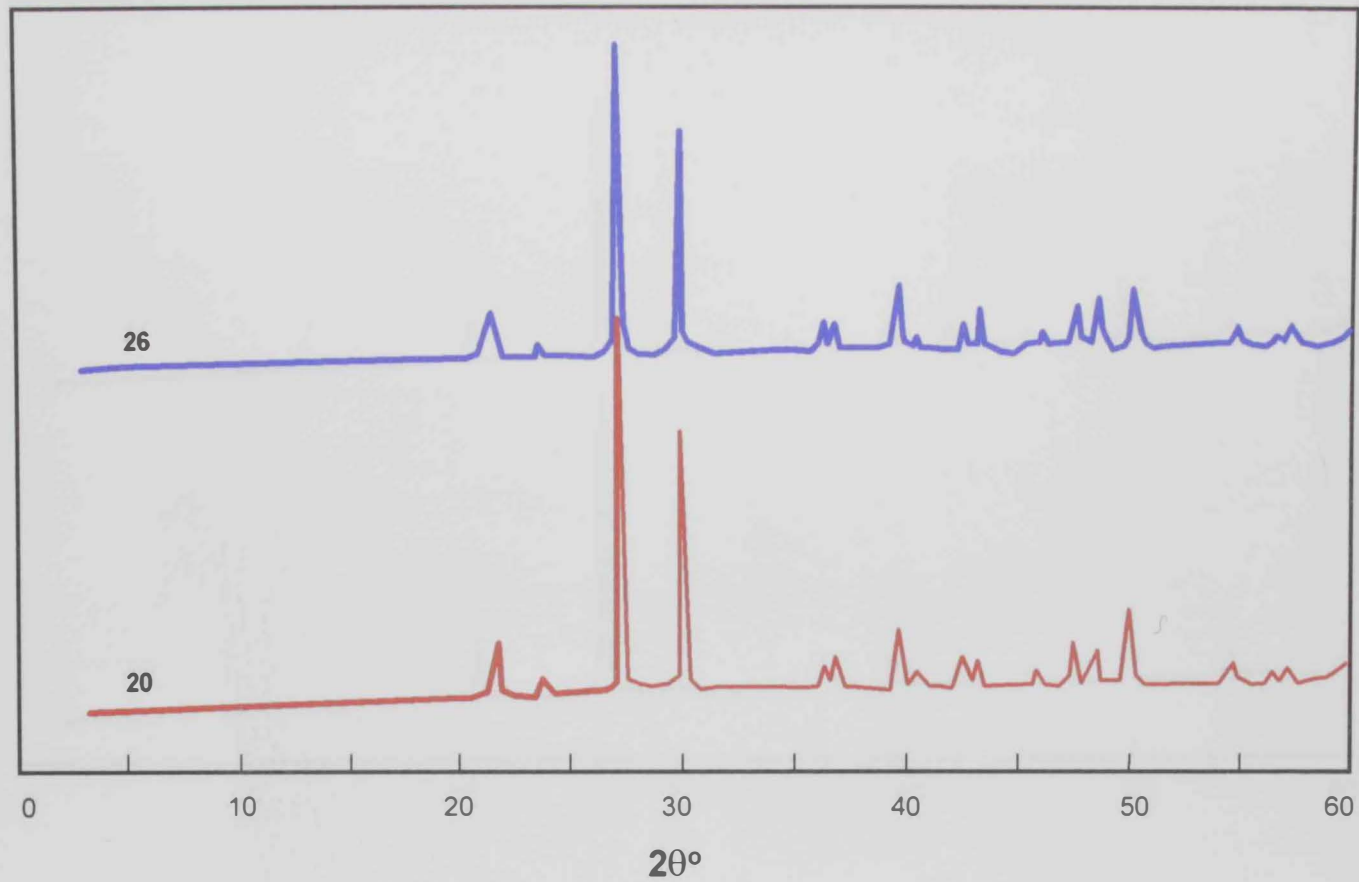


Fig. 4.3 (Cont.): X-ray diffraction patterns of Saram chert samples

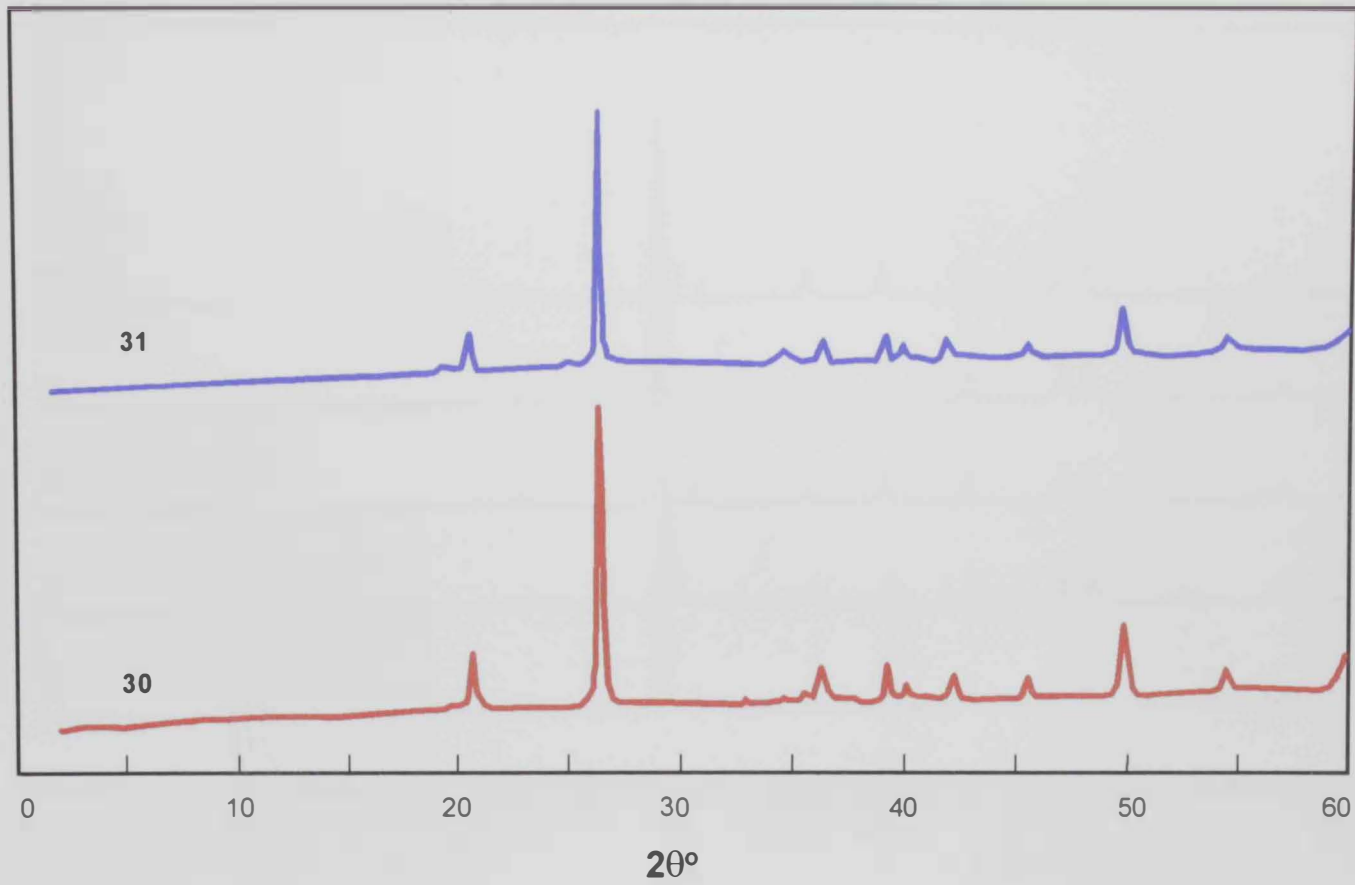


Fig. 4.4: X-ray diffraction patterns of Al Rams chert samples

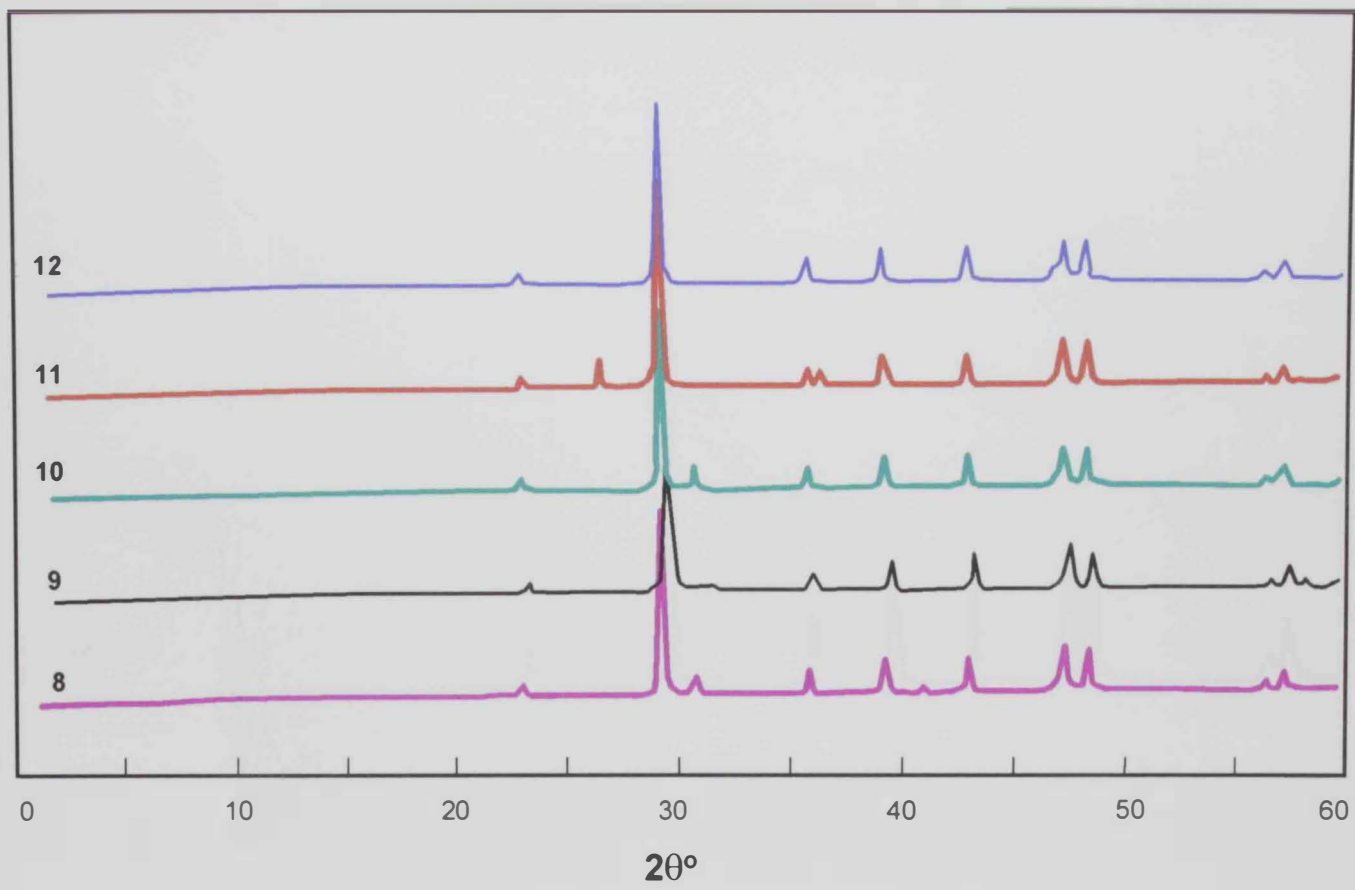


Fig. 4.5: X-ray diffraction patterns of Idan carbonate samples

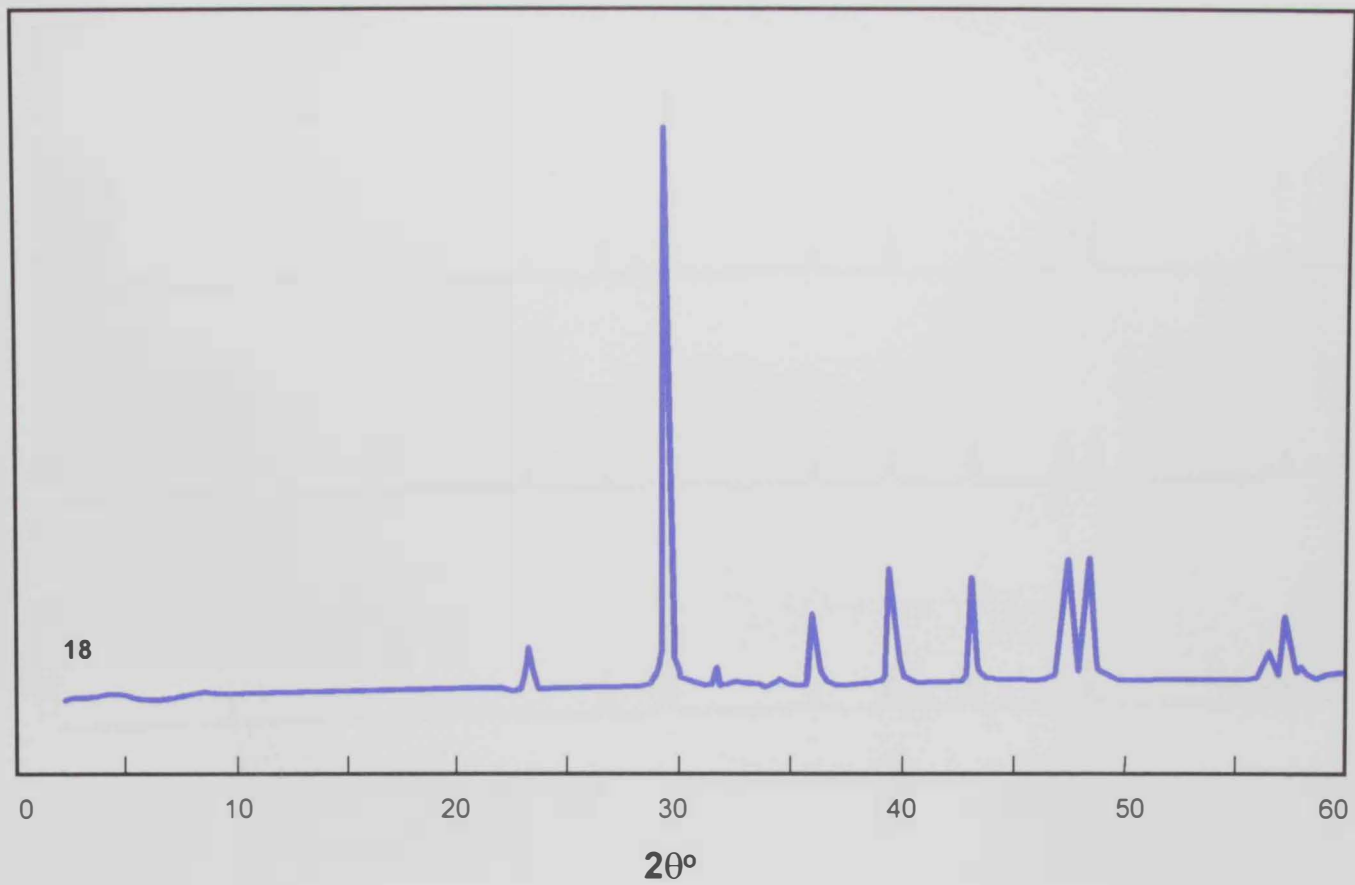


Fig. 4.6: X-ray diffraction patterns of Al Gail carbonate sample

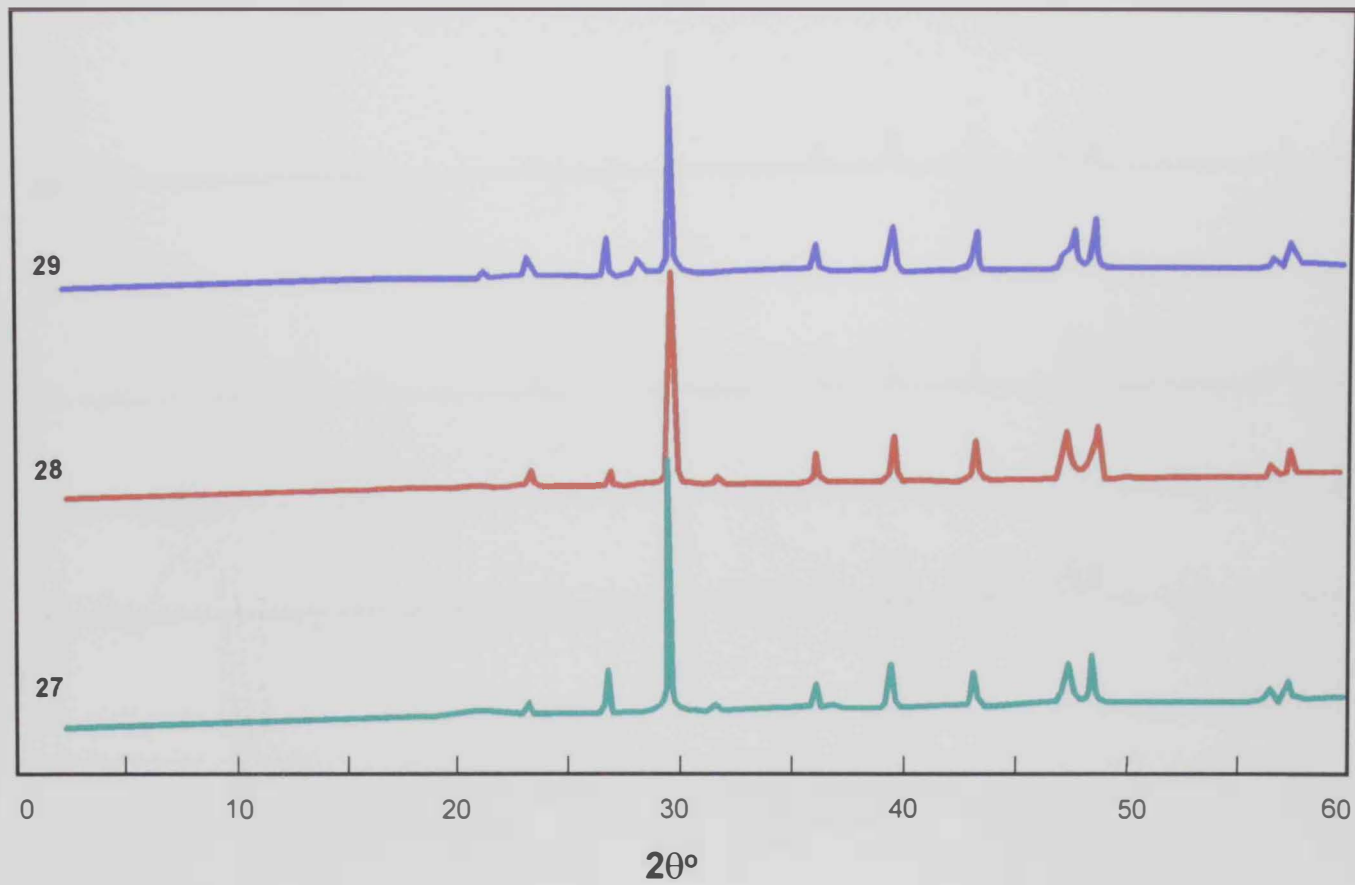


Fig. 4.7: X-ray diffraction patterns of Saram carbonate samples

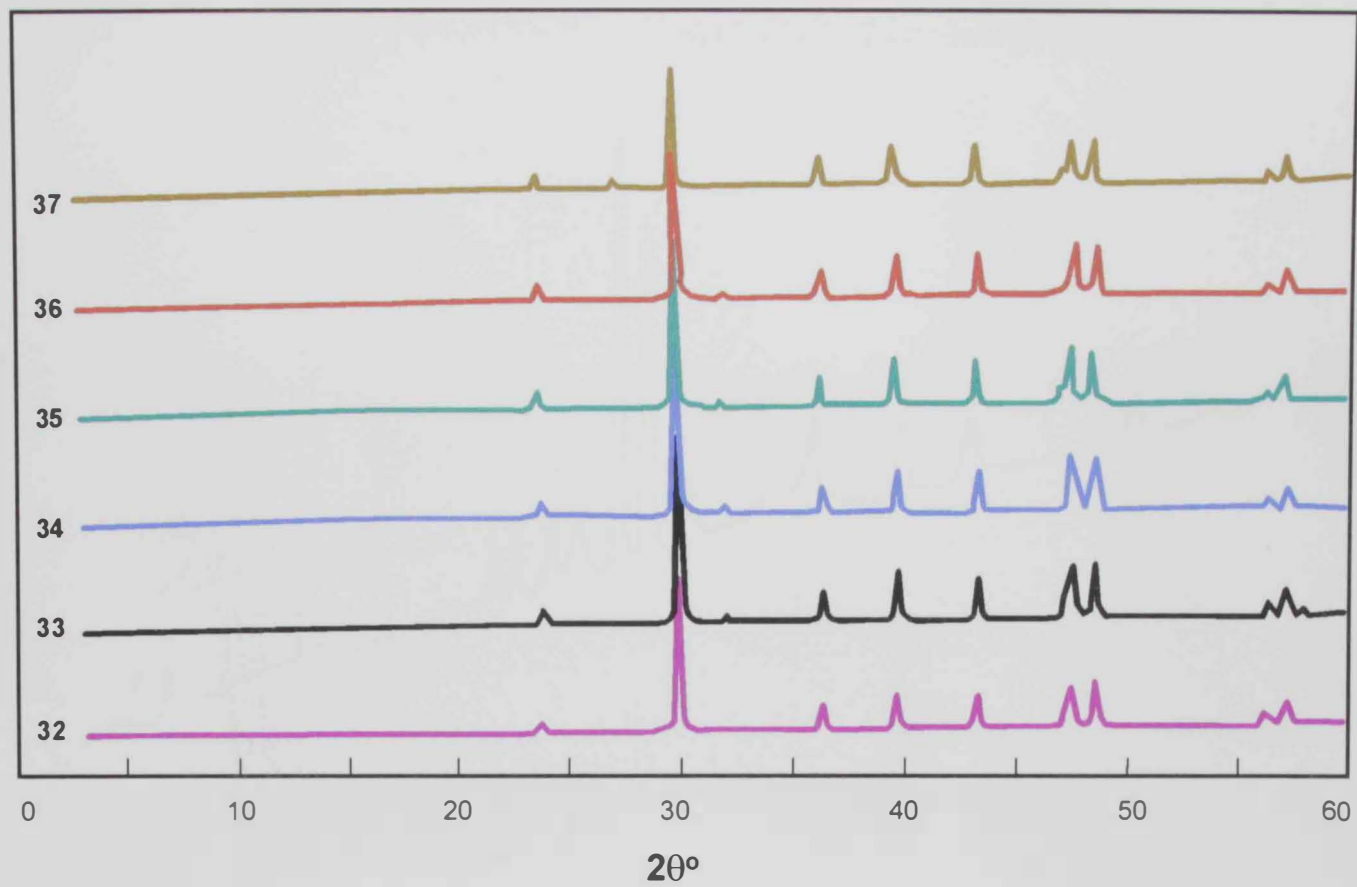


Fig. 4.8: X-ray diffraction patterns of Khor Khowair carbonate samples

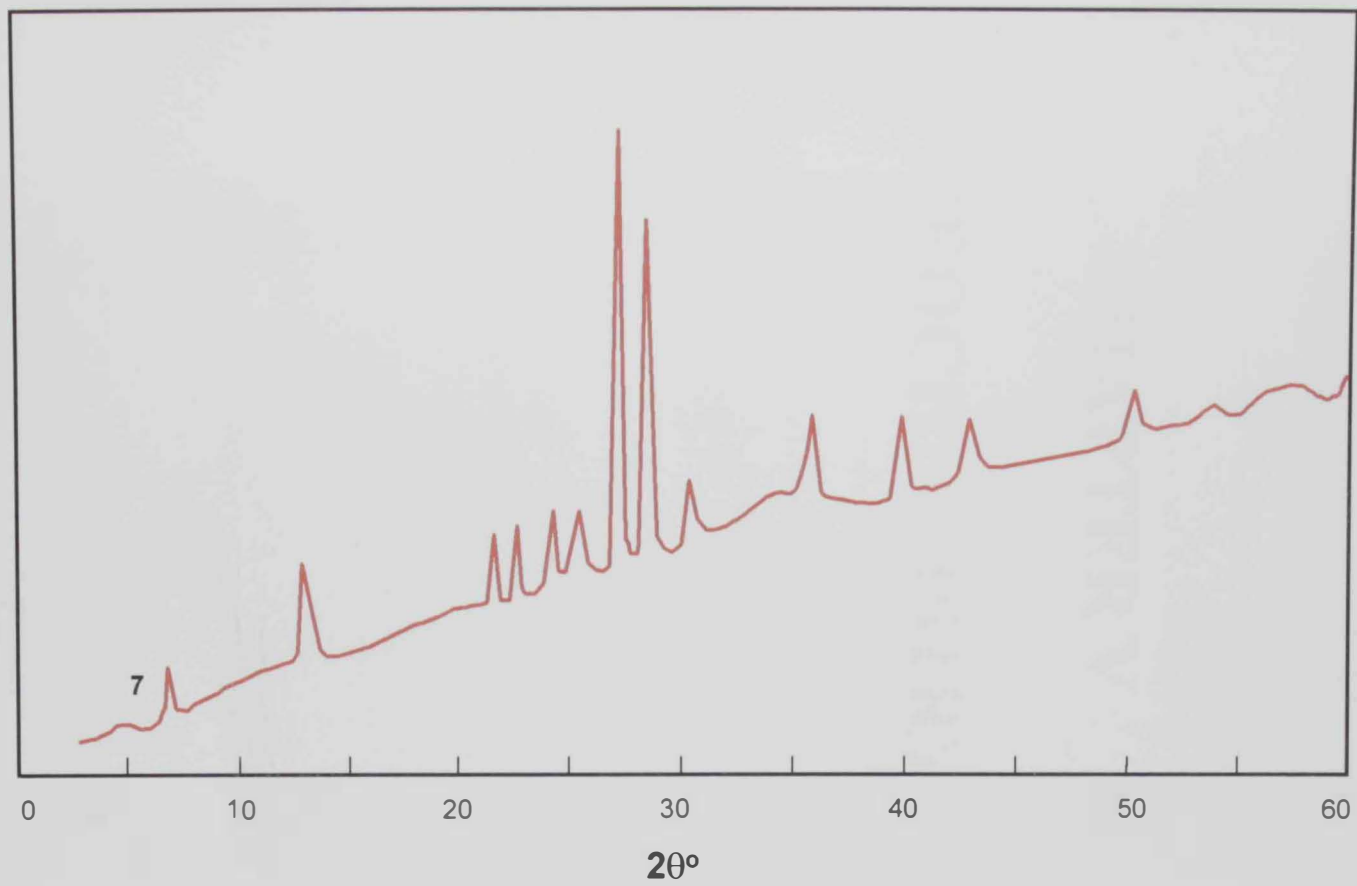


Fig. 4.9: X-ray diffraction patterns of Idan diabase sheet sample

CHAPTER V

GEOCHEMISTRY

CHAPTER V

GEOCHEMISTRY

The geochemical data obtained for the studied rocks are given in Tables (5.1) and (5.2). These data are in accordance with those obtained from petrographic investigation and XRD analysis and indicate that the studied chert can be classified into three lithologic groups; namely: i) red ribbon radiolarian cherts (or radiolarites, R), ii) calcareous chert (CC), and iii) siliceous mudstones (SM). These lithologic groups constitute alternating beds of different relative abundances and thicknesses within the studied chert sequences. For example, SM and R are markedly abundant, whereas CC is rare in Idan exposures. The exposures at Wadi Saram are characterized by the common occurrence of alternating beds of CC and R; the abundance of the latter lithology increases upwards in the section. On the other hand, Al Rams sections are characterized by the dominance of SM. It is worthy to mention that the chert sequences at Idan and Al Rams are highly dismembered and tectonized, and hence, it was difficult to sample a complete sequence. However, a well-developed chert sequence is exposed at Wadi Saram and, therefore, was used as the main site of sampling in order to assess the vertical variation in element concentrations within this sequence.

5.1 Distribution of Elements

5.1.1 Major Elements

The concentrations of the major elements in the studied rocks (Table 5.1) show marked variations from one area to the other. This could be attributed largely to differences in the relative abundances of the various rock lithologies among these areas taking into consideration the fact that comparable rock lithologies in the three areas show closely

Table (5.1) Major and Minor elements composition of the various rock types and sand dunes.

Area	Chert Samples																Limestone Samples								Sand Dunes		
	Idan						Al Gail				Saram				Al Rams		Idan	Khor Khowair		Al Gail	Saram		Al Gail	Al Helailah	Al Jazeerah		
	SM	R	CC	R	CC	SM	SM	CC	R	R	CC	CC	R	R	SM	SM											
Sample No Elements	1	2	3	4	5	6	13	14	15	16	17	20	21	22	30	31	8	32	33	36	18	28	29	38	39	40	
SiO ₂	77.10	93.34	48.52	89.89	63.60	87.00	78.51	73.62	96.38	96.44	70.29	71.80	98.00	92.93	85.49	71.24	0.02	0.04	0.06	0.33	0.02	7.45	14.45	57.81	34.17	48.97	
Al ₂ O ₃	7.75	2.01	3.33	1.81	2.91	4.02	8.09	2.16	0.38	0.39	2.39	1.03	0.32	0.88	5.02	11.10	0.64	0.76	0.61	0.70	0.68	2.09	5.58	3.12	1.58	4.41	
Fe ₂ O ₃	5.65	1.80	1.74	1.40	1.35	3.16	4.12	1.39	0.89	0.90	1.44	1.39	0.72	1.13	3.09	4.05	0.04	0.13	0.04	0.20	0.09	0.72	0.99	2.01	0.89	1.82	
Fe ₂ O ₃ (H)*	3.39	-	-	-	-	1.90	2.48	-	-	-	-	-	-	-	1.86	2.43	-	-	-	-	-	-	-	-	-	-	-
MgO	1.50	0.45	0.99	1.35	6.32	1.21	1.43	0.81	0.09	0.09	1.55	0.31	0.05	0.38	1.18	2.41	1.53	0.58	0.23	0.50	0.27	1.14	0.96	4.28	1.69	2.42	
CaO	0.45	0.22	22.98	1.37	9.25	0.48	0.50	11.32	0.79	0.80	11.47	13.07	0.26	2.13	0.33	0.47	54.24	54.53	55.47	54.38	55.22	47.93	43.07	15.35	31.48	21.14	
Na ₂ O	0.19	0.09	0.05	0.30	0.39	0.10	0.78	0.08	0.07	0.07	0.10	0.05	0.03	0.03	0.42	0.70	0.01	0.01	0.01	0.01	0.01	0.21	0.59	0.46	0.29	0.53	
K ₂ O	1.99	0.40	0.58	0.37	0.63	0.43	2.10	0.34	0.05	0.05	0.37	0.09	0.07	0.10	0.75	2.39	0.04	0.05	0.04	0.04	0.04	0.04	0.11	0.75	0.34	0.82	
TiO ₂	0.57	0.11	0.18	0.09	0.18	0.24	0.46	0.12	0.05	0.05	0.16	0.05	0.02	0.06	0.28	0.78	0.01	0.01	0.01	0.01	0.02	0.07	0.15	17.00	0.15	0.23	
P ₂ O ₅	0.11	0.01	0.02	0.06	0.08	0.02	0.16	0.14	0.04	0.06	0.07	0.02	0.02	0.05	0.06	0.11	0.01	0.02	0.02	0.01	0.01	0.07	0.02	0.01	0.06	0.01	
MnO	0.39	0.29	0.14	0.01	0.09	0.01	0.09	0.07	0.02	0.02	0.12	0.18	0.01	0.04	0.04	0.08	0.02	0.01	0.01	0.01	0.01	0.16	0.30	0.03	0.02	0.04	
L.O.I	4.20	1.30	21.40	3.30	15.20	3.10	3.60	10.20	1.10	1.00	12.10	12.00	0.50	2.30	3.30	6.80	43.40	43.60	43.40	43.70	43.60	40.00	36.80	15.70	28.5	20.50	
Tot/c	0.01	0.04	5.60	0.49	3.62	0.07	0.05	2.57	0.21	0.20	2.93	3.35	0.06	0.51	0.05	0.08	12.23	12.13	12.13	12.32	12.23	11.12	10.48	3.70	7.60	5.15	
Tot/s	0.01	0.01	0.01	0.01	0.16	0.01	0.01	0.01	0.01	0.01	0.03	0.11	0.02	0.01	0.01	0.01	0.02	0.02	0.01	0.02	0.02	0.04	0.04	0.10	0.07	0.01	
Sum	99.94	100.07	99.94	100.03	100.04	99.82	99.88	100.30	99.69	99.97	100.13	100.05	100.1	100.11	100.0	100.17	99.89	99.73	99.83	99.86	99.93	99.88	100.04	99.89	99.0	100.8	

* Calculated Hematite

SM = Siliceous mudstone

R = Radiolarite

CC = Calcareous chert

similar compositions. Silica concentration is quite constant throughout most of the sections in the three areas. R beds contain 90 – 98 % SiO₂, and SM beds have 71-87% SiO₂. However, CC beds show much lower SiO₂ content (49% to 72%) which may reflect the dilution effect of carbonates and, to a lesser extent, the contributions from detrital clay sources. It has often been suggested that cherts overlying ophiolites might contain a direct component of volcanic-hydrothermal silica (Barrett, 1981). However, the lack of silica enrichment in cherts near the ophiolitic basement precludes a significant contribution from a hydrothermal source.

The relatively high abundance of Fe, particularly in SM samples from Idan and Al Rams, can be attributed to proximity to the ophiolitic outcrops. Iron is dominantly present as hematite and also in detrital clays. The contribution of iron from detrital clays can be estimated using the average Fe₂O₃ / Al₂O₃ ratio which is about 0.4:1 for pelagic clays (average for Pacific Clays is 0.41:1; Conan, 1976; and average for SM beds in Apennines, Italy is 0.38:1; Barrett, 1981). This ratio is multiplied by the total iron content and the obtained value is subtracted from total Fe₂O₃ to give the Fe₂O₃ present as hematite. As shown in Table (5.1), the calculated hematite is relatively high in the majority of SM samples from the three studied areas. This Fe enrichment can be attributed to the discharge of hydrothermal solutions at the spreading axis which results in the precipitation of Fe-hydroxides (cf. Bostrom, 1973; Dymond *et al*, 1973). Hematite is formed in a later phase by dehydration of Fe-hydroxides during diagenesis (Bischoff, 1969).

Major element variations within the Wadi Saram sequence show regular and consistent trends. Al₂O₃ and TiO₂ decrease regularly upwards in the section (Table 5.1). Most of the previous workers on chert sequences from various Mesozoic orogenic belts elsewhere in the world have found that Al can be attributed almost entirely to a detrital source (cf. Bostrom and Peterson, 1969; Steinberg and Marin, 1978; Karl, 1984). They

emphasized that aluminum to metal ratios are useful in discriminating sediment sources. Moreover, due to the immobility and the low solubility of Ti with respect to the hydrothermal elements, it has not been considered significant in hydrothermal, biogenic, authigenic, or residual sediments (Bostrom *et al*, 1971). Thus, as in the case of Al, Ti is considered to represent a terrigenous source component (including volcanic ash) (Karl, 1984). The terrigenous source for both Al and Ti could be confirmed by the significant positive correlation between the two elements in the studied cherts (Fig. 5.1). Bostrom and Peterson (1969) showed that a value of less than 0.4 for the ratio $Al / (Al+Fe+Mn)$ is indicative of transition metal enrichment by hydrothermal processes. The majority of the studied cherts have $Al / (Al+Fe+Mn)$ ratios >0.4 . The plot of this ratio versus Ti (Fig. 5.2) reveals that all the R, SM and CC samples from both Idan and Al Rams have important contributions from terrigenous sources in their genesis. However, the R samples from Wadi Saram, which are exposed in the upper part of the section occurring up-section, have $Al / (Al+Fe+Mn)$ ratios < 0.4 reflecting a pelagic domain during sedimentation. Thus, there is a change up-section in Wadi Saram, from a setting with predominantly terrigenous influence to a setting of pelagic deposition. Bostrom (1973) developed a diagram for representing the relative contributions of terrigenous (Al, Fe, Ti) and hydrothermal (Fe, Mn) components in pelagic sedimentation based on the relation between $Al / (Al+Fe+Mn)$ vs Fe/Ti . Fig. 5.3 shows that most of the SM samples from the studied areas fall close to the ideal mixing curve between hydrothermal metalliferous sediments (as defined on the East Pacific Rise) and average terrigenous matter. The SM and CC samples overlap and cluster around the composition of typical pelagic clays and siliceous ooze. On the other hand, the R samples plot further to the left roughly parallel to the curve, and close to the biogenic matter composition (non-biogenic fraction is 20-50% hydrothermal). On the Ti –

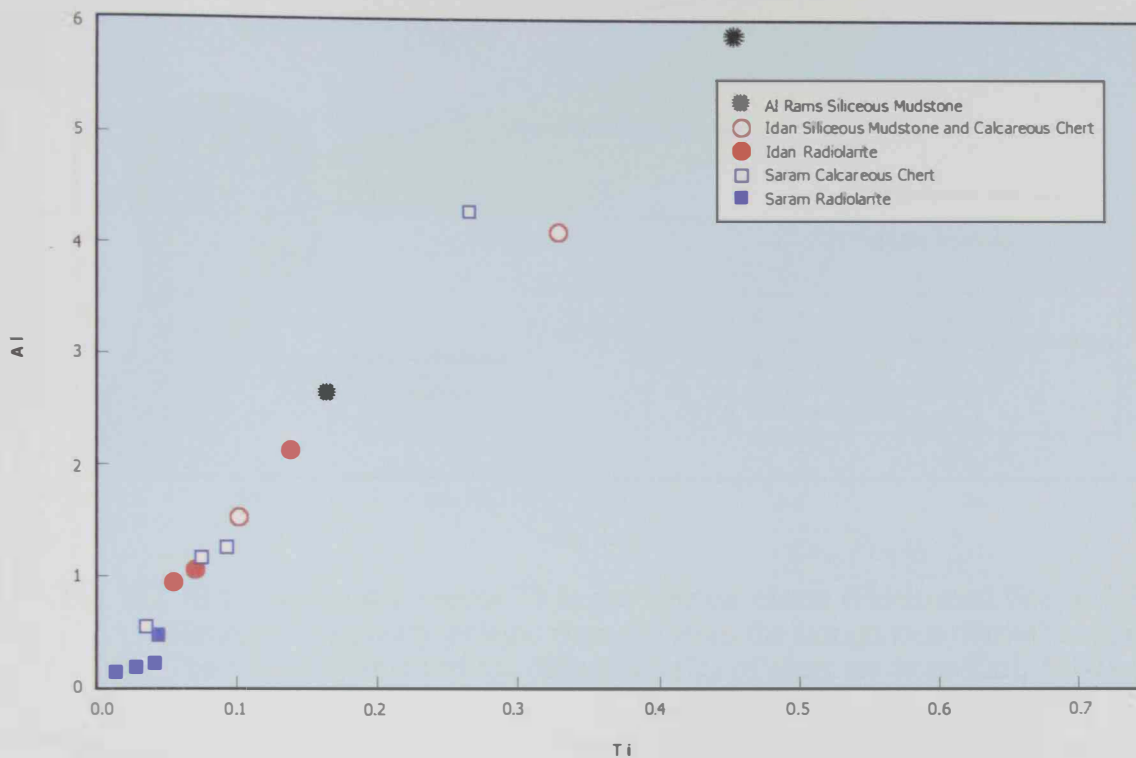


Fig. 5.1 A binary relationship of Al versus Ti for the studied cherts.

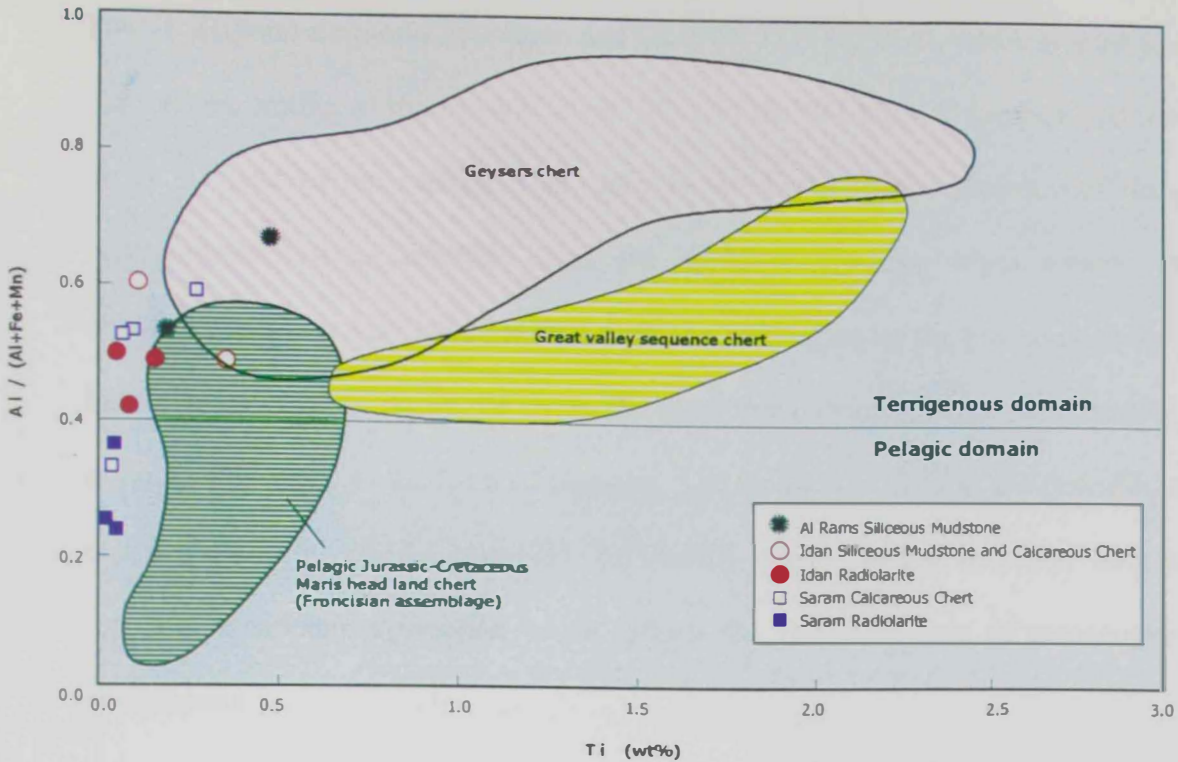


Fig. 5.2 Al to metal ratio versus Ti in the studied cherts (Horizontal line at 0.391 distinguishes purely pelagic deposits from the terrigenous detrital material. The boundary line and the different fields of chert are from Karl, 1984).

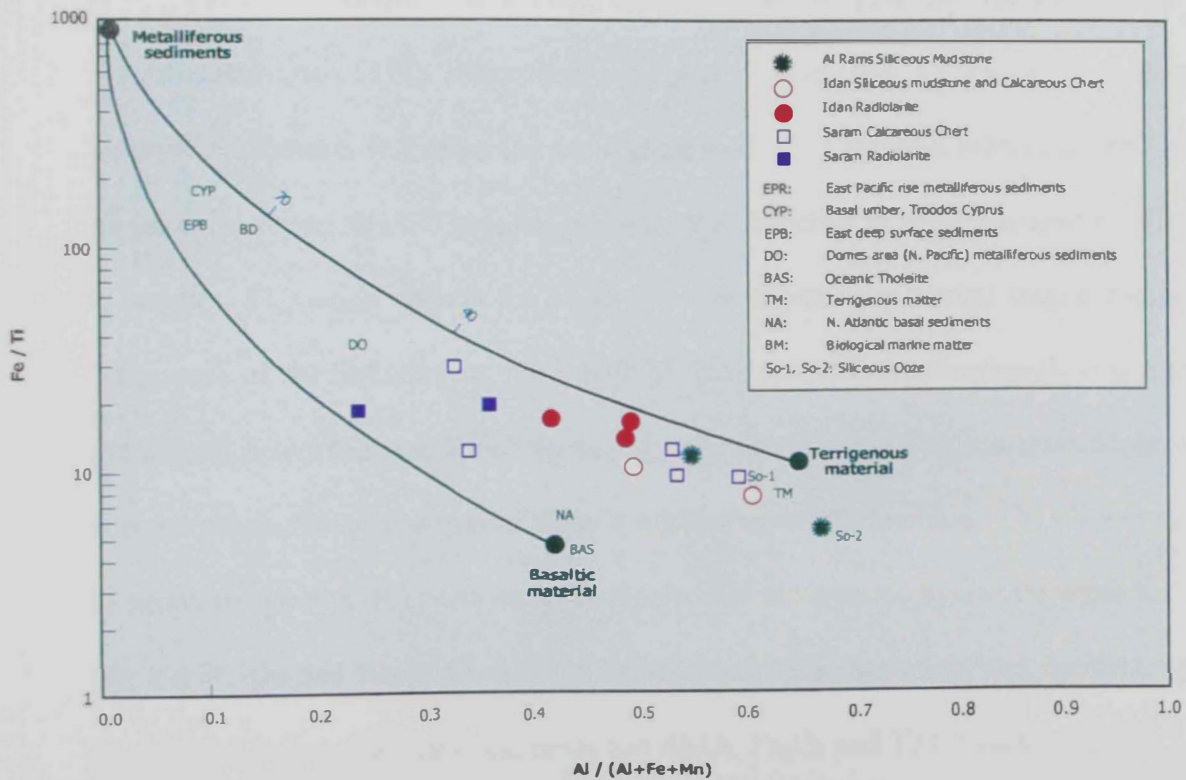


Fig. 5.3 Fe / Ti versus Al / (Al+Fe+Mn) for the studied cherts (Data points are after Barrett, 1981).

Zr – Y diagram proposed by Pearce and Cann (1973) (Fig. 5.4), which is used to identify the tectonic setting of the basaltic levels. Most of the SM and CC samples plot very close or in the field of arc basalts. This may be attributed to the presence of fine-grained volcanogenic detritus inherited from the mafic crust. Also, MgO content increases downwards, which may have resulted from the weathering of the basement rocks and the formation of chlorite. Again, Fe shows the same trend which reflects the increasing rate of accumulation of Fe in the form of hematite. The increase of K₂O at the base also signifies contribution from detrital materials, particularly clays. On the contrary, SiO₂ contents increase remarkably up-section which reflects the decreased role of terrigenous source components.

5.1.2 Trace elements

Table 5.2 presents the average trace-element compositions for the studied cherts. The concentration of HFS (High Field Strength) elements (e.g. Zr, Ga) and LIL (Large Ion Lithophile) elements (e.g. Rb, Th) are highest in the SM samples relative to the CC and R samples. However, the CC samples are still more enriched in these elements relative to the R samples. This again reflects the important role played by a detrital source component in the genesis of the SM samples since most of these elements are dominantly concentrated in the detrital heavy minerals (such as zircon and hematite) and clay minerals. Moreover, the concentrations of these elements show a gradual upwards decrease in Wadi Saram section in which the pelagic R cherts exist. A dominantly terrigenous source for elements such as Nb, Zr, Y, Ga and Rb in the studied cherts could be indicated by the significant positive correlations between all these elements and Al₂O₃, Fe₂O₃ and TiO₂ (Tables 5.3 and 5.4).

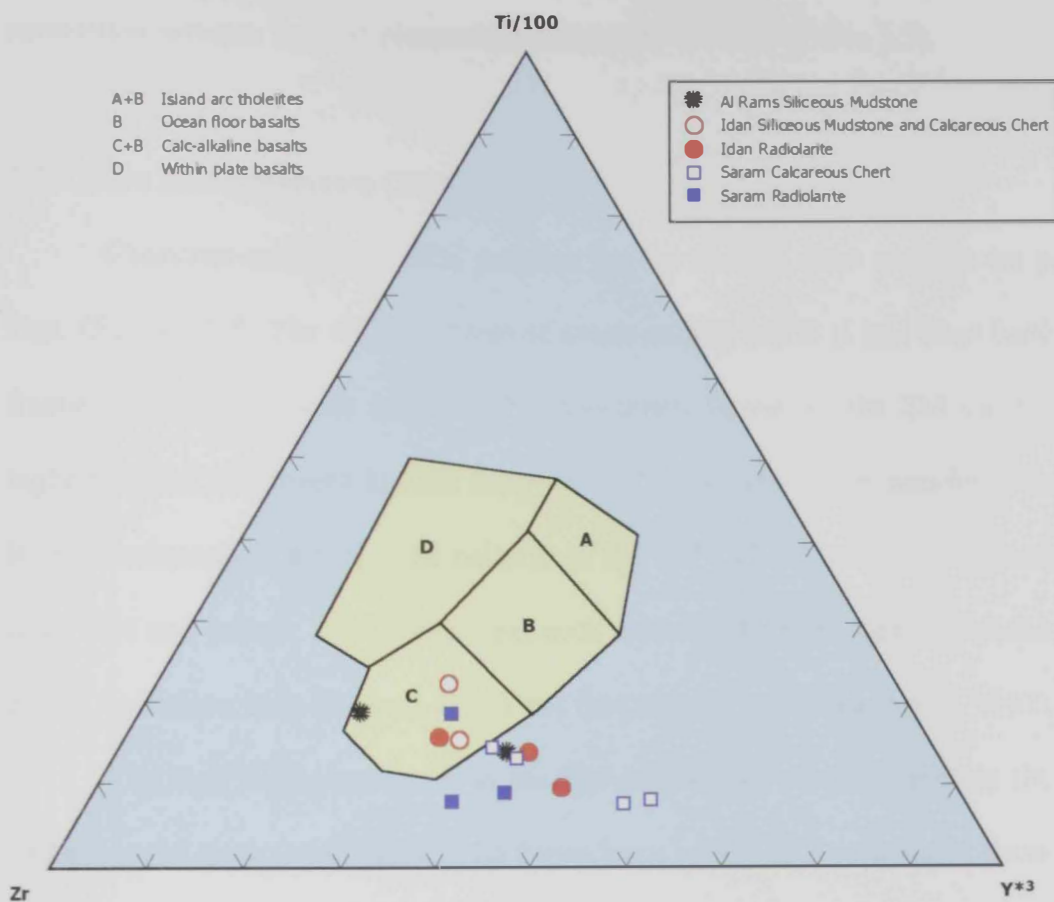


Fig. 5.4 Plot of Ti/100, Zr & Yx3 for the studied cherts (diagram adopted by Pearce & Cann, 1973).

The concentration of Sr shows the highest levels in the CC samples. This can be attributed to the substitution of Sr for Ca in calcite as indicated by the significant positive correlation between the two elements as will be shown later (Table 5.5).

5.1.3 Rare Earth Elements (REE)

Chondrite-normalized REE patterns for the studied chert samples are presented in Figs. (5.5) to (5.7). The different types of cherts exhibit LREE (Light Rare Earth Elements) fractionated patterns with moderate Eu anomalies. However, the SM samples show the highest overall enrichment in REE followed by the CC whereas R samples have the lowest REE abundances. (Fig.5.7). The patterns of the SM and CC samples are closely similar to other SM and pelagic clays worldwide, such as the SM of the Jurassic bedded chert from North Apennines, Italy (Barrett, 1981) and the pelagic clays (Haskin *et al*, 1968).

The high REE abundances in the SM samples are clearly related to the dominance of intermixed clays and hematite. The dependence of the REE contents in these samples on the terrigenous materials is manifested by the significant positive correlation between all REE and Al_2O_3 , Fe_2O_3 , K_2O and P_2O_5 . Again, this positive correlation is depicted in the binary variation plots between the Total REE (ΣREE) and the major oxides that signify a terrigenous source component such as Al_2O_3 , Fe_2O_3 , TiO_2 , and K_2O (Figs. 5.8 to 5.11), together with some trace elements that are mainly concentrated in detrital minerals such as Zr (Fig. 5.12). On the other hand, the relationships between the ΣREE and each of SiO_2 and CaO show no obvious correlation (Figs. 5.13 and 5.14).

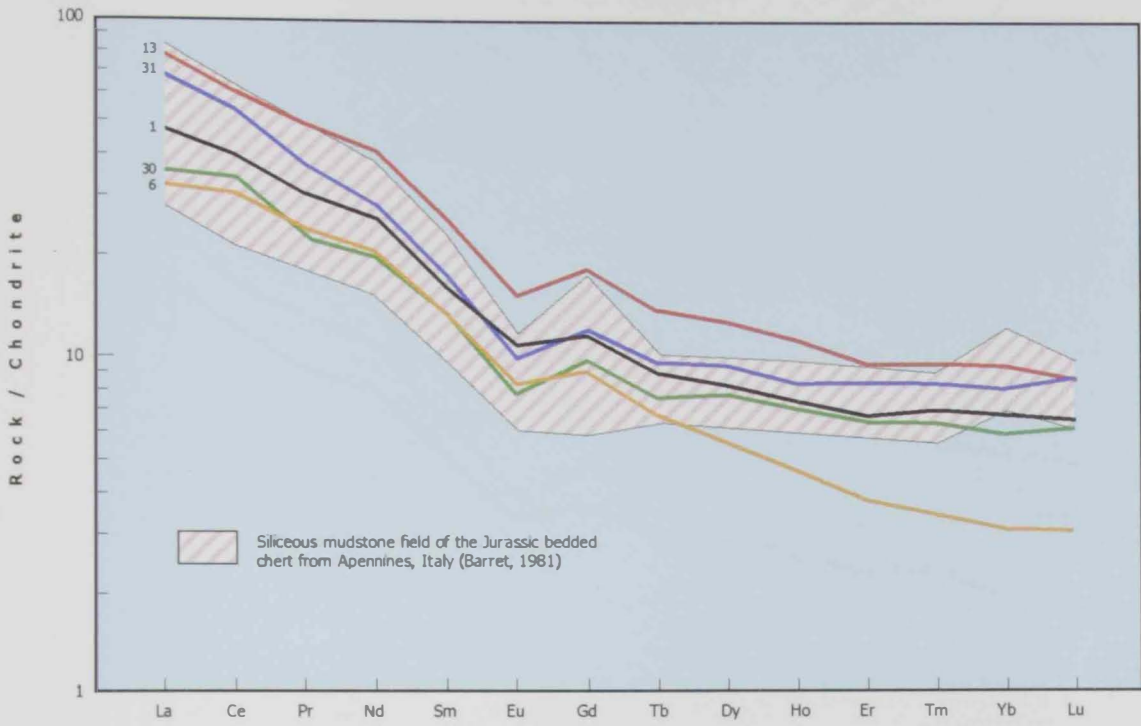


Fig. 5.5 Chondrite-normalized REE patterns for the siliceous mudstones.

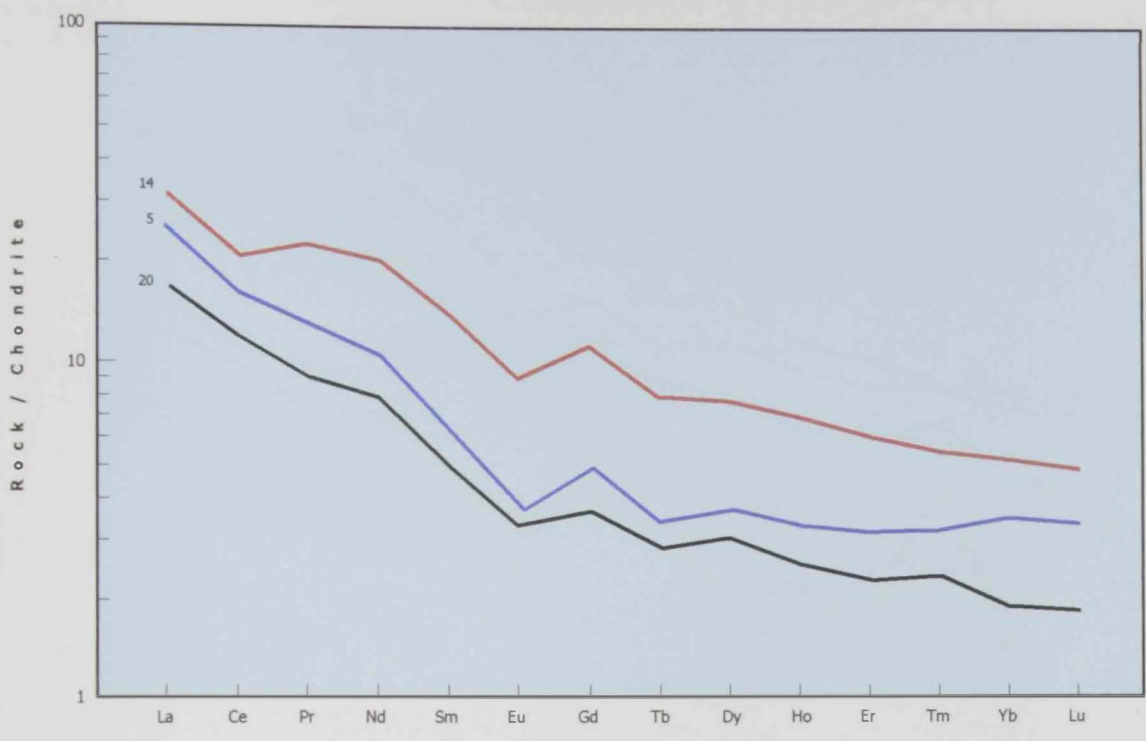


Fig. 5.6 Chondrite-normalized REE patterns for the calcareous cherts.

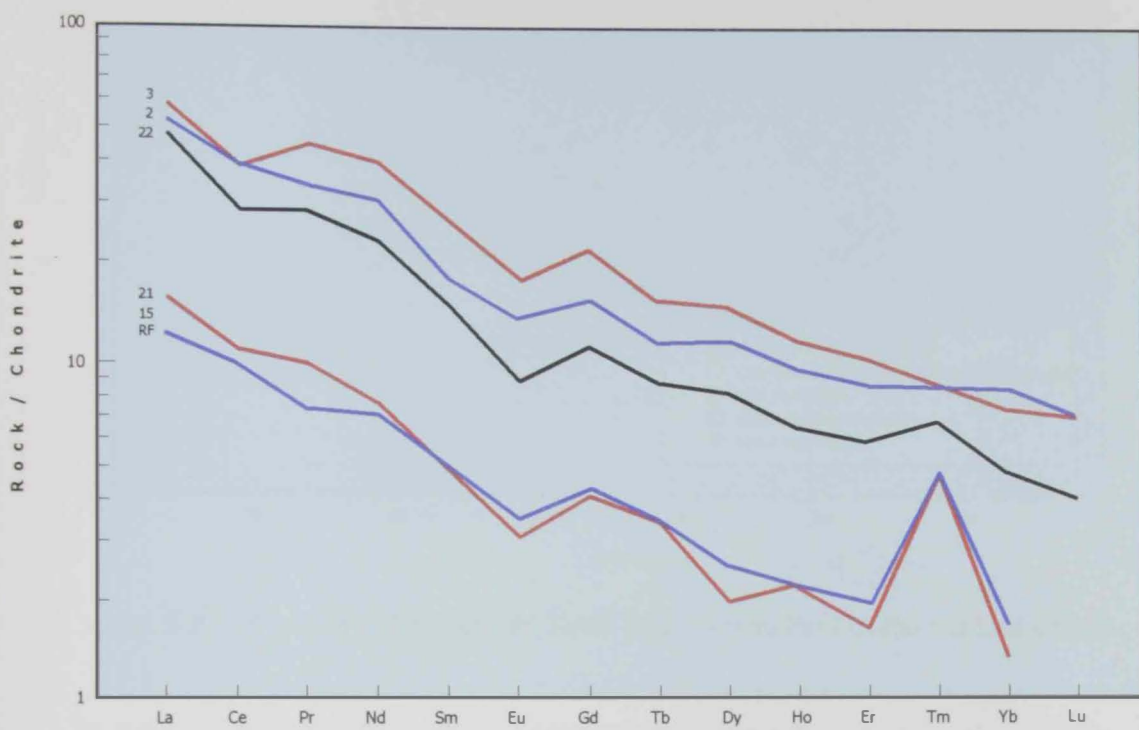


Fig. 5.7 Chondrite-normalized REE patterns for the radiolarites.

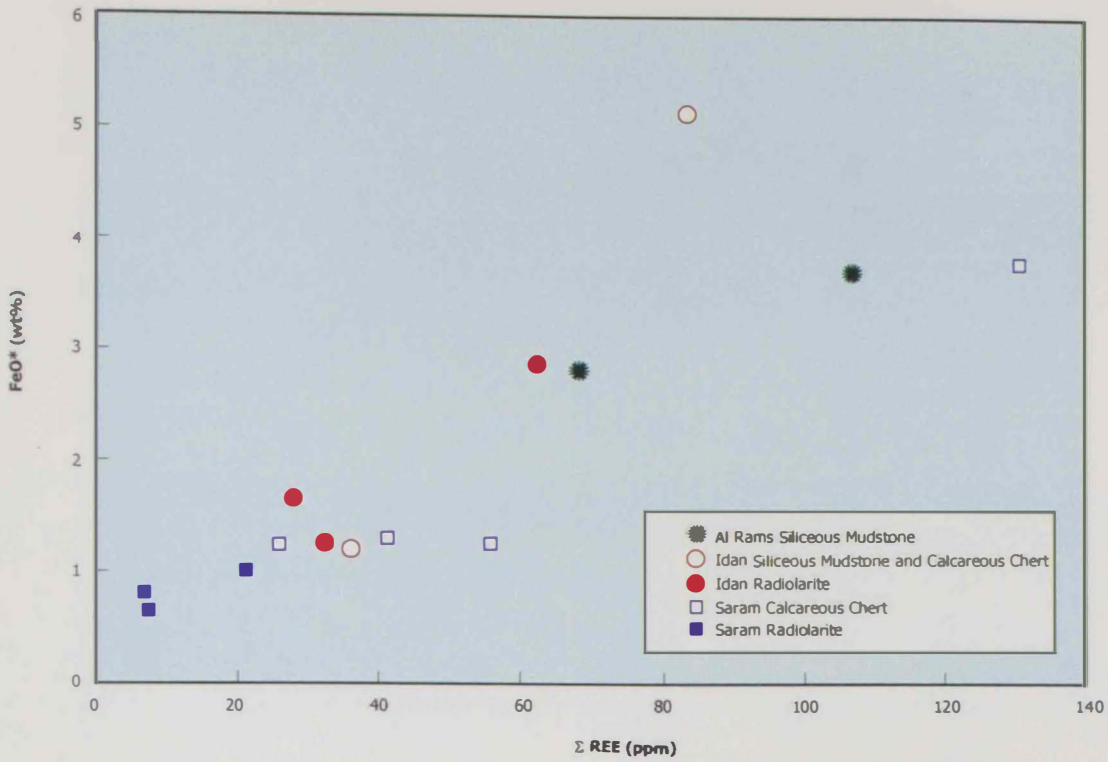


Fig. 5.8 A binary relationship of Total REE versus FeO in the studied cherts.

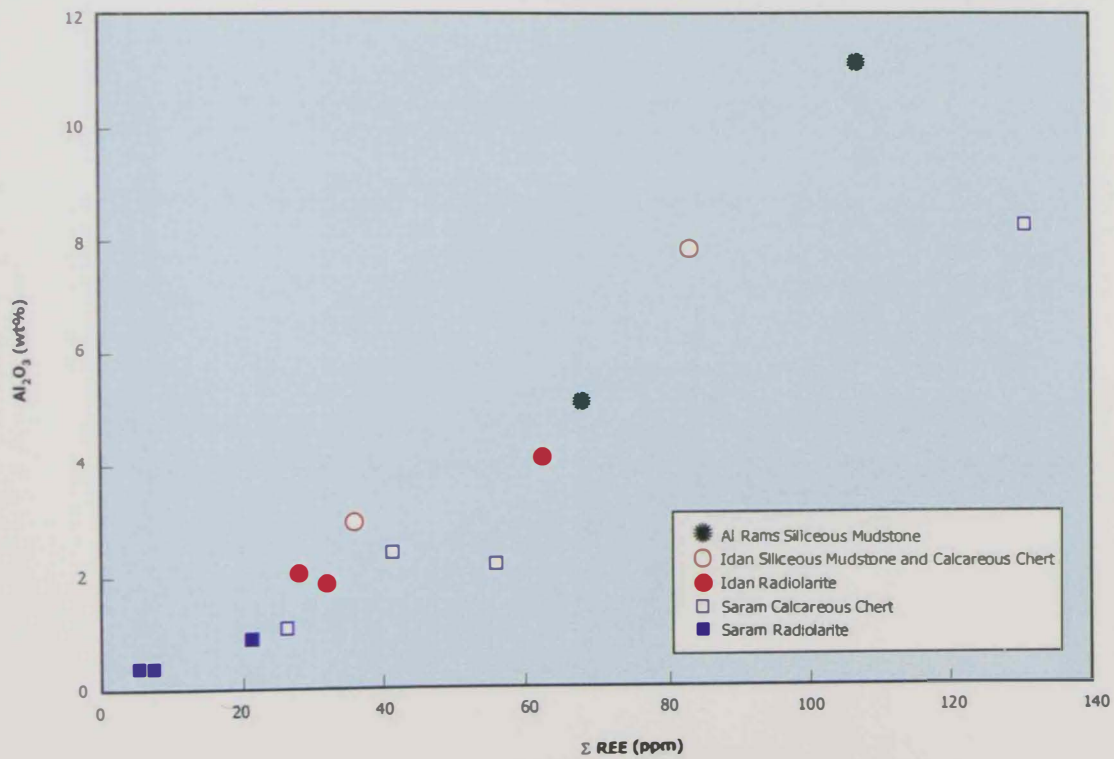


Fig. 5.9 A binary relationship of Total REE versus Al₂O₃ in the studied cherts.

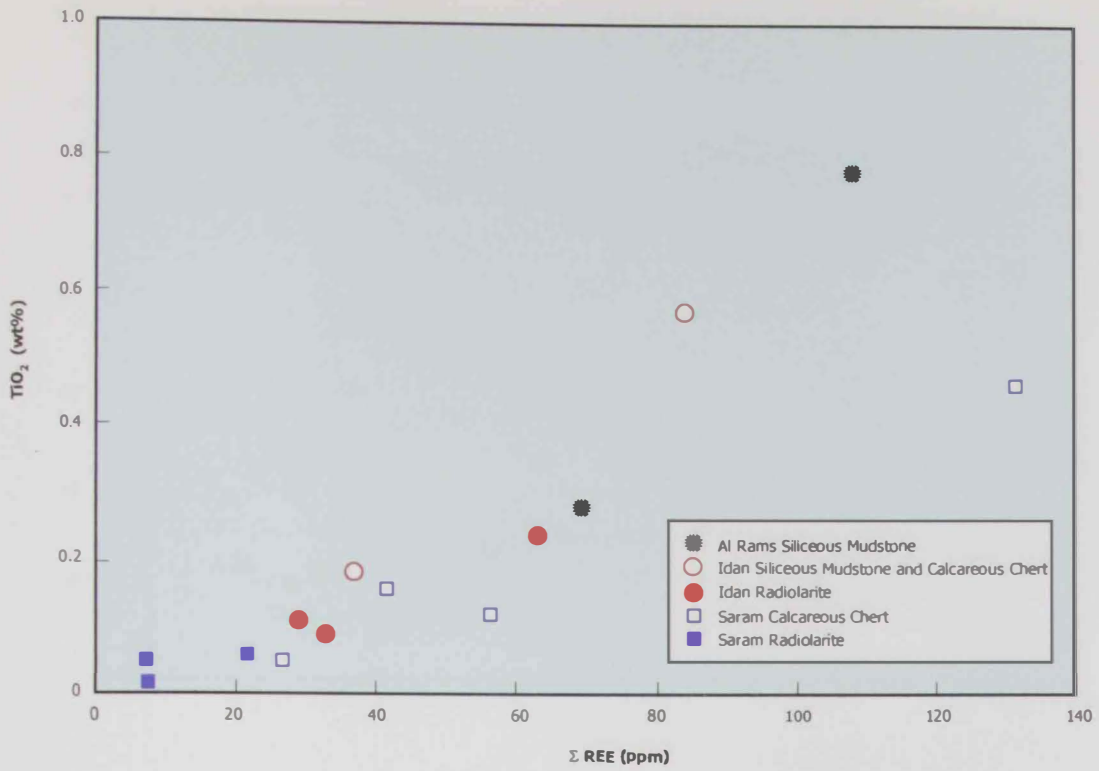


Fig. 5.10 A binary relationship of Total REE versus TiO₂ in the studied cherts.

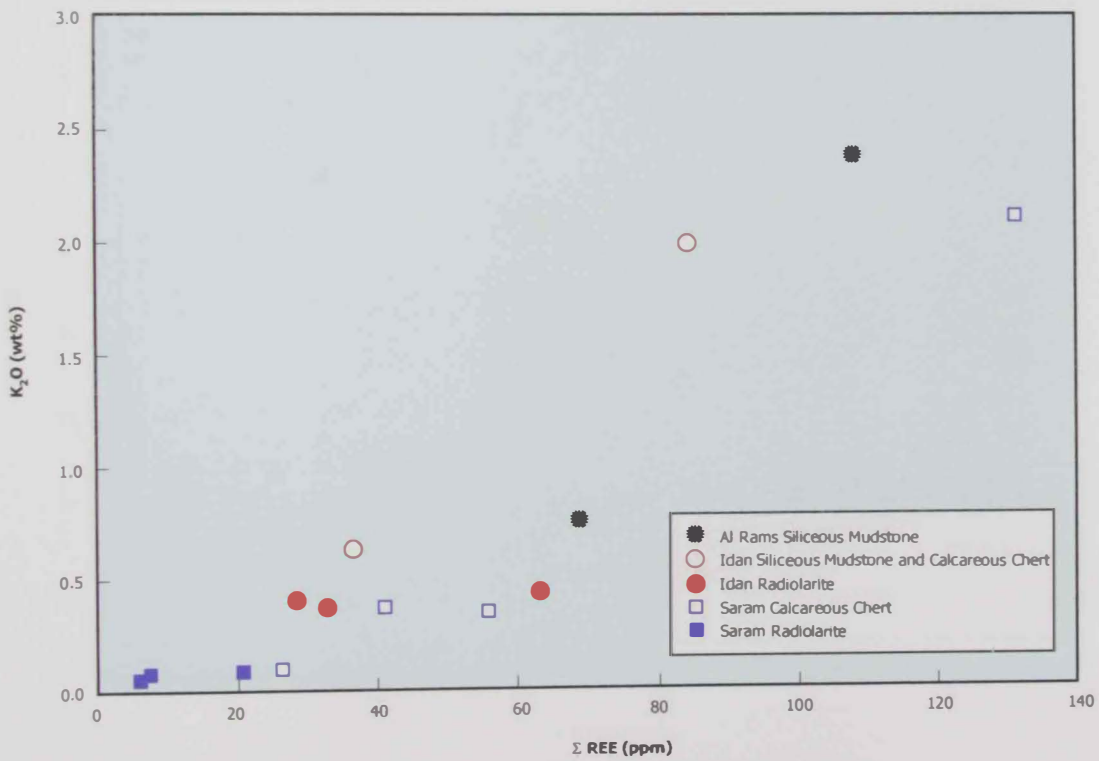


Fig. 5.11 A binary relationship of Total REE versus K₂O in the studied cherts.

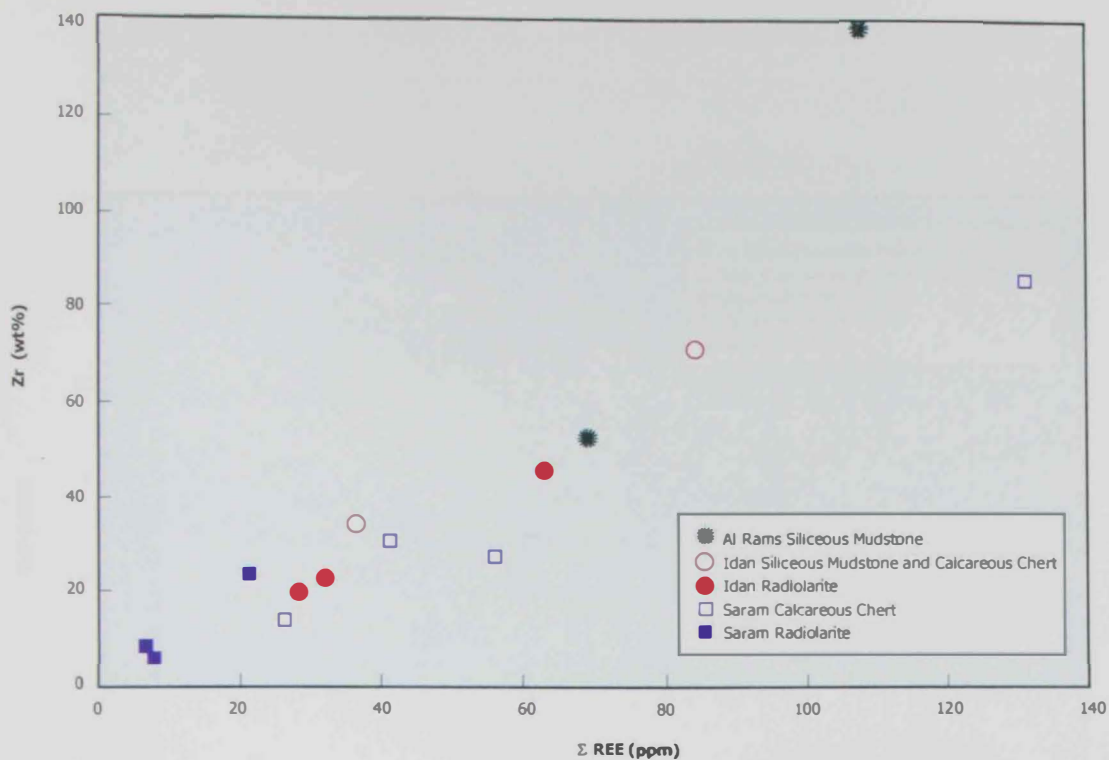


Fig. 5.12 A binary relationship of Total REE versus Zr in the studied cherts.

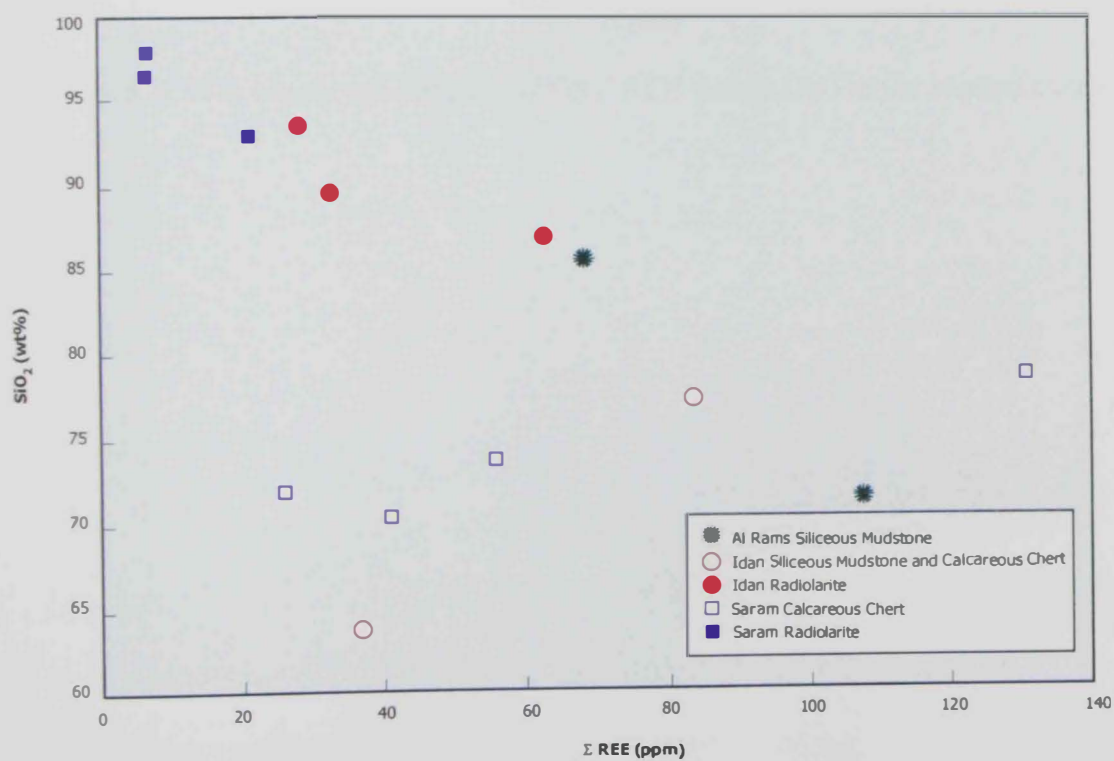


Fig. 5.13 A binary relationship of Total REE versus SiO₂ in the studied cherts.

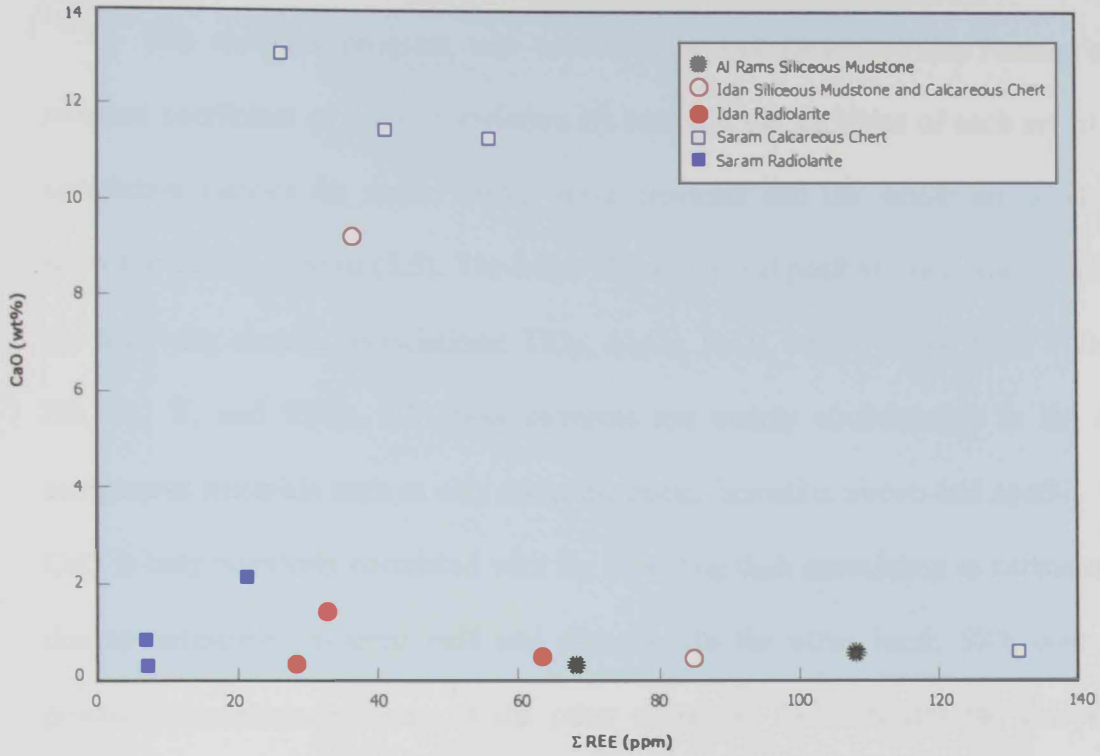


Fig. 5.14 A binary relationship of Total REE versus CaO in the studied cherts.

5.2. Multivariate Statistics

5.2.1 Correlation Coefficients

The statistica program was used for the calculation of the Pearson's product-moment coefficient of linear correlation (r) between the variables of each set of data. The correlation matrices for major oxides, trace elements and the whole set of elements are shown in Tables (5.3) to (5.5). The tables show that real positive correlations exist between the following element associations: TiO_2 , Al_2O_3 , FeO_2 , MgO , Na_2O , K_2O , P_2O_5 , Rb, Ga, Nb, Zr, Y, and REEs. All these elements are mainly concentrated in the detrital or terrigenous materials such as clay minerals, micas, hematite, zircon and apatite. Moreover, CaO is only positively correlated with Sr, reflecting their association in carbonate minerals due to similarities in ionic radii and charges. On the other hand, SiO_2 does not show positive correlation with any of the other elements. This indicates the independence of silica deposition to the other sources such as the terrigenous or the carbonate materials. The significant negative correlation between SiO_2 and each of CaO and Sr may be attributed to difference in depositional conditions, the diagenetic cementation with carbonate or replacement of silica by calcite.

5.2.2 Cluster Analyses

Cluster analysis is a multivariate technique extensively used by numerical taxonomists (Sokal and Sneath, 1963). It depends on sample being defined by a number of attributes or variables. A data matrix is obtained consisting of a number of samples with their corresponding set of coded or quantified characters. Similarly, coefficients are calculated between each pair of samples or variables depending on whether samples (Q-mode) or variables (R-Mode) are being clustered. Most clustering methods consist of grouping the samples or variables on the basis of the computed similarity coefficient and

Table (5.3) The correlation matrix of major oxides data in the studied cherts.

Variables	SiO ₂	TiO ₂	Al ₂ O ₃	Fe ₂ O ₃	MnO	MgO	CaO	Na ₂ O	K ₂ O	P ₂ O ₅
SiO ₂	1.00*	-0.30	-0.32	-0.16	-0.17	-0.48*	-0.81*	-0.17	-0.29	-0.24
TiO ₂	-0.30	1.00*	0.99*	0.89*	0.24	0.30	-0.27	0.74*	0.97*	0.60*
Al ₂ O ₃	-0.32	0.99*	1.00*	0.89*	0.20	0.31	-0.25	0.79*	0.97*	0.62*
Fe ₂ O ₃	-0.16	0.89*	0.89*	1.00*	0.40	0.14	-0.35	0.58*	0.88*	0.52*
MnO	-0.17	0.24	0.20	0.40	1.00*	-0.02	0.05	-0.12	0.28	-0.01
MgO	-0.48*	0.30	0.31	0.14	-0.02	1.00*	0.12	0.46*	0.30	0.32
CaO	-0.81*	-0.27	-0.25	-0.35	0.05*	0.12	1.00*	-0.33	-0.27	-0.12
Na ₂ O	-0.17	0.74*	0.79*	0.58*	-0.12	0.46*	-0.33	1.00*	0.80*	0.66*
K ₂ O	-0.29	0.97*	0.97*	0.88*	0.28	0.30	-0.27	0.80*	1.00*	0.69*
P ₂ O ₅	-0.24	0.60*	0.62*	0.52*	-0.01	0.32	-0.12	0.66*	0.69*	1.00*

* Significant at 95% level

Table (5.4) The correlation matrix of minor elements data in the studied cherts

Variables	Rb	Sr	Ga	Nb	Zr	Y	Th	U	TREE
Rb	1.00*	0.14	0.98*	0.94*	0.96*	0.80*	0.97*	0.40	0.91*
Sr	0.14	1.00*	0.11	0.15	0.12	0.25	0.13	-0.32	0.20
Ga	0.98*	0.11	1.00*	0.97*	0.99*	0.80*	0.98*	0.47*	0.91*
Nb	0.94*	0.15	0.97*	1.00*	0.98*	0.74*	0.95*	0.48*	0.85*
Zr	0.96*	0.12	0.99*	0.98*	1.00*	0.78*	0.97*	0.50*	0.89*
Y	0.80*	0.25	0.80*	0.74*	0.78*	1.00*	0.87*	0.09	0.95*
Th	0.97*	0.13	0.98*	0.95*	0.97*	0.87*	1.00*	0.41	0.96*
U	0.40	-0.32	0.47*	0.48*	0.50*	0.09	0.41	1.00*	0.22
TREE	0.91*	0.20	0.91*	0.85*	0.89*	0.95*	0.96*	0.22	1.00*

* Significant at 95% level

Table (5.5) The correlation matrix of major oxides and trace elements in the chert samples from the studied area.

Variable	SiO ₂	TiO ₂	Al ₂ O ₃	Fe ₂ O ₃	MnO	MgO	CaO	Na ₂ O	K ₂ O	P ₂ O ₅	Rb	Cs	Sr	Ga	Nb	Zr	Th	U	TREE
SiO ₂	1.00	-0.30	-0.32	-0.16	-0.17	-0.48	-0.81*	-0.17	-0.29	-0.24	-0.34	-0.36	-0.85*	-0.27	-0.37	-0.31	-0.28	0.37	-0.30
TiO ₂	-0.30	1.00	0.99*	0.89*	0.24	0.30	-0.27	0.74*	0.97*	0.60*	0.98*	0.80*	0.12	0.99*	0.94*	0.97*	0.95*	0.49	0.87*
Al ₂ O ₃	-0.32	0.99*	1.00	0.89*	0.20	0.31	-0.25	0.79*	0.97*	0.62*	0.98*	0.82*	0.15	0.99*	0.95*	0.98*	0.98*	0.40	0.93*
Fe ₂ O ₃	-0.16	0.89*	0.89*	1.00	0.40	0.14	-0.35	0.58*	0.88*	0.52*	0.86*	0.67*	0.10	0.87*	0.73*	0.80*	0.84*	0.28	0.85*
MnO	-0.17	0.24	0.20	0.40	1.00	-0.02	0.05	-0.12	0.28	-0.01	0.20	0.02	0.33	0.17	0.03	0.09	0.08	-0.08	0.12
MgO	-0.48	0.30	0.31	0.14	-0.02	1.00	0.12	0.46	0.30	0.32	0.39	0.58*	-0.01	0.30	0.37	0.31	0.27	-0.19	0.24
CaO	-0.81*	-0.27	-0.25	-0.35	0.05	0.12	1.00	-0.33	-0.27	-0.12	-0.24	-0.17	0.85*	-0.29	-0.17	-0.25	-0.27	-0.56*	-0.21
Na ₂ O	-0.17	0.74*	0.79*	0.58*	-0.12	0.46	-0.33	1.00	0.80*	0.66*	0.81*	0.73*	-0.09	0.79*	0.81*	0.81*	0.85*	0.30	0.81*
K ₂ O	-0.29	0.97*	0.97*	0.88*	0.28	0.30	-0.27	0.80*	1.00	0.69*	0.98*	0.80*	0.13	0.95*	0.89*	0.93*	0.95*	0.39	0.91*
P ₂ O ₅	-0.24	0.60*	0.62*	0.52*	-0.01	0.32	-0.12	0.66*	0.69*	1.00	0.68*	0.73*	0.09	0.60*	0.56*	0.60*	0.68*	0.13	0.75*
Rb	-0.34	0.98*	0.98*	0.86*	0.20	0.39	-0.24	0.81*	0.98*	0.68*	1.00	0.87*	0.14	0.98*	0.94*	0.96*	0.97*	0.40	0.91*
Cs	-0.36	0.80*	0.82*	0.67*	0.02	0.58*	-0.17	0.73*	0.80*	0.73*	0.87*	1.00	0.08	0.83*	0.83*	0.81*	0.83*	0.27	0.82*
Sr	-0.85*	0.12	0.15	0.10	0.33	-0.01	0.85*	-0.09	0.13	0.09	0.14	0.08	1.00	0.11	0.15	0.12	0.13	-0.32	0.20
Ga	-0.27	0.99*	0.99*	0.87*	0.17	0.30	-0.29	0.79*	0.95*	0.60*	0.98*	0.83*	0.11	1.00	0.97*	0.99*	0.98*	0.47	0.91*
Nb	-0.37	0.94*	0.95*	0.73*	0.03	0.37	-0.17	0.81*	0.89*	0.56*	0.94*	0.83*	0.15	0.97*	1.00	0.98*	0.95*	0.48	0.85*
Zr	-0.31	0.97*	0.98*	0.80*	0.09	0.31	-0.25	0.81*	0.93*	0.60*	0.96*	0.81*	0.12	0.99*	0.98*	1.00	0.97*	0.50	0.89*
Th	-0.28	0.95*	0.98*	0.84*	0.08	0.27	-0.27	0.85*	0.95*	0.68*	0.97*	0.83*	0.13	0.98*	0.95*	0.97*	1.00	0.41	0.96*
U	0.37	0.49	0.40	0.28	-0.08	-0.19	-0.56*	0.30	0.39	0.13	0.40	0.27	-0.32	0.47	0.48	0.50	0.41	1.00	0.22
TREE	-0.30	0.87*	0.93*	0.85*	0.12	0.24	-0.21	0.81*	0.91*	0.75*	0.91*	0.82*	0.20	0.91*	0.85*	0.89*	0.96*	0.22	1.00

* Significant at 95% level.

gradually admitting more as the similarity coefficient is lowered. Other clusters are eventually initiated until, finally, all the samples are linked. Various clustering methods exist depending on the criterion of entry of a sample into a cluster e.g. weighted and unweighted pair-group average linkage, and single-linkage methods (Sokal and Sneath, 1963). The end product of the clustering procedure can be represented as two-dimensional hierarchical diagrams called “dendrograms”.

Three methods of cluster analysis were carried out during the course of the present work; namely: (i) Weighted Pair Group average Method (WPGM); (ii) Unweighted Pair Group average Method (UPGM); and (iii) Single-Linkage Method (SLM). Generally, it has been found that the pair-group methods UPGM and WPGM have the highest cophenetic correlation coefficients, and that the Single Linkage has the lowest. Therefore, the Single Linkage method is least used by numerical taxonomists. Gower (1967) recommended WPGM for general purpose classification, whereas Farris (1969) found that the cophenetic correlation coefficient is maximized by UPGM. This latter method (UPGM) has found a wide acceptance among numerical taxonomists and, therefore, it has been utilized in the work. Also, a wide variety of similarity coefficients exists. In the present study, two similarity coefficients were used: correlation (r) and distance coefficients. However, the correlation coefficients usually produce a better-classification dendrogram and are, therefore, more reliable than taxonomic distance as a measure of similarity of geochemical entities.

(1) R-mode cluster analysis

Twenty-eight major and trace elements in the studied chert samples were considered for R-mode cluster analysis. The obtained dendrogram (Fig. 5.15) shows that at linkage distance of one, three distinct clusters are apparent: (i) CaO and Sr; (ii) MgO, P₂O₅,

Lu, Yb, Tm, Ce, Eu, Tb, Gd, Sm, Nd, Pr, Er, Ho, Dy, Y, FeO, Zr, Nb, Rb, K₂O, Ga, Al₂O₃ and TiO₂; (iii) SiO₂. The first cluster comprises an association of elements of the carbonate minerals. It is well known that Sr is closely associated with Ca in the carbonate minerals due to their similarities in both ionic radii and charges. Therefore, Ca is readily replaced by Sr in the mineral structure. The second cluster includes an association of most of the elements. This association is clearly related to the terrigenous source component and hematite. This cluster is also subdivided into several sub-clusters (A, B, C, D, E, F and G). Sub-cluster (A) includes only MgO and may be related to the alteration of the oceanic crust and the formation of the mineral chlorite. Sub-cluster (B) contains only P₂O₅, which may be related to some phosphatic components such as the mineral apatite. The sub-cluster (C) represents the rare earth elements together with Y. This association is mainly related to detrital minerals that concentrate REEs. The sub-cluster (D) includes FeO which is clearly related to the mineral hematite. The sub-cluster (E) is mainly related to the mineral zircon since it contains only Zr and Nb; elements that are known to concentrate in this mineral. The sub-cluster (F) includes K₂O and Rb that are mainly concentrated in micas and clay minerals. The sub-cluster (G) contains Ga, Al₂O₃ and TiO₂, a typical association of detrital clays and volcanogenic detritus. Ga is known to replace and closely associates Al due to similarity in ionic radii and charges. The third cluster includes only SiO₂, which indicates the independence of the silica contents of the chert samples to terrigenous and carbonate materials. This is further confirmed by the lack of significant correlations between silica and each of the other elements (Table 5.5).

A similar dendrogram (Fig.5.16) was produced by considering only fourteen elements and total of all REEs (TREE). The dendrogram is more simple, however, it gives the same cluster result of the three groups of elements at (1.1) r. except for the fact that the sub-cluster (C) in cluster II becomes more simple and is represented only by TREE and Y.

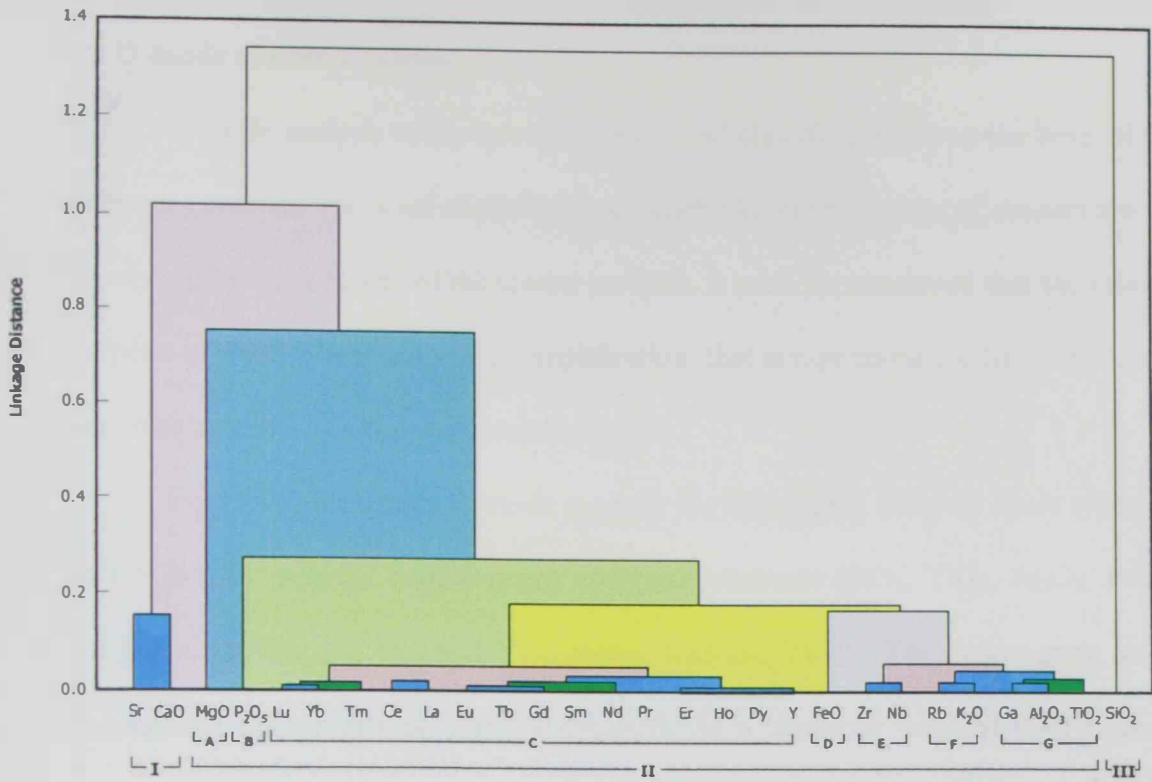


Fig. 5.15 Dendrogram (R-mode) of major and trace elements.

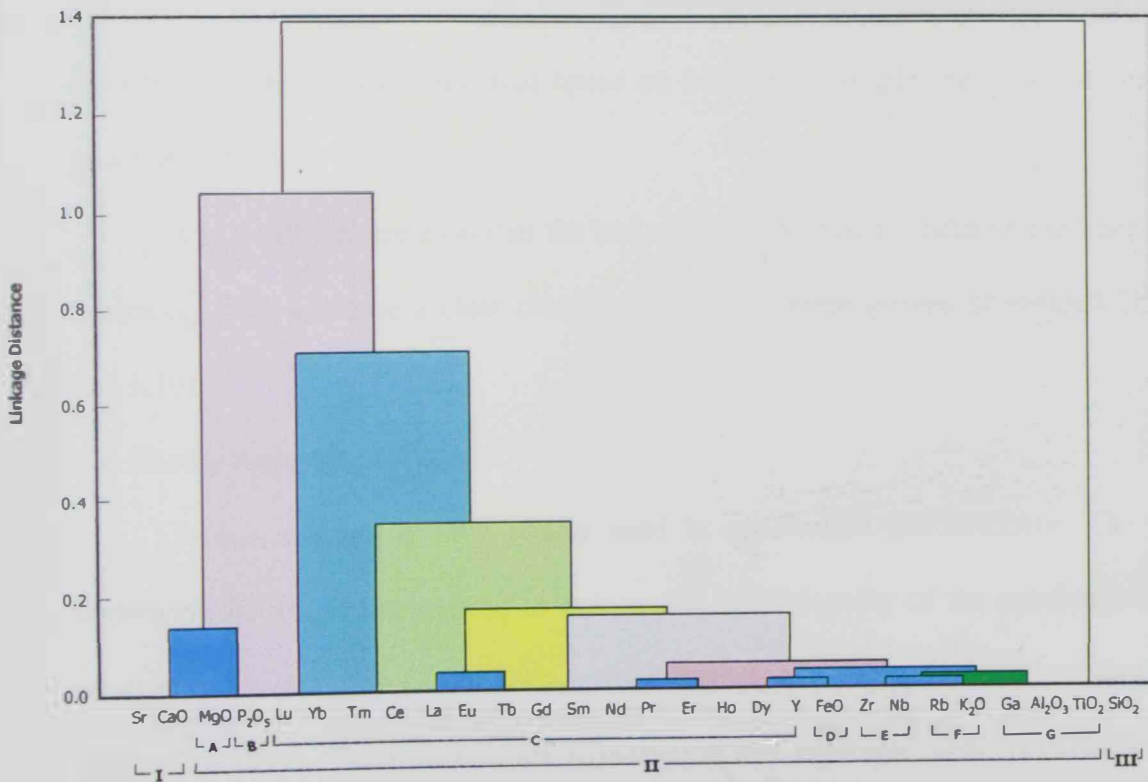


Fig. 5.16 Dendrogram for the studied chert samples using the 14 elements and REE.

(2) Q-mode cluster analysis

Q-mode analysis endeavors to compare and classify samples on the basis of their different contents. The level of similarity at which clusters or groups of clusters are taken is only a subjective aspect of the cluster analysis. It must be mentioned that the prime purpose of multivariate analysis is simplification; that is expressing the large number of variables in terms of a few interpretable ones.

Fig (5.17) illustrates Q-mode analysis for the studied different chert types by using of UPGM for selected twelve major and trace elements (SiO_2 , TiO_2 , Al_2O_3 , FeO , MgO , CaO , Rb , Sr , Ga , Nb , Zr , and Y) together with the TREE. The dendrogram in Fig 5.17 summarizes the groups of clusters obtained. At a similarity level of 0.85 r, three main groups of clusters are shown. The first group includes mainly the SM samples, the second group is restricted to the CC samples, whereas the third group contains only the R samples. The important feature revealed by applying this analysis is the close conformity between the obtained classification and that based on both the petrographic observations and the geochemical data.

It is worthy to mention that the use of either the major oxides or the trace elements separately does not give a clear clustering of the different groups of samples (Figs. 5.18 and 5.19).

(3) Factor Analysis

Factor analysis is now widely used in exploration geochemistry. The intention underlying its use is the attempt to reduce the dimensionality of the geochemical data by constructing a set of new variables termed factors, which are fewer in number than the original variables. These factors are hypothetical and represent linear combinations of the original variables. The methodology of factor analysis is quite complex. Details have been given by various workers (e.g. Harman, 1976; Joreskog *et al*, 1976; Davis, 1973). The first

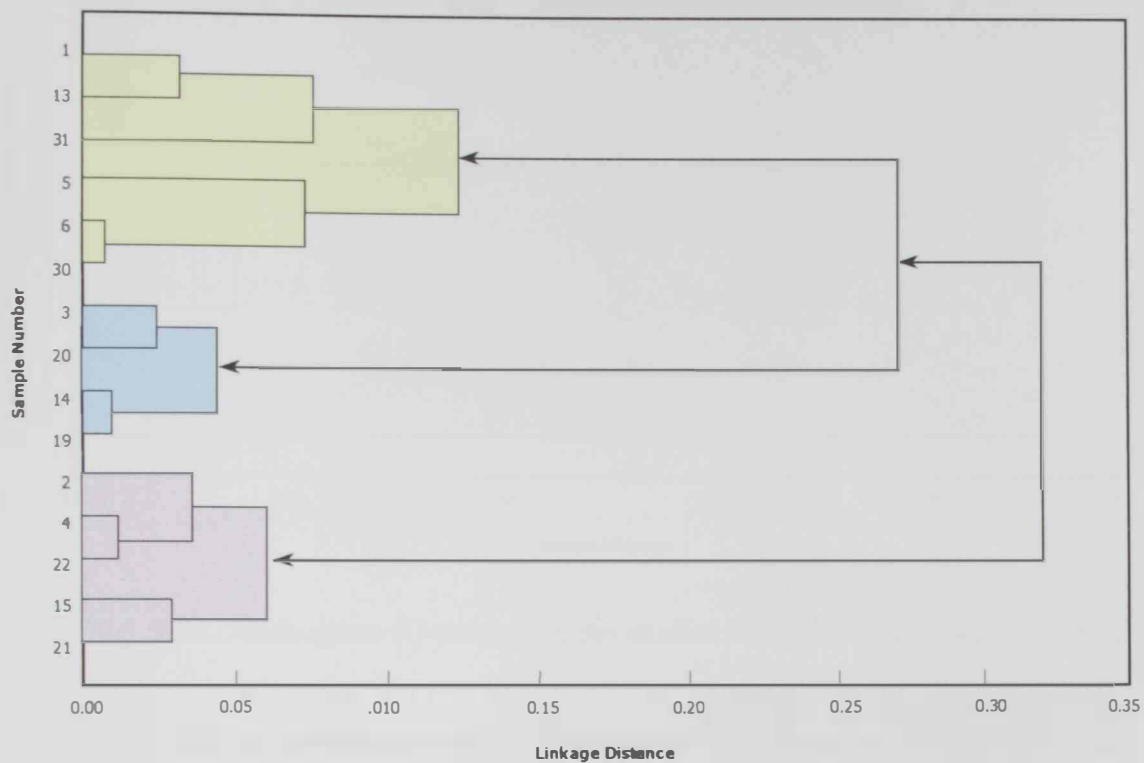


Fig. 5.17 Dendrogram (Q-mode) for the studied cherts by using selected major and trace elements.

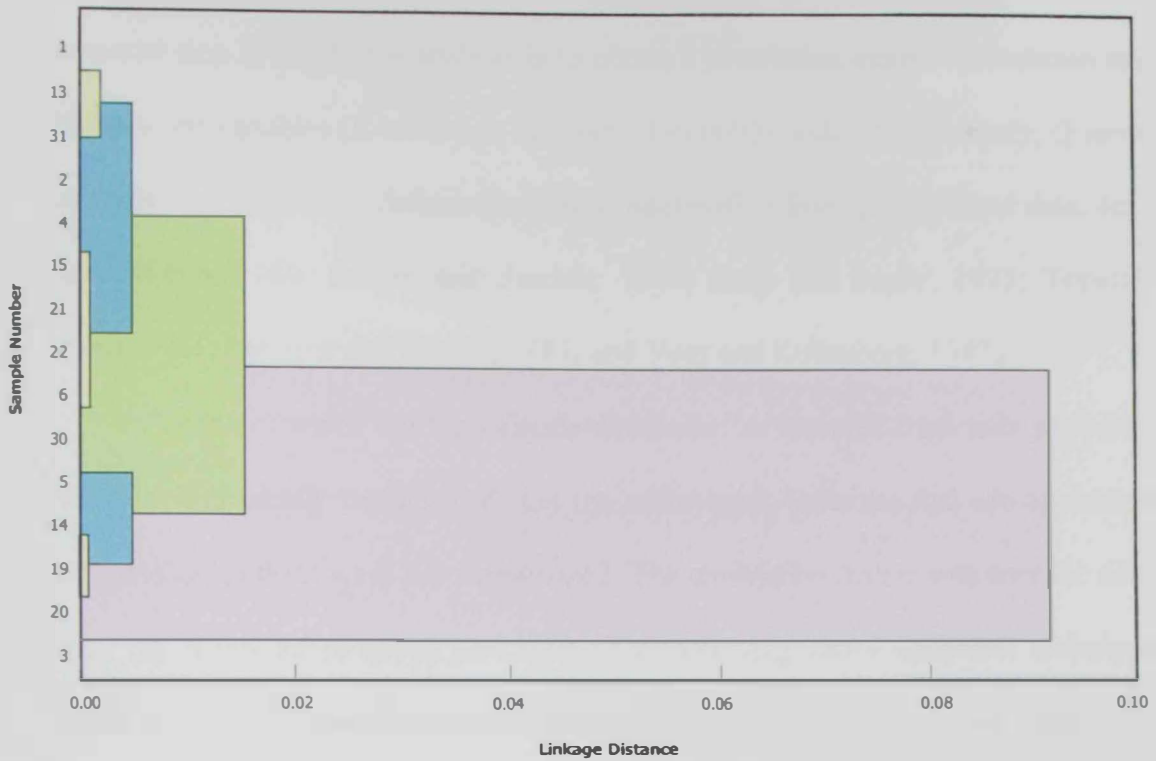


Fig. 5.18 Dendrogram (Q-mode) for the studied cherts by using major oxides.

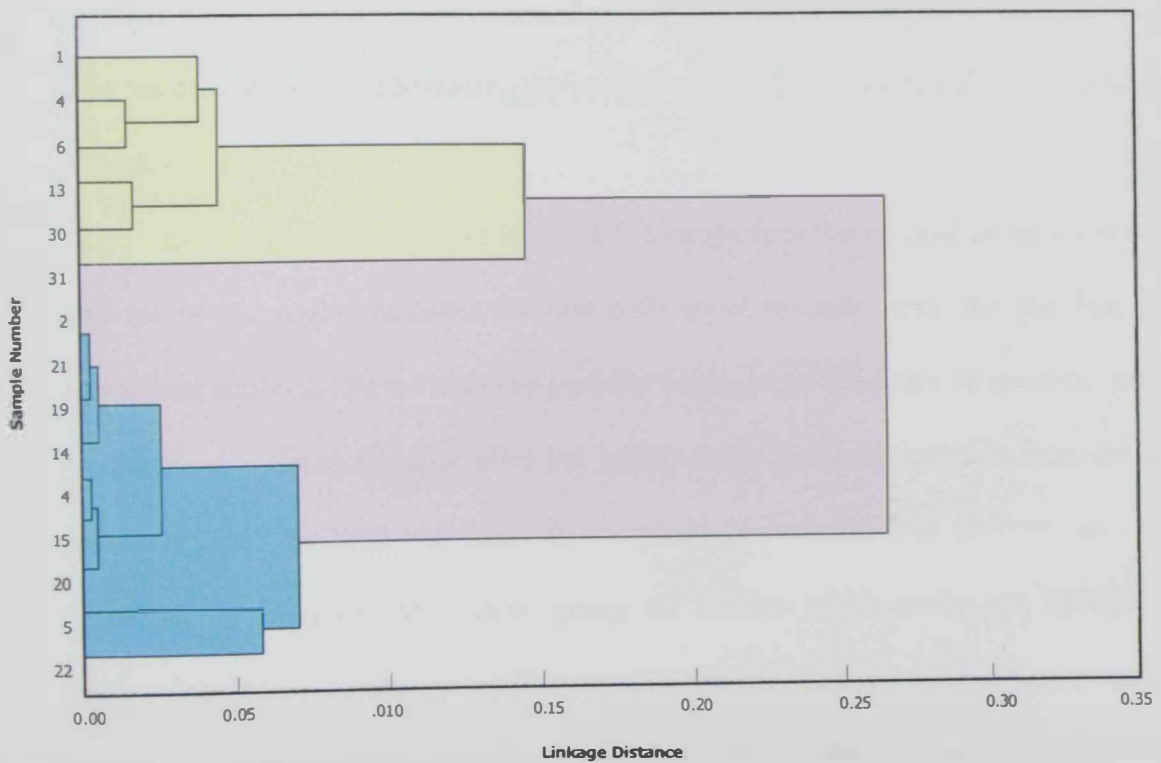


Fig. 5.19 Dendrogram (Q-mode) for the studied cherts by using trace elements together with the Tree.

essential step in any factor analysis is to obtain a correlation matrix. Correlation may either be between variables (R-mode) or between objects (Q-mode). In this study, Q-mode factor analysis was applied to deduce geological information from geochemical data. (cf. Saager and Esselaar, 1969; Saager and Sinclair, 1974; Hesp and Rigby, 1975; Tripathi, 1979; Ajayi, 1981; Buttener and Saager, 1983; and Vogt and Kollenberg, 1987).

Variables which are lognormally distributed as revealed from their probability plots were logarithmically transformed. On the other hand, variables that are approximated by normal distributions were not transformed. The correlation matrix was used for direct input into the SPSS subprogram FACTOR. The following factor-analytical techniques were tried: principal component method (PA 1), wherein t leading diagonal values of unity in the correlation matrix remain unchanged, and principal factoring method (PA 2), in which at the time of factoring 1's are replaced by communalities in the main diagonal of the correlation matrix. It is worth-mentioning that the two methods gave very similar results after varimax rotation. Therefore, the results of the first method will be discussed in the present study.

The second step in factor analysis is to transform the original set of variables into a new set of composite variables that are orthogonal to each other. So, the first principal component accounts for as much as possible of the total variability of the data, the second for the most residual variance after the effect of the first component is removed and this continues until the total variability is completely exhausted. The process can be simply visualized as insertion of a new group of factors which really are at right angles (uncorrelated) into another group that are not, and the relation between the two groups are defined by mathematical transform equations. The cosine of the angles between the original variables and the factors are a measure of the loadings of the former on the latter. The immediate result of the initial factoring is the extraction of an unrotated factor matrix.

The sum of squared loadings of any element (row) is termed the communality. It expresses the amount of total variability of each element explained in a given factor solution. On the other hand, the sum of squares for each of the columns the eigen values and represent the amount of variance accounted for by each factor. They are commonly re-expressed as percentage total to explain the proportion of the total variability accounted for by this new set of variables. Usually, the first few components explain most of the variance in the data. For factor analytical purposes, these components are commonly retained for further rotation. This arises a question about the correct number of factors to be extracted in the final solution. Actually, there are no statistically based tests and the final choice is only a subjective assessment based either on a single or many criteria. Subprogram FACTOR automatically deletes all factors with an associated eigen value of less than 1.0. Four rotational methods are available in the subprogram and the user has the choice to apply either orthogonal or oblique rotation. The rotation process tends to rotate the initial factors in order to maximize the contrast of the element loadings, so high loadings tend to ± 1.0 and low ones to 0.0. Consequently, rotation is advantageously applied to get a simpler and a more interpretable factor pattern. The most common by used Kaiser's varimax orthogonal rotation method is followed in the present study.

The obtained rotated factor matrix is used to calculate the exact factor-score coefficients (in case of PA1). The latter are subsequently used to get the factor scores for every individual case and are written on a raw-output-data file. It must be noted that the scores of each factor are standardized, i.e. they have zero mean and unit variance. Factor scores reflect the strength and importance of each factor in every individual case. So, factor analysis introduces additional advantage in geochemical data reduction and interpretation by producing a fewer number of factor score maps instead of the large number of the

original variable maps which are difficult to grasp and interpret all the information included in them.

The R-mode factor analysis of the studied chert samples produced 2 factors model accounting for 85.85% of the data variability. This is considered an appropriate solution in terms of the geochemical data and geological observations (Table 5.6).

Table (5.6) R-Mode Varimax rotated Factor matrix for the studied chert samples.

Variable	Factor 1	Factor 2	Communality
SiO ₂	-0.213433	-0.961189	0.999833
TiO ₂	0.977398*	0.075989	0.998186
Al ₂ O ₃	0.986440*	0.101748	0.999334
Fe ₂ O ₃	0.906029*	-0.079492	0.986251
MgO	0.293610	0.549491	0.997235
CaO	-0.356572	0.875847*	0.999802
K ₂ O	0.97835*	0.078915	0.996644
P ₂ O ₅	0.689251	0.165587	0.947743
Rb	0.982056*	0.141071	0.997663
Ga	0.983133*	0.053403	0.998509
Zr	0.961164*	0.101460	0.994343
TREE	0.937724*	0.096765	0.991795
Variance %	68.12	17.43	-----

The communalities show that all the elements are reasonably well accounted for by this model.

Factor 1 (terrigenous source): explained most of the geochemical data variations. It accounts for 68.12% of the variability model. The association (TiO₂, Al₂O₃, FeO, K₂O, P₂O₅, Rb, Ga, Zr & TREE) represents the terrigenous source component. These elements refer to the various varieties of detrital materials such as clay minerals and micas (Al₂O₃, K₂O, Rb, Ga), hematite and iron oxides (FeO, TiO₂), and detrital zircon (Zr, TREE).

Factor 2 (carbonate minerals): accounts for additional 17.43% of data variability. It is a bipolar factor where CaO is positively loading and SiO₂ is negatively loading on this factor. The high positive loading of CaO indicates the role played by cementation and

other diagenetic processes by carbonate minerals. On the other hand, the negative loading of SiO_2 indicates that the secondary carbonate replacement occurred at the expense of silica in the chert samples. The loading of the different elements on both factor 1 and factor 2 is illustrated in Fig (5.20).

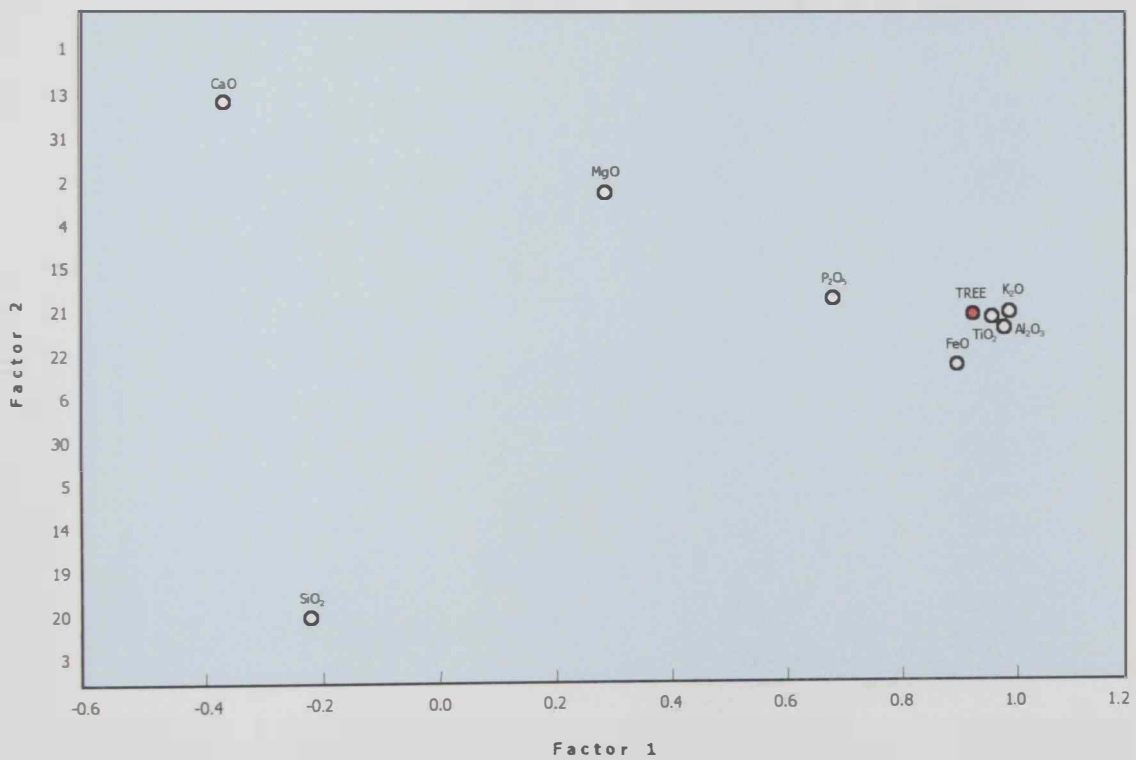


Fig. 5.20 The loading of the representative major and trace elements in the chert samples on both factor 1 and factor 2.

CHAPTER VI

ECONOMIC POTENTIAL

CHAPTER VI

ECONOMIC POTENTIAL

6.1 Introduction

The world as we know it today would be inconceivable without the use of cement. Cement is one of the most important building materials because of its versatility, durability, ease of working and last, but not the least, low price.

Cement is a hydraulic binder. It consists mainly of compounds of calcium oxide, silica, alumina and iron ore. The main raw materials used in the cement manufacturing are: limestone, shale, clay, silica, bauxite, laterite, iron ore and gypsum. Except gypsum, the other raw materials are used for making clinker which is an intermediate product for making cement. Gypsum is added in order to adjust the properties of cement like setting time and strength.

Limestone is the major source for making cement. Calcium carbonates of all geological formations satisfy the requirements for the production of Portland cement. Limestone usually contains admixtures of clay substances or iron oxides, which influences its colour. The purest grades of limestone are calcspar (calcite) and aragonite.

A limestone with a minimum of 45% – 50% CaO , maximum 3% – 3.5 % MgO , 0.6 % alkalis , 0.25 % P₂O₅ ,0.5 % Mn₂O₃, 1.3 % TiO₂ and 0.015 – 0.02 % chloride is regarded as cement grade limestone. This is suited for the production of clinker with good burnability, which results in higher production of clinker.

The melting point of limestone is about 2200 °C which has to be lowered to 1350° – 1450 °C for excellent burnability in order to give good clinker. This is possible through the use of iron ore, laterite or hematite . Sometimes even bauxite is required to compensate alumina requirement.

Material rich in silica such as sandstone, clay, shale or dune sand are used for the preparation of the ground raw meal to make clinker. The usage of silica as a raw material depends on the chemical composition of limestone available for use. Generally, before selecting the silica source, its reactivity should be checked for using as a potential raw material for cement industry. Silica enriched in quartz is not preferable in the cement industry because of its poor reactivity. Also, alkalis and chloride contents present in the silica play a major role in selecting the silica source. Moreover, silica with higher alkali and chloride contents is not suitable as a raw material since it causes operational problems in the pyro-processing and also affects the quality of cement.

Bauxite and iron ore are rich in Al_2O_3 and Fe_2O_3 ; respectively. They are used in the cement manufacturing process as a flux to reduce the clinkering temperature. The use of these raw materials depends on composition of the limestone and siliceous additives.

Gypsum ($\text{CaSO}_4 \cdot 2\text{H}_2\text{O}$) is ground along with clinker to make cement. It is used to modify the setting property of cement. It is also one of the essential raw materials for producing any type of cement. The sources of gypsum are marine rocks and industrial byproducts.

6.2 Ras Al-Khaimah Cement History

Ras Al-Khaimah is the northernmost Emirate of the United Arab Emirates. It is famous for its mountains, farms, beaches and archaeological sites. In 1972, Ras Al-Khaimah witnessed the emergence of a new era in the industrial sector of the United Arab Emirates. The cement industry, which is the second largest industry after Oil, commenced in that year with the establishment of the first cement factory in the country. The Union Cement Company (U.C.C) of Ras Al-Khaimah was the first plant to start operation and is still one of the largest companies. The production in 1974 was 500,000 tons. Today, there are ten

cement factories (four of them in Ras Al Khaimah, 3 produce gray cement, and 1 for white cement) spread over the UAE to meet the growing demand for cement in the field of developing activities.

The annual production capacity of Ras Al-Khaimah cement companies as in today is over than three and half million tons per year. The plants are located about one kilometer from the excellent port of Mina Saqar, and about the same distance from the Ras Al Khaimah mountains that provide abundant supply of high and consistent quality limestone. These factories produce the following types of cement :

- Ordinary Portland Cement type 1 (OPC1): produced by the Union Cement Company (UCC), the Gulf Cement Company (GCC), and the Ras Al Khaimah Cement Company (RAKCC).
- Moderate Sulfate Resistant Cement (MSRC): produced by the Union Cement Company (UCC), the Gulf Cement Company (GCC), and the Ras Al Khaimah Cement Company (RAKCC).
- High Sulfate Resistant Cement (HSRC): produced by the Union Cement Company (UCC) and the Gulf Cement Company (GCC).
- Oil well Cement (OC): produced by the Union Cement Company (UCC).
- White Cement (WC): produced by the Ras Al-Khaimah White Cement Company (RAKWCC).

6.3 The Cement Production Process

The essential raw materials used for the production of cement are: limestone, silica, iron ore, gypsum and bauxite. Several processes are conducted to produce cement from these raw materials. The process used by the Ras Al-Khaimah Cement Company is summarized in the following:

First phase: Extracting (Quarrying) and crushing the raw materials:

Raw Materials (limestone and silica rocks) are extracted from the mountains in the Ras Al-Khaimah Emirate. The crushed raw materials are transported to the companies using trucks and conveyor belts (Fig. 6.1).

Second phase: Grinding and storage of raw materials:

The crushed raw materials (limestone, silica, iron ore and bauxite) are transported to the Raw Mill (tube grinding machine). After grinding, a mixed powder component (the kiln feed or raw meal) is obtained.

Third phase: Clinker production:

From the storage silo, the kiln feed enters the kiln which burns the materials up to 1000° - 1400 °C to get the clinker product. Then, by the conveyor belt, it is transported to the clinker yards or silos for storage.

Fourth phase: Cement grinding and storage:

After getting clinker products, the cranes or the conveyors shift the clinker from the yards to the cement mill hopper. The cement mill grinds the clinker with a little amount of gypsum to get the finished cement product. This latter product is transported through the production pipeline to the cement storage silo.

Final phase: Cement packing and loading.

In the packing plant, cement is packed in two ways: either in small bags (50 kg), or big bags (1.5 ton). Also, it can be loaded directly to the bulk trucks.

A flowchart illustrating sample points throughout the production lines for raw materials, semi finished products and finished products is shown in Fig. (6.2).

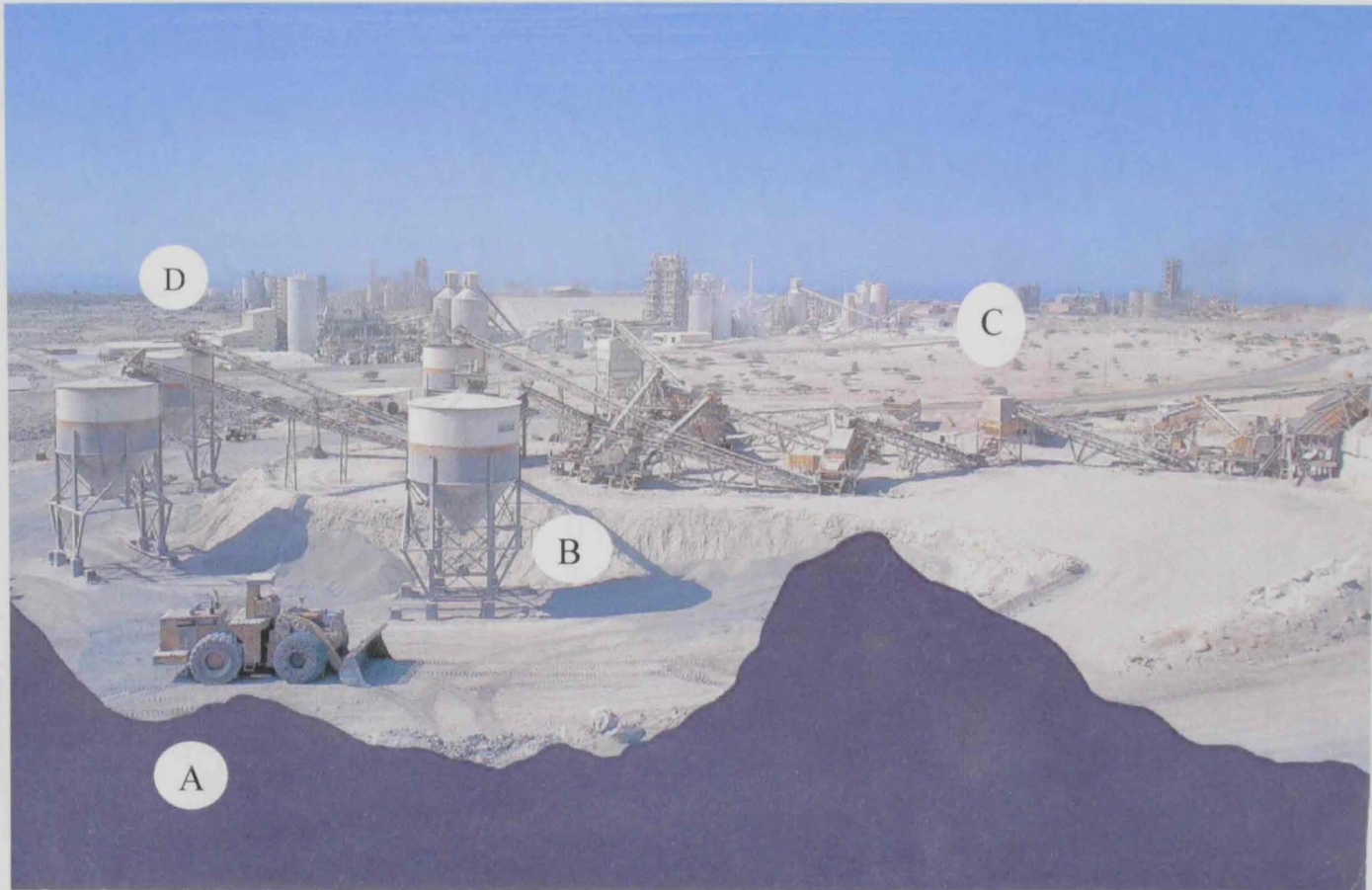


Fig.6.1 A panorama (looking North) of the limestone quarry in Khor Khowair (A), the limestone crushers (B), the cement companies (C) and the port of Mina Saqr (D).

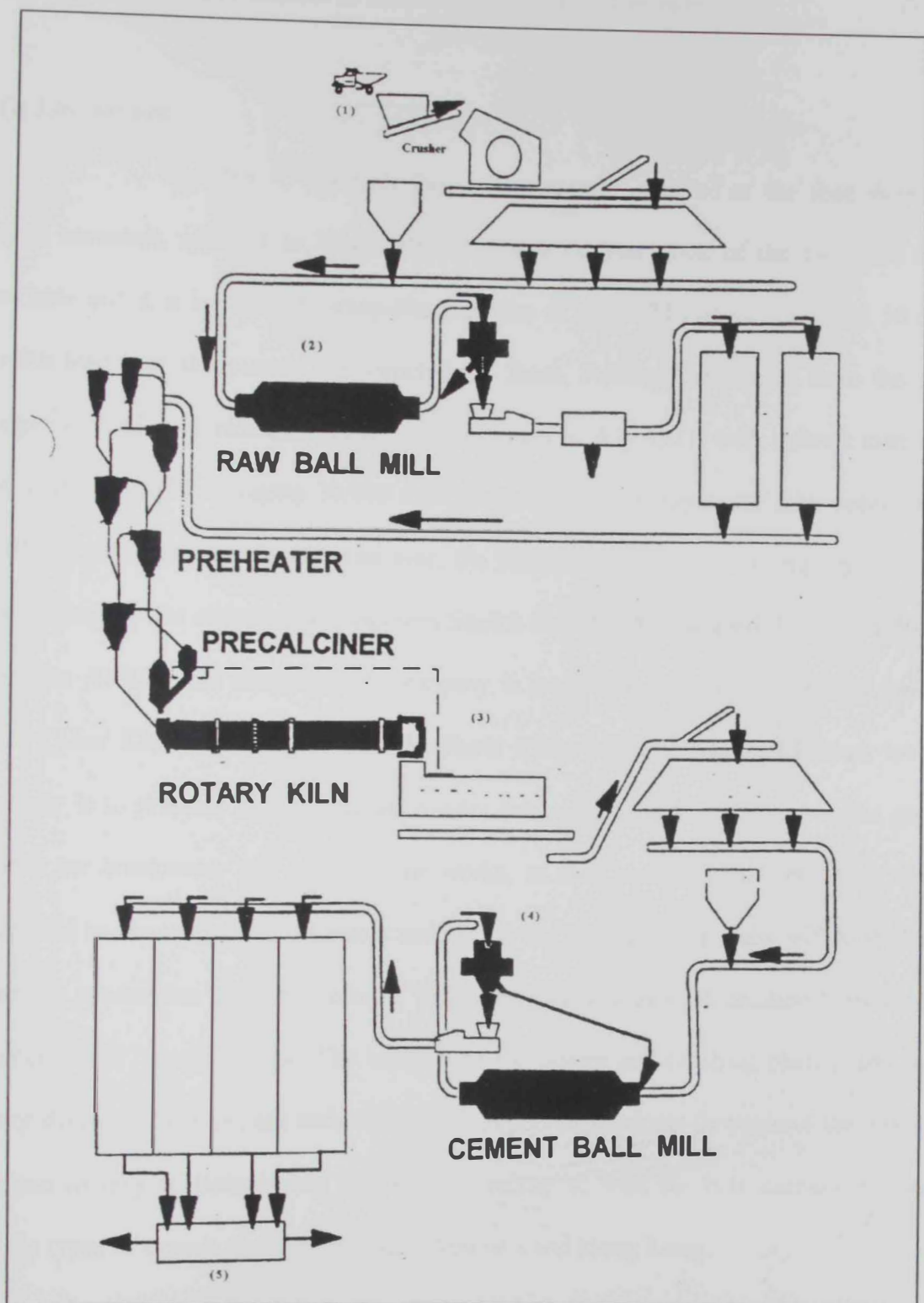


Fig.6.2 A flow chart showing the various stages of cement preparation in the cement plant.

6.4 Raw Materials Available in the Ras Al-Khaimah Emirate

(i) Limestones

The Ras Al-Khaimah limestone quarry is situated at the foot slopes of a steep mountain adjacent to Wadi Ghalilah (Fig.6.3). The slope of the mountain face is variable and it is locally very steep-Sharp gullies of up to 20 meters depth and 50 meters width lead into the present top bench back faces. Primary extractions from the quarry began in 1968 by Helde and Franke and continued to July 1971, with a direct sales of run of quarry material averaging 20,000 tons per year and total aggregate sales approximately 200,000 tons per year. In the same year, the Ras Al Khaimah Rock Company (RRC) was established by the order of His Highness Sheikh Saqr bin Mohammed Al Qasimi, Ruler of the Ras Al Khaimah Emirate. This company is located in the Ras Al Khaimah industrial area (Khor Khowair) (Figs.6.4 & 6.5), about 35km north of Ras Al Khaimah town. Its activity is to produce high quality aggregates for concrete and road construction projects, rocks for breakwater and other marine works, as well as high grade limestone which is supplied to the nearby cement plants and also to the steel plants in India and Australia. The present production capacity exceeds 15,000,000 million tons of crushed hard limestone material and "armour" rock. The location of the quarry and crushing plants, next to Port Saqr deepwater harbor, has assisted RRC to export its products throughout the whole Gulf region (mainly to Bahrain and Kuwait), as well as to load the bulk carriers and various other types of vessels destined for India, Australia and Hong Kong.

In 1975, a new company was established for the same business (Stevin Rock Company; SRC). It is a European owned and managed quarry and rock contractor that has been operating both within the UAE and internationally. The company is firmly established as the leading quarry in the Gulf region for the production and commercial

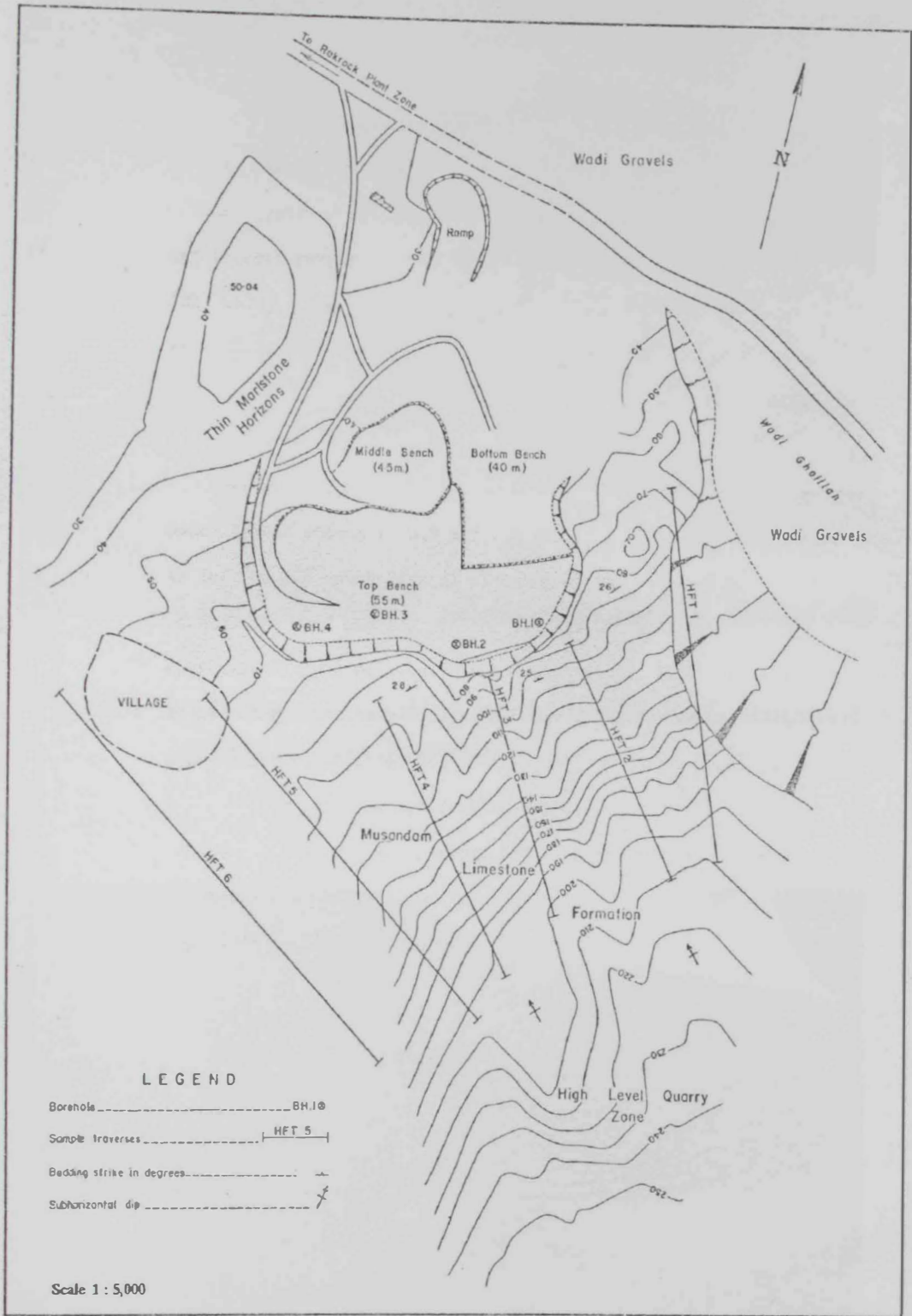


Fig. 6.3 A map of the Ras the Al Khaimah limestone quarry in Khor Khowair (Masri *et al.*, 1972).



Fig. 6.4 A photograph (looking north) of the RRC limestone quarry in Khor Khowair.



Fig. 6.5 A close up view (looking east) of the limestone quarry in Khor Khowair showing the extensive thickness (average about 1500 m) of the limestone succession.

supply of rock materials used in coastal protection projects (Fig. 6.6).

The SRC quarry at Khor Khowair produces and sells high-grade limestone materials to the construction companies throughout the Gulf region. It was constructed near the Ras Al Khaimah Rock Company (RRC) limestone quarry. The quarry equipment levels, access roads, selection yards and stockpiling areas were all constructed in such a way to ensure a production level capability of 150,000 tones per week (8 million tones per year) of coastal protection rocks. In order to complement the supply of rock materials, SRC has the facility to produce high quality concrete aggregates, with a production capacity of some 1.8 million tones per year. Hence, it can be ensured that the Khor Khowair limestone rock quarry supplies the market with more than 23 million tones of limestone per year. The Ras Al-Khaimah cement plants consume more than 4 million tons of limestone per year of the total rock quarry production.

The limestones available in the Ras Al Khaimah belt (Khor Khowair) represent one of the best deposits in the world in term of quality and consistency. These high quality limestones can be used for producing all types of Portland cement including white cement. They constitute huge reserves and are presently used as the sole source for the cement industry in Ras Al Khaimah.

The limestones studied in the present work comprise those of Khor Khowair and the rocks exposed at Idan, Al Gail and Saram. Table (5.1) shows a comparison between their chemical compositions and the data provided by the Ras Al Khaimah Cement Company (RAKCC) laboratories for Khor Khowair limestones. This table reveals the following:

- (a) The data obtained in the present study for the Khor Khowair limestones are closely similar to those provided by the RAKCC laboratories. However, the



Fig. 6.6 A photograph (looking East) of the limestone quarry of the Steven Rock Company (SRC). Which is located very close to the Port of Mina Saqr.

studied limestones contain slightly higher concentrations of CaO and lower proportions of SiO₂, MgO and Fe₂O₃.

- (b) The limestones of Idan and Al Gail are, to a great extent, compositionally similar to those of Khor Khowair which are used by RAKCC. Differences are represented only by the presence of slightly higher concentrations of MgO in Idan limestones and CaO in those of Al Gail. This permits the consideration of limestone exposures in those two localities for possible future demands.
- (c) The Saram limestones are markedly compositionally different from those of Khor Khowair. They are remarkably more depleted in CaO and enriched in SiO₂, Al₂O₃ and FeO₃.

Table (6.1) Comparison between the chemical compositions of the studied limestones and those used in RAKCC

Element Oxide	Present Study				RAKCC*	Standards for Portland Cement	
	Saram	Idan	Al Gail	Khor Khowair		British	American
CaO%	43.1 – 47.9	54.20	55.22	54.4 – 55.5	51.0 – 54.0	-	
SiO ₂ %	7.4 – 14.4	0.02	0.02	0.04 – 0.33	1.5 – 3.5	N.S.**	N.S.**
Al ₂ O ₃ %	2.1 – 5.6	0.60	0.68	0.61 – 0.76	0.4 – 1.2	N.S.	Max. 6.0
FeO ₃ %	0.7 – 1.0	0.04	0.09	0.04 – 0.2	0.1 – 0.4	N.S.	Max. 6.0
MgO%	1.0 – 1.1	1.53	0.27	0.23 – 0.58	0.6 – 0.8	Max. 5.0	Max. 6.0

* RAKCC: data supplied by the Ras Al Khaimah Cement Company Laboratories

** NS : not specified in standard

(1)Silica

Silica, either in the form of rock or dune sands, is available in abundance in UAE. However, there are no big reserves for silica in the surroundings of Ras Al-Khaimah Emirate. The main source of silica which is used by many cement companies in Ras Al-Khaimah is represented by a few chert exposures (Fig. 6.7) as those in Al Rams and Idan (present study area). However, the use of chert as a source of silica in the cement production is not highly recommended. This is attributed to the high hardness of chert



Fig. 6.7 A photograph showing the red banded ribbon cherts in the Idan silica rock quarry of the Ras Al Khaimah Rock Company.

material which leads to high abrasive effects on the crushing machines and also high consumption of energy. Therefore, other alternative sources for silica are required, particularly for the future planning.

Dune sands, which can be used as a potential source of silica, are abundant in the United Arab Emirates. Most of these dunes consist of loose sediments that can be easily quarried and grinded. Also, these dune sands consist of fine and well-sorted grains properties that are recommended during the mill operation.

Earlier attempts have been made by the cement companies at Ras Al Khaimah to assess the cement production. It was found that these dune sands have very homogenous chemical compositions. However, the averages of SiO_2 , Al_2O_3 and Fe_2O_3 contents in these sands are relatively lower than those in the silica source rocks. This requires the addition of imported materials to the raw meal. Therefore, the overall costs upon using dune sands as silica source will be increased and, consequently, the sands were not economically recommended.

An attempt has been made in the present study to test the suitability of sand dunes in the surroundings of Ras Al Khaimah as a silica source. The chemical compositions of two samples representing the coastal and inland dunes at Al Gail and Al Helailah, respectively have been determined (Chapter V). The obtained chemical data were compared with those of cherts and dune sands previously analyzed by Ras Al Khaimah Cement Company (RAKCC) Table (6.2). The results obtained reveal the following:

- (a) The studied Idan cherts have lower SiO_2 and higher CaO concentrations when compared with those used by RAKCC. This may be attributed to the fact that the studied rocks comprise several samples that represent the calcareous cherts. On the other hand, the studied Al Rams cherts are more enriched in Al_2O_3 ,

MgO and Na₂O and depleted in CaO relative to the RAKCC cherts. This may be attributed to the presence of siliceous mudstones.

- (b) The chemical compositions of the studied Al Gail cherts is closely similar to those presently used by RAKCC and, hence, can be considered as a source of silica in future planning. On the other hand, Saram cherts have higher CaO and Lower Al₂O₃ and Fe₂O₃ contents when compared with the RAKCC cherts.
- (c) The studied dune sands have lower SiO₂, Al₂O₃ and Fe₂O₃ concentration than those in cherts. This finding is in accordance with that previously reached by RAKCC.
- (d) Sand dunes of Al Gail are compositionally similar to those tested by RAKCC; except for their slight relative enrichment in Fe₂O₃, CaO and MgO at the expense of SiO₂, Al₂O₃ and K₂O. On the other hand, the Al Helailah dune sands are compositionally different from those tested by RAKCC. The former sands have much higher proportions of CaO and lower concentrations of the other major elements and, hence, cannot be considered as silica source.

Table (6.2) Comparison between the chemical compositions of the obtained cherts, dune sands and those used by RAKCC.

Element Oxide	Chert					Dune Sand		
	Present Study				RAKCC	Present Study		RAKCC
	AL Gail	Saram	Idan*	Al Rams*		Al Gail	Al Helailah	
SiO ₂ %	73.62 – 96.44	70.29 – 98.00	48.52 – 93.34	71.24 – 85.49	81.72	57.81	34.82	68.37
Al ₂ O ₃ %	0.38 – 8.09	0.32 – 2.39	1.81 – 7.75	5.02 – 11.1	4.72	3.12	1.58	3.78
FeO ₃ %	0.89 – 4.12	0.74 – 1.44	1.35 – 5.65	3.09 – 4.05	3.16	2.01	0.89	1.77
CaO%	0.5 – 11.32	0.26 – 13.07	0.22 – 22.98	0.33 – 0.47	1.84	15.35	32.00	11.42
MgO%	0.09 – 1.43	0.05 – 1.55	0.45 – 6.32	1.18 – 2.41	1.22	4.28	1.69	2.22
K ₂ O%	0.05 – 2.10	0.07 – 0.37	0.37 – 1.99	0.75 – 2.39	1.07	0.75	0.34	1.11
Na ₂ O%	0.07 – 0.78	0.03 – 0.10	0.05 – 0.39	0.42 – 0.70	0.31	0.46	0.29	0.26

* cherts are presently used by cement companies in Ras Al Khaimah

CHAPTER VII

**SUMMARY AND
CONCLUSIONS**

CHAPTER VII

SUMMARY AND CONCLUSIONS

The present study deals with the Jurassic limestones and Upper Cretaceous siliceous rocks exposed at Ras Al Khaimah Emirate. The objectives of the study are three-fold: (i) to determine the petrographic and mineral characteristics of the rocks; (ii) to investigate their geochemical attributes; and (iii) to assess their suitability as raw materials for the cement industry in the Emirate.

The materials used in the present study comprise samples representing the cherts, limestones and dune sands. Twenty-one chert samples were collected from the Hawasina succession in two quarries in addition to some exposures at Al Gail and Saram. Fifteen limestone samples were collected from the Khor Khowair quarry. The coastal and inland sand dunes at Al Helailah and Al Gail; respectively are represented by three samples. One sample was collected from a diabase sheet structurally interbedded with the cherts in the Hawasina succession.

Microscopic examination has been carried out on a total of 37 thin sections and three grains mounts prepared from the various rock types and the loose dune sands. X-ray diffractometry has been utilized to investigate the mineral composition of the various rocks. Samples collected from the sand dunes were subjected to heavy mineral separation. The obtained light and heavy fractions were examined microscopically and their constituents were quantitatively determined by counting of about 300 grains in each slide. In addition, chemical analyses were conducted on all samples to determine the concentrations of the major oxides and some trace and rare earth elements.

Microscopic examination of thin sections prepared from the various sedimentary lithologies revealed the presence of two main facies: the chert facies and the carbonate

facies. Based on their composition, each of these two facies could be subdivided into a number of subfacies.

The chert facie was recorded in all the studied localities except Khor Khowair. The delineated subfacies include: ferruginous radiolarian ribbon chert, carbonaceous radiolarian ribbon chert, colloform ribbon chert, calcareous chert and siliceous mudstone. These subfacies are variably recorded in the different localities. They show several evidences of diagenetic effects including: cementation, dissolution, replacement and neomorphism.

The carbonate facies was recorded in all the studied localities. Based on the textural classification of Dunham (1962), these carbonates comprise lime mudstone, wackestone, packstone and crystalline limestone. The wackestones are represented by two types: peloidal bioclastic wackestone and *Orbitolina* bioclastic wackestone. The packstones, on the other hand, consist of algal bioclastic packstone, pelecypodel bioclastic packstone or *Orbitolina* peloidal bioclastic packstone. The crystalline limestones are rare and their presence is restricted to Idan area. All the carbonate rocks display evidences of extensive diagenesis including: dissolution, cementation, compaction, replacement and neomorphism.

The studied sand dunes are of two types: carbonate and noncarbonate. The former type is represented by the coastal dunes whereas the latter type constitutes the inland dunes.

The detailed mineral compositions of the studied rocks have been further assessed utilizing X-ray diffractometry. The results obtained revealed that the cherts consist of (in order of decreasing abundance): quartz, calcite, dolomite and hematite. Quartz is the only major component in the rocks of all localities except for some exposures in Saram where calcite also represents a major constituent. The latter mineral is a subordinate or minor

component in some other calcareous cherts in Al Gail and Saram. The presence of dolomite is limited to the calcareous cherts of Idan in which it represents a subordinate or minor component. Hematite was detected in the ferruginous radiolarian chert of Idan. The limestones, on the other hand, are made up of (in order of decreasing abundance): calcite, quartz sand dolomite. Calcite is the sole major component in all the studied carbonates. Quartz exists as a subordinate constituent in some lime mudstones and wackestones of Saram. The presence of dolomite is limited to the packstones of Idan in which the mineral represents a minor component.

The light fractions of the Al Helailah coastal sand dunes consist of carbonate lithoclasts and quartz together with minor proportions of skeletal grains and traces of feldspars and chert. Their heavy fractions are made up of pyroxenes and opaques in addition to traces of hornblende, garnet, rutile, tourmaline and epidotes. The light and heavy fractions of Al Gail inland dunes are compositionally similar to those of Al Helailah except for the absence of skeletal grains and the presence of traces of monazite. Quantitative comparison between the two types of dune sands revealed that the light fractions of Al Helailah coastal dunes contain higher concentrations of carbonate lithoclasts and skeletal grains and lower proportions of quartz and chert. Also, the heavy fractions of Al Helailah dunes are slightly more enriched in opaques, pyroxenes, epidote and hornblende and depleted in rutile, tourmaline, garnet and monazite.

The obtained geochemical data are in accordance with the results of petrographic studies and XRD analysis. These data confirm the classification of the studied cherts into three types; namely: (i) red ribbon radiolarian cherts or radiolarites (R); (ii) calcareous cherts (CC), and (iii) siliceous mudstones (SM).

Comparable rock lithologies in the studied areas show closely similar major element compositions. Silica concentrations do not show marked variations throughout

most of the stratigraphic sections. They are 90%-98% for R beds, 71% – 87% for SM beds and 49% - 72% for CC beds.

The high values of Al / (Al+Fe+Mn) ratio in the R, SM and CC samples from both Idan and Al Rams indicate a major role played by terrigenous sources in their genesis. The decrease in this ratio upwards in the chert section of Wadi Saram reflects a change up-section from a setting with predominantly terrigenous influence to a setting of pelagic deposition. Again, the increase in TiO₂, Al₂O₃, MgO, Fe₂O₃ and K₂O contents downwards in the section an increase in proportions of reflects detrital materials inherited from the underlying ophiolitic section.

The relative enrichment of the studied cherts, particularly SM samples, in the HFS (High Field Strength) elements is mostly attributed to the important role played by a detrital source component in their genesis. This is because most of the HFS elements are concentrated in detrital heavy minerals such as zircon, hematite and clay minerals.

The cherts exhibit LREE (Light Rare Earth Elements) fractionated patterns with moderate Eu anomalies. The SM samples have the highest REEs abundances. The positive correlations between the total REE and the detrital indicators such as Al₂O₃, Fe₂O₃, TiO₂, and K₂O signify contributions from terrigenous sources in the origin of these cherts.

R-mode cluster analysis for major and trace elements exhibits three main element associations or clusters. The first cluster is for carbonate minerals (Ca & Sr), the second cluster includes the terrigenous source components (REE, MgO, P₂O₅, FeO, Zr, Nb, Rb, K₂O, Ga, Al₂O₃ and SiO₂), whereas the third cluster is only devoted for silica. On the other hand, Q-mode cluster analysis proved to be successful in discriminating between the three major chert lithologies including R, SM and CC types.

R-mode factor analysis produced 2 factor model accounting for 85.85% of the data variability. Factor 1 (terrigenous source) accounts for 68.12% of the variability model and

includes the association TiO_2 , Al_2O_3 , FeO , K_2O , P_2O_5 , Rb , Ga , Zr and REE . Factor 2 (carbonate minerals) accounts for 17.43% of data variability and is a bipolar factor where CaO is positively loaded and SiO_2 is negatively loaded on it. This indicates the carbonate replacement in the cherts at the expense of silica.

In the present work an attempt has been made to assess the suitability of the studied limestones and cherts as raw materials for cement production. A comparison has been made between the chemical compositions of the studied limestones and those of Khor Khowair presently used by the Ras Al Khaimah Rock Company. This comparison revealed the following:

- (i) The studied Khor Khowair limestones contain slightly higher concentrations of CaO and lower proportions of SiO_2 , MgO and Fe_2O_3 .
- (ii) The limestones of Idan and Al Gail are, to great extent, compositionally similar to those of Khor Khowair. Differences are represented only by the slight relative enrichment of Idan limestones in MgO and those of Al Gail in CaO . This permits the consideration of the limestone exposures in these two localities for possible future needs.
- (iii) The Saram limestones are markedly compositionally different from those of Khor Khowair; being depleted in CaO and enriched in SiO_2 , Al_2O_3 and Fe_2O_3 .
- (iv) The studied Idan cherts have lower SiO_2 and higher CaO concentrations when compared with those presently used by RAKCC. Al Rams cherts are more enriched in Al_2O_3 , MgO and Na_2O and depleted in CaO . Saram cherts have higher CaO and lower Al_2O_3 and Fe_2O_3 contents. On the other hand, Al Gail cherts are closely similar to those exploited by RAKCC and, hence, can be considered as a source of silica in future planning.

The suitability of sand dunes in the surroundings of Ras Al Khaimah as a source of silica has been also tested. The chemical data of the sands collected from the coastal and

inland dunes at Al Gail and Al Helailah; respectively were compared with those of cherts and dune sands analyzed earlier by the RAKCC. This comparison revealed the following:

- (i) The studied dune sands have lower SiO_2 , Al_2O_3 and Fe_2O_3 concentrations than those reported for cherts.
- (ii) Sand dunes of Al Gail are compositionally similar to those tested earlier by RAKCC; except for their slight relative enrichment in Fe_2O_3 , CaO and MgO at the expense of SiO_2 , Al_2O_3 and K_2O . On the other hand, Al Helailah dune sands are relatively more enriched in CaO and depleted in other major elements and, hence, cannot be considered as a possible silica source for cement productions.

REFERENCES

REFERENCES

- Allemann, F., and Peters, T., 1972, The Ophiolite Radiolarite belt of the North Oman Mountains. *Eclogue Geologica Helvetica*, 65, pp. 657-697.
- Ager, D. V., 1981, Major marine cycles in the Mesozoic. *Journal of the Geological Society*, 138, pp. 159-1611.
- Ajayi, T. R., 1981, Statistical analysis of stream sediments data from the Ife-Ilesha area of Southwest Nigeria. *J. Geochemist Explorer*. 15: 539-548
- Barrett, T. J., 1981, Chemistry and Mineralogy of Jurassic bedded chert overlying Ophiolites in the North Apennines, Italy: *Chemical Geol.*, 34. 289-317
- Barrette, P.D., and Calon, T.J., 1987, Re-imbrications of the Hawasina allochthons in the Sufrat and Dawd range, Oman Mountains. *Journal of Structural Geology*, 9, pp. 859-867.
- Bechennic, F., Le Metour, J., Rabu, D., Boudillon De-Grissac, Ch., De Wever, P., Beurrier, M. and Villey, M., 1990, The Hawasina Nappes: Stratigraphy, palaeogeography and structural evaluation of a fragment of the south-Techyan passive continental margin. *Geol. Society* 40, 213-223.
- Bernoulli, D. and Weissert, H., 1987, The upper Hawasina nappes in the central Oman Mountains: stratigraphy, palinspastics and sequence of nappe emplacement. *Geodynamica Acta*, 1, pp. 47-58.
- Biehler, J., Chevalier, C., and Ricateau, R., 1975, Carte geologique de la peninsula de Musandam. Edition B.R.G.M., Orleans, France.
- Bishoff, J. L., 1969, Goethite-hematite stability relations in the reference to sea water and the Red Sea brine system. In: E. T. Degens and D. A. Ross (Editions), *Hot Brines and Recent Heavy Metal Deposits in the Red Sea*, Springer, New York, N. Y. pp. 402-406.
- Bostrom, K., 1973, The origin and fate of ferromanganoan active ridge sediments. *Stockholm Contrib. Geol.*, 27: 147-243.
- Bostrom, K. and Peterson, N. N. A., 1969, Origin of Aluminum-poor ferromanganoan sediments in areas of high heat flow on the East Pacific Rise: *Marine Geology*, v. 7, p. 427-447.
- Bostrom, K., Farquharson, B., and Eyl, W., 1971, Submarine Hot springs as a source of active ridge sediments: *chemical geology*, v. 10, 184-203.
- Bowna, A. H., 1962, *Sedimentology of Some flysch deposits*. Elsevier, Amsterdam.

- Buttner, W. and Sagar, R. 1983, Factor analysis of stream sediment data for the Vicinity of the Zinc-Lead occurrences of S-Carl (Unteregadine Switzerland), In: Schneider J. (Ed.), Mineral Deposits of Alps and of the Alpin Epoch in Europe. Springer xevlag. Hidelberg. 231-239.
- Cooper, D.J.W., 1986, The Hamrat Duru Group: evolution of a Mesozoic passive carbonate margin in the Oman Mountains. University of Edinburgh PhD, thesis.
- Cooper, D.J.W., 1987, Hamrat Duru Group: revised stratigraphy of a Mesozoic deep-water passive margin in the Oman Mountains. University of Edinburgh, PhD thesis.
- Cooper, D.J.W., 1988, Structure and sequence of thrusting in deep-water sediments during ophiolite emplacement in the south-central Oman Mountains. *Journal of Structural Geology*, 10, pp. 473-485.
- Cooper, D.J.W., 1990, Sedimentary evaluation and palaeogeographical reconstruction of the Mesozoic continental rise in Oman: evidence from the Hamrat Dura Group. In: Robertson, A. H. F., Searle, M. P. & Ries, A. C. (eds) *The Geology and Tectonics of the Oman Region*. Geological Society, London, Special Publication, 49, 161-187.
- David, M., Camiglio, C. & Darling, R., 1974, Progresses in R- and Q-mode analysis: Correspondence analysis and its application to the study of geological processes. *J. Earth. Sci.*, 2: 131-146.
- Davis, J. C., 1973, *Statistic and Cluster Analysis in Geology*. 1st edition. Wiley, New York, 550p.
- Dunham, R. J., 1962, Classification of carbonate rocks according to depositional textures, in W. E. Ham (ed.), *Classification of carbonate rocks*. Am. Assoc. Petroleum Geologists Mem. 1, p. 108-121.
- Dymond, J., Corliss, J. B., Heath, G. R., Field, C. W., Dasch, E. J. and Veeh, H. H., 1973, Origin of metalliferous sediments from the Pacific Ocean. *Bull. Geol. Soc. Am.*, 84: 3355-3372.
- Falcon, N.L., 1967, The geology of the north-east margin of the Arabian basement shield. *Advancement of Science*, 24, pp. 31-42.
- Farris, J. S., 1969, On the Cophenetic correlation coefficient. *Cist. Zool.*, 18, 279-285.
- Glennie, K.W., Boeuf, M.G.A., Hughes Clark, M.W., Moody-Stuart, M., Pilaar, W.F.H., and Reinhardt, B.M., 1973, Late Cretaceous nappes in the Oman Mountains and their geologic evolution. *American Association of petroleum Geologists Bulletin*, 57, pp. 5-27.

- Glennie, K.W., Boeuf, M.G.A., Hughes Clark, M.W., Moody-Stuart, M., Pilaar, W.F.H., and Reinhardt, B.M., 1974, The Geology of Oman Mountains: Konin. Neder. Geol. Mijubouw. Genoot. Verdh. 3, part 1, 432 p.
- Glennie, K.W., 1995, The geology of the Oman mountains and an outline of their origin: Scientific Press Ltd., Bucks, United kingdom.
- Graham, G. M., 1980, Structure and Sedimentology of the Hawasina Window, Oman Mountains. Ph D thesis, Open University, Milton Keynes, UK.
- Gower, J. C., 1967, A comparison of some methods of cluster analysis biometrics. 32. 623-637.
- Harland, W. B., Cox, A. V., Llewellyn, P. G., Pickton, C. A. G., Smith, A. G. & Walters, R., 1982, A geologic time scale. Cambridge University Press, Cambridge.
- Harman, H. H., 1976, Modern Factor analysis. University of Chicago Press. Chicago, III. 482 pp.
- Haskin, L. A., Haskin, N. A., Frey, F. A. and Wildeman, T. R., 1968, Relative and absolute abundances of the rare earths. In: L. H. Ahrens (Editor), Origin and Distribution of the Elements. Pergamon, London, pp. 889-912.
- Hedberg, H. D., 1976, International Stratigraphic guide: a guide to stratigraphic classification, terminology and procedure. John Wiley, New York.
- Hesp, W. R., and Rigby, D., 1975, Aspects of tin metallogenesis in the Tasman Geosyncline, Eastern Australia as reflected by cluster and factor analysis. J. Geochem. Explore. 4: 234-347.
- Hiscott, R. N. & Middleton, G. V., 1979, Depositional mechanisms of thick-bedded sand stones at the base of a submarine slope, Tourelle Formation (lower Ordovician), Quebec, Canada. In: Doyle, L. F. & Pilkey, O. H. (eds) Geology of Continental Slope. Special Publication of the Society of Economic Mineralogists and Paleontologists, 27, 307-326.
- Hudson, R.G.S., Browne, R.N., and Chatton, M., 1954a, The structure and stratigraphy of the Jabel Qamar area, Oman. Proceeding of the Geological Society of London, 1513, xcix-civ.
- Hudson, R.G.S., Mcgugan, A., and Morton, D.M., 1954b, The structure of the Jabel Hagab area, Trucial Oman. Quarterly Journal of the Geological Society of London, 110, pp. 121-152.
- Hudson, R.G.S., and Chatton, M., 1959, The Musandam limestone (Jurassic to Lower Gretaceous) of Oman, Arabia: Museum National D'histoire Naturelle, Paris, v. 7, pp. 69-91.

- Hudson, R.G.S., 1960, The Permian and Triassic of the Oman Peninsula, Arabia: The Geological Magazine, v. XCVII, no. 4, pp. 299-308.
- Hughes Clark, M. W., 1988, Stratigraphy of rock crust nomenclature in the oil producing area of Interior Oman, Journal of Petroleum Geology. 11, 5-60.
- Holland, C. H., Audley-Charles, M. G., Basselt, M. G., Gowre, J. W., Carry, D., Fitch, F. J., Hancock, J. M., House, M. R., Ingham, J. K., Kent, P. E., Morton, N., Ramsbottom, W. H. C., Rawson, R. E., Smith, D. B., Stubblefield, C. J., Torrens, H. S., Wallace, P. & Woodland, A. W., 1978, A guide to stratigraphical procedure. Geological Society, London Special report 11.
- IWACO, 1986, Groundwater study: report submitted to the Ministry of Agriculture and Fisheries, United Arab Emirates.
- Joroskog, K. G., Klovan, J. E., and Reyment, R. A., 1976, Geological factor analysis. Elsevier, Amsterdam, 178.
- Karl, S. M., 1984, Sedimentologic, diagenetic, and geochemical analyses of Upper Mesozoic ribbon cherts from the Franciscan assemblage at the Main Headlands, California. In M. C. Blake, Jr. (ed.), Franciscan Geology of Northern California. Soc. Econ. Paleontologists and Mineralogists, Pacific Section, Los Angeles, 71-88.
- Lees, G.M., 1928, The geology and tectonics of Oman and of part of southeastern Arabia. Quarterly Journal of the Geological Society of London, 84, pp. 585-670.
- Lippard, S.J., and Rex, D.C., 1982, K-Ar ages of alkaline igneous rocks in the northern Oman Mountains, N.E. Arabia, and their relation to drifting, passive margin development and destruction of the Oman Tethys. Geological Magazine, 119, pp.497-503.
- Lippard, S.J., Smewing, J.D., Rothery, D.A., and Browning, P., 1982, The Geology of the Dibba zone, Northern Oman Mountains: a preliminary study. Journal of the Geological Society of London, 139, pp. 59-66.
- Lowe, D. R., 1982, Sediment gravity Flow II. Deposition models with special reference to deposition of high density turbidite currents. Journal of Sedimentary Petrology, 52, 279-297.
- Masri, M. R., Brown, N. B., Chatten, J., Cement Raw Materials-Ras Al Khaimah. Arab Development Company and Robertson Research International, v1, 1972.
- Nie, N. H., Hull, C. H., Jenkins, J. G., Steinburnner, T. & Bent, D. H., 1975, Statistical Package for the Social Sciences (SPSS) 2nd edn. Graw Hill, New York. 676pp.
- Norusis, M. J., 1986, Statistical package for the Social Sciences (PS/PC+) SPSS Inc. 444N. Michigan Avenue. Chicago Illinois.

- Patton, T. L. & O'Connor, S. J., 1988, Cretaceous flexural history of the northern Oman Mountain foredeep, United Arab Emirates, *American Association of Petroleum Geologists Bulletin*, 72, 797-809.
- Pearce, J. A. and Cann, J. R., 1973, Tectonic setting of basic volcanic rocks determined using trace element analyses: *Earth and Planetary Science letters*, v. 19, p. 29-300.
- Rabu, D., Le Metour, J., Bechenec, F., Beurriet, M., Villey, M. & Bourdillon-Jeucly De Grissac, 1990, Sedimentary aspects of the Eo-Alpine cycle on the Northeast edge of the Arabian Platform (Oman Mountains). In: Robertson, A. H. F., Searle, M. P. & Ries, A. C. (eds) *The Geology and Tectonics of the Oman Region*. Geological Society, London, Special Publication, 40, 49-68.
- Ricateau, R., and Riche, P. H., 1980, Geology of the Musandam Peninsula (Sultanate of Oman) and its surroundings. *Journal of Petroleum Geology*, 3, pp. 139-152.
- Robertson, A. H. F., 1987, The transition from a passive margin to an Upper Cretaceous foreland basin related to ophiolite emplacement in Oman Mountains. *Geological Society of America Bulletin*, 99, 633-653.
- Robertson, A. H. F., Searle, M. P. & Ries, A. C. (eds), 1990, *The Geology and Tectonics of the Oman Region* Geological Society Special Publication. 49, 3-25.
- Saagar, R. Esselaar, P. A., 1969, Factor analysis of geochemical data for the Basal rock, Orange Free State gold field, South Africa, *Econ. Geol.*, 64: 446-451
- Saagare, R. Sinclair, A. J., 1974, Factor analysis of stream sediment geochemical data from the Mount Nansen Area, Yukon Territory, Canada, *Econ. Geol.* 243-252.
- Searle, M.P., and Malpas, J., 1980, The structure and metamorphism of rocks beneath the Semail ophiolite of Oman and their significance in ophiolite obduction. *Transactions of the Royal Society of Edinburgh: Earth Sciences*, 71, pp. 213-28.
- Searle, M.P., and Malpas, J., 1982, Petrochemistry and origin of subophiolitic metamorphic and related rocks in the Oman Mountains. *Journal of the Geological Society of London*, 139, pp. 235-248.
- Searle, M. P., Lippard, S.J., Smewing, J.D., and Rex, D.C., 1980, Volcanic rocks beneath the Semail Ophiolite in the northern Oman Mountains and their tectonic significance in the Mesozoic evolution of Tethys. *Journal of the Geological Society of London*, 137, pp. 589-604.
- Searle, M.P., and Graham, G.M., 1982, 'Oman Exotics' Oceanic stages of continental rifting. *Geology*, 10, pp. 43-49.
- Searle, M.P., James, N.P., Calon, T.J, and Smewing, J.D., 1983, Sedimentological and structural evolution of the Arabian continental margin in the Musandam Mountains and Dibba zone, United Arab Emirates. *Geological Society of America Bulletin*, 94, pp. 1381-1400.

- Searle, M.P., 1985, Sequence of thrusting and origin of culminations in the northern and central Oman Mountains. *Journal of Structural Geology*, 7, pp. 129-143.
- Searle, M.P., 1988a, Thrust tectonics of the Dibba zone and the structural evolution of the Arabian continental margin along the Musandam mountains (Oman and United Arab Emirates). *Journal of the Geological Society*, 145, pp. 43-54.
- Searle, M.P., 1988b, Structure of the Musandam Culmination (Sultanate of Oman and the United Arab Emirates) and the Strait of Hormuz syntaxis. *Journal of the Geological Society*, 145, pp. 831-845.
- Sokal, R. R. & Sneath, P. H. A., 1963, *Principals of numerical taxonomy* (London and Sanfrancisco: Freeman) 359p.
- Steinberg, M., and Mpodozis-Marin, C., 1978, Classification geochemique des radiolarites et des sediments silicieux oceaniques, signification paleoceanographique: *Oceanologica Acta* I, p. 359-367.
- Stocklin, J., 1968, Structural history and tectonics of Iran: A review. *American Association of Petroleum Geologists Bulletin*, 52, 1229-1258.
- Stocklin, J., 1974, Possible ancient continental margins in Iran. In: Burk, C. L. & Drake, C. L. (eds) *The Geology of Continental Margins*. New York, Springer, 873-887.
- Tucker, L. R., 1971, Relation of Factor scan estimates to their use. *Psychometrica*, 3b: 427-436.
- Tripathi, V. S., 1979, Factor analysis in geochemical exploration. *J. Geochem. Explor.* 2: 262-275.
- Tucker, M.E., 1974, Sedimentology of Paleozoic pelagic limestones: the Devonian Griotte (southern France) and Cephalopodenkalk (Germany). In: Jenkyns, H. C. and Hsu, K.J. *pelagic sediments on Land and under the sea*. Special Publication of the International Association of sedimentologists, 1, pp. 71-92.
- United Arab Emirates National Atlas, 1993.
- Vail, P. R., Mitchum, F.M.Jr., and Thompson, J.III., 1977, Seismic stratigraphy and global changes in sea level, part 4: global cycles or relative changes of sea level. In: *Seismic stratigraphy applications to hydrocarbon exploration*. American Association of Petroleum Geologists Memoir, 26, pp. 83-97.
- Vogt, J. H., and Kollenberg, W., 1987, Genetic implications of geochemical factor analysis in sediment-hosted Cu-Pb-Ba mineralization. *Mineral Deposita*, 22: 151-160.
- Watts, K. F., 1990, Mesozoic Palaeogeography of the Oman Mountains-Carbonate slope facies marking the Arabian platform margin. In: Robertson, A. H. F.,

Searle, M. P. & Ries, A. C. (eds) *The Geology and Tectonics of the Oman Region*. Geological Society, London, Special Publication, 49, 139-159.

Watts, K. F., and Garrison, R. E., 1986, Sumeini Group, Oman-evaluation of Mesozoic carbonate slope on a south Tethyan continental margin. *Sedimentary Geology*, 48, 107-168.

White, R.S., and Ross, D.A., 1979, Tectonics of the Western Gulf of Oman. *Journal of Geophysical Research*, 84, pp. 3479-3489.

ARABIC SUMMARY

الهيكلية والمعادن الثقيلة المعتمة ومعادن بيروكسين وايبيدوت وهورنبلند بينما تحتوي على نسب أقل من الشرت ومعادن كوارتز وروتيل وتورمالين وجارنت ومونازيت .

وقد أكدت نتائج التحاليل الكيميائية لصخور الشرت وجود عدد من السحنات هي: الراديولاريت والشرت الجيري والصخر الغريني الليسي، وتميز كل من هذه السحنات بخصائص كيميائية متجانمة من ناحية محتواها من العناصر الرئيسية والنادرة ، وتواجد السليكا SiO_2 بأعلى تركيزاتها (90 - 98%) في سحنة راديولاريت ، بينما سجلت أقل التركيزات في سحنة الشرت الجيري، ومن ناحية أخرى فإن القيم المرتفعة للنسبة $Al / (Al + Fe + Mn)$ في معظم السحنات تشير إلى أهمية الدور الذي لعبته المصادر الفتاتية في تكوينها ونشأتها ، ويؤكد ذلك أيضا الارتفاع النسبي في تركيزات كل من TiO_2 , Al_2O_3 , MgO , Fe_2O_3 بالإضافة إلى العناصر ذات جهد التأين المرتفع . وتميز صخور الشرت بأنماط توزيع ثرية بالعناصر الأرضية النادرة الخفيفة ذات شذوذ سالب متوسط لعنصر الأوروبيوم . وقد أوضحت نتائج التحليل الإحصائي التجميعي **R-mode cluster analysis** إلى وجود ثلاثة تجمعات إحداهما لمعادن الكربونات والثاني للمكونات الأرضية والثالث للسليكا ، ومن ناحية أخرى فقد تمخض تحليل المعامل الإحصائي عن نموذج ذو معاملين يمثل حوالي 85.85% من التغير في النتائج ، ويرتبط المعامل الأول في هذا النموذج بالمكونات الأرضية بينما يمثل المعامل الثاني المكونات الكربوناتية .

وتشير نتائج الدراسات التي أجريت إلى أن معظم الأحجار الجيرية وبعض الصخور السليسية (الشرت) موضوع الدراسة تتشابه في تركيبها مع تلك التي تستخدم حاليا في صناعة الأسمنت في شركات راس الخيمة مما يجعل من الممكن أخذها في الاعتبار في حالة أية احتياجات مستقبلية محتملة ، وعلى العكس من ذلك فإن الخصائص التكوينية لرمال الكثبان موضوع الدراسة - خاصة الشاطئية - لا تسمح بالاستفادة منها كمصدر للسليكا في صناعة الأسمنت .

بتروولوجية وجيو كيميائية والإمكانات الاقتصادية لبعض الأحجار الجيرية والصخور السليسية بشمال دولة الامارات العربية المتحدة

تتضمن هذه الرسالة نتائج مجموعة من الدراسات البتروولوجية والمعدنية والجيوكيميائية التي أجريت على الأحجار الجيرية التابعة لمكون المسندم (الجوراسي) والصخور السليسية الواقعة ضمن مجموعة الحواسنة (الكريتاسي العلوي) ، بالإضافة إلى الكثبان الرملية الشاطئية والداخلية وذلك بعدة مناطق بإمارة رأس الخيمة الواقعة في الجزء الشمالي من دولة الامارات العربية المتحدة ، وقد شملت تلك الدراسات الفحص الميكروسكوبي للشرائح الصخرية ، وفصل المعادن الثقيلة والخفيفة برواسب رمال الكثبان وتحليل الصخور باستخدام حيود الأشعة السينية بالإضافة إلى التحاليل الكيميائية للتعرف على توزيع العناصر الرئيسية وبعض العناصر النادرة والشحيحة .

وقد أوضحت نتائج الدراسات المختلفة أن الصخور السليسية (الشيرت) يمثلها عدد من السحنات هي الشيرت الشريطي الراديولاري الحديدي ، والشيرت الشريطي الراديولاري الكربوني ، والشيرت الشريطي الكولوفورمي ، والشيرت الجيري ، والصخر الغريني السليسي . وتتكون هذه الصخور من معادن كوارتز وكالسيت ودولوميت وهيماتيت (مرتبة طبقا للتناقص في درجة الانتشار) . وتتواجد الأحجار الجيرية في شكل عدد من السحنات النسيجية هي:

Crystalline carbonate, packstone, wackestone, lime mudstone

وتتكون هذه الأحجار بصفة أساسية من معدن كالكيت بالإضافة إلى نسب أقل من معدني كوارتز ودولوميت . وقد لوحظ أن العمليات اللاحقة للترسيب (مثل الانضغاط والإذابة والالتحام والإحلال والاستحداث) قد لعبت دورا هاما في تغيير الخصائص الأصلية (سواءا النسيجية أو التكوينية) للصخور وبصفة خاصة الأحجار الجيرية . ومن ناحية أخرى فقد أوضحت المقارنة بين القطفات الخفيفة والثقيلة لرمال كل من الكثبان الشاطئية والكثبان الداخلية أن الأولى تحتوي على تركيزات أعلى من الكسورات الصخرية الجيرية والحبيبات الحفرية



بتروولوجية وبيوكيميائية والإمكانات الاقتصادية
لبعض الأحجار الجيرية والصخور الطليسية
بشمال دولة الامارات العربية المتحدة

إعداد

محمد احمد علي إبراهيم
شركة اسمنت رأس الخيمة
بكالوريوس علوم
(1995)

رسالة مقدمة إلى

كلية العلوم - جامعة الامارات العربية المتحدة
لاستكمال متطلبات الحصول على درجة الماجستير
في علوم البيئة



كلية العلوم
جامعة الامارات العربية المتحدة
ديسمبر 2001 م